



**HAL**  
open science

## Small molecules regulated bone resorption and enzyme activity in osseous cells

Zhongyuan Ren

► **To cite this version:**

Zhongyuan Ren. Small molecules regulated bone resorption and enzyme activity in osseous cells. Biochemistry [q-bio.BM]. Université Claude Bernard - Lyon I; Jilin University (Changchun, Chine), 2014. English. NNT: 2014LYO10291 . tel-01128220

**HAL Id: tel-01128220**

**<https://theses.hal.science/tel-01128220>**

Submitted on 9 Mar 2015

**HAL** is a multi-disciplinary open access archive for the deposit and dissemination of scientific research documents, whether they are published or not. The documents may come from teaching and research institutions in France or abroad, or from public or private research centers.

L'archive ouverte pluridisciplinaire **HAL**, est destinée au dépôt et à la diffusion de documents scientifiques de niveau recherche, publiés ou non, émanant des établissements d'enseignement et de recherche français ou étrangers, des laboratoires publics ou privés.

THESE EN COTUTELLE

Pour obtenir le grade de Docteur délivré par

Jilin University

et

Université Claude Bernard Lyon 1

Ecole Interdisciplinaire Sciences-Santé

Spécialité : Biochimie

Présentée et soutenue publiquement le 5 décembre 2014

Par

Zhongyuan Ren

## **Small Molecules regulated Bone Resorption and Enzyme Activity in osseous cells**

Rapporteurs : Dr. Joanna Bandorowicz Pikula  
Pr. Jean-Marie Ruyschaert  
Pr. Xiao Zha

Membres du Jury : Dr. Saida Mebarek (Co-directrice)  
Pr. Yuqing Wu (Co-directrice)  
Pr René Buchet (Co-directeur)  
Pr. Xuexun Fang  
Dr. Pierre Jurdic  
Dr. Hong-Wei Li  
Pr. Xiao Zha

## UNIVERSITE CLAUDE BERNARD - LYON 1

### **Président de l'Université**

**M. François-Noël GILLY**

Vice-président du Conseil d'Administration

M. le Professeur Hamda BEN HADID

Vice-président du Conseil des Etudes et de la Vie  
Universitaire

M. le Professeur Philippe LALLE

Vice-président du Conseil Scientifique

M. le Professeur Germain GILLET

Directeur Général des Services

M. Alain HELLEU

### ***COMPOSANTES SANTE***

Faculté de Médecine Lyon Est – Claude Bernard

Directeur : M. le Professeur J. ETIENNE

Faculté de Médecine et de Maïeutique Lyon Sud – Charles  
Mérieux

Directeur : Mme la Professeure C. BURILLON

Faculté d'Odontologie

Directeur : M. le Professeur D. BOURGEOIS

Institut des Sciences Pharmaceutiques et Biologiques

Directeur : Mme la Professeure C.  
VINCIGUERRA

Institut des Sciences et Techniques de la Réadaptation

Directeur : M. le Professeur Y. MATILLON

Département de formation et Centre de Recherche en  
Biologie Humaine

Directeur : Mme. la Professeure A-M. SCHOTT

### ***COMPOSANTES ET DEPARTEMENTS DE SCIENCES ET TECHNOLOGIE***

Faculté des Sciences et Technologies

Directeur : M. F. DE MARCHI

Département Biologie

Directeur : M. le Professeur F. FLEURY

Département Chimie Biochimie

Directeur : Mme Caroline FELIX

Département GEP

Directeur : M. Hassan HAMMOURI

Département Informatique

Directeur : M. le Professeur S. AKKOUCHE

Département Mathématiques

Directeur : M. Georges TOMANOV

Département Mécanique

Directeur : M. le Professeur H. BEN HADID

Département Physique

Directeur : M. Jean-Claude PLENET

UFR Sciences et Techniques des Activités Physiques et

Directeur : M. Y. VANPOULLE

## Sportives

Observatoire des Sciences de l'Univers de Lyon

Polytech Lyon

Ecole Supérieure de Chimie Physique Electronique

Institut Universitaire de Technologie de Lyon 1

Ecole Supérieure du Professorat et de l'Education

Institut de Science Financière et d'Assurances

Directeur : M. B. GUIDERDONI

Directeur : M. P. FOURNIER

Directeur : M. G. PIGNAULT

Directeur : M. C. VITON

Directeur : M. A. MOUGNIOTTE

Directeur : M. N. LEBOISNE

## Acknowledgements

*This thesis was prepared at the University Claude Bernard Lyon 1, UMR 5246 CNRS, UMR 5242 IGFL, in Lyon (France) and at Jilin University, Key Laboratory for Supramolecular Structure and Materials, in Changchun (China) under the co-supervision of Professor René BUCHET, Dr. Saida Mebarek and Professor Yuqing WU. I would like to thank them for their guidance, encouragement, and enthusiasm.*

*I am very grateful Dr. Saida Mebarek. I would never have been able to finish my works and dissertation without her helps. A special thank is also addressed to Prof. Pierre Jurdic for giving me the opportunity to work in his laboratory of IGFL and for his guidance.*

*I wish to thank following people for their suggestions, discussions, teaching and technical help:*

*Jilin University (China):*

*Hongwei LI*

*Yuan YUE*

*Jian SUN*

*Yang GAO*

*Shi JIN*

*Xiaoyu YUAN*

*Dong PAN*

*Jiao LIU*

*Dongdong ZHENG*

*Xingpeng WANG*

*Teng ZHANG*

*Dingyi FU*

*Pengfan GAO*

*Xingfeng REN*

*Laboratory ODMB (Lyon):*

*Anne BRIOLAY*

*Françoise BESSON*

*Carole BOUGAULT*

*Loïc J. BLUM*

*David MAGNE*

*Leyre BRIZUELA*

*Laurence BESUEILLE*

*Dina ABDALLAH*

*Le Duy DO*

*Michèle BOSCH*

*Maya FAKHRY*

*Abdelkarim ABOUSALHAM*

*Renaud RAHIER*

*Aurélie FÉLIZARD*

*Laboratory of IGFL (Lyon):*

*Justine BACCHETTA*

*Fabienne COURY*

*Nathalie DEMONCHEAUX*

*Irma MACHUCA-GAYET*

*Kélig PERNELLE*

*Many thanks to Prof. Jean-Marie Ruyschaert, Prof. Joanna Bandorowycz-Pikula and Prof. Xiao Zhafor having accepting to review my Ph. D thesis. I would like to thank to Dr. Geraldine Bechkoff for her pionneering work on infrared enzymatic assay. We thank Dr M.O Platt (Coulter Department of Biomedical Engineering, Georgia Institute of Technology, Atlanta, GA, USA) for providing helpful advice on zymography.*

*To my parents, Wei REN and Xiufang BI,*

*My family, my friends,*

# CONTENTS

<b>CHAPTER I: Introduction</b> -----	<b>8</b>
1. Bone Metabolism-----	<b>9</b>
2. Bone resorption and formation-----	<b>9</b>
3. Communications between osteoclasts and osteoblasts-----	<b>10</b>
4. Cathepsin K is necessary for bone resorption in osteoclasts -----	<b>10</b>
5. Inhibition of Cathepsin K for the treatment of Osteoporosis and Osteoarthritis -----	<b>11</b>
6. Cathepsin K inhibitors -----	<b>11</b>
7. Biomarker of bone formation in osteoblasts: Alkaline phosphatases -----	<b>14</b>
8. State of art of phosphatase activity assays-----	<b>15</b>
<b>CHAPTER II: AIMS</b> -----	<b>17</b>
<b>CHAPTER III: MATERIAL AND METHODS</b> -----	<b>21</b>
<b>CHAPTER IV: RESULTS AND DISCUSSIONS</b> -----	<b>37</b>
Part 1: Effects of Azanitrile Cathepsin K Inhibitors on Mineralization and Bone Resorption -----	<b>38</b>
Part 2: Direct determination of pyrophosphate hydrolysis in Matrix Vesicles by Infrared Spectroscopy-----	<b>49</b>
Part 3: An infrared assay of the kinetics of phosphate-release from physiological substrates in living cells -----	<b>59</b>
<b>CHAPTER V: CONCLUSIONS AND REMARKS</b> -----	<b>71</b>
<b>REFERENCES</b> -----	<b>74</b>
<b>LIST OF PUBLICATIONS</b> -----	<b>89</b>
<b>LIST OF PRESENTATIONS</b> -----	<b>90</b>
<b>SUBSTANTIAL FRENCH SUMMARY</b> -----	<b>91</b>
<b>FRENCH ABSTRACT</b> -----	<b>108</b>



## Abbreviations

$\alpha$ -MEM	- $\alpha$ -Minimum Essential Media
AA	-ascorbic acid
A-M-P	- 2-amino-2-methyl-1-propanol
AP	-alkaline phosphatase
APS	- Ammonium persulfate
AR-S	-alizarin Red-S
ATPase	-adenosine triphosphatase
$\beta$ -GP	- $\beta$ -glycerophosphate
bis- <i>p</i> -NPP	-bis- <i>p</i> -nitrophenyl phosphate
BCA	-bisinchoninic acid assay
Cat	-Cathepsin
CatK	-Cathepsin K
CKI	-Cathepsin K inhibitor
CPC	- Cetylpyridinium Chloride
DMEM	-Dulbecco modified Eagles medium
DMSO	-Dimethyl Sulphoxide
DTT	-DL-Dithiothreitol
E-64	-commercial cathepsin inhibitors
ePP <sub>i</sub>	-extracellular pyrophosphate
EDTA	-Ethylene Diamine Tetraacetic Acid
FBS	-fetal bovine serum
FTIR	-Fourier transformed infrared spectroscopy
G-1-P	-glucose-1-phosphate

HA	-hydroxyapatite
HEPES	-2-[4-(2-Hydroxyethyl)-1-piperazinyl]ethanesulfonic acid solution
IC <sub>50</sub>	-concentration to inhibit half the enzymatic activity
IR	-infrared spectroscopy
K <sub>m</sub>	-Michaelis-Menten constant
K <sub>i</sub>	-Inhibition constant
M-CSF	-Macrophage Colony Stimulating Factor
MMP	-matrix metalloprotease
MTT	-3-(4,5-dimethylthiazol-2-yl)-2,5-diphenyltetrazolium bromide
MVs	-matrix vesicles
NADP	-Nicotinamide Adenine Dinucleotide Phosphate
NPP1	-nucleoside triphosphate pyrophosphatase phosphodiesterase 1
OA	-Osteoarthritis
OB	-Osteoblast
OC	-Osteoclast
ODN	-Odanacatib, inhibitor of cathepsin K (actually at clinical phase III for the treatment of osteoporosis)
OP	-Osteoporosis
PAGE	-polyacrylamide gel electrophoresis
PBS	-phosphate-buffered saline
<i>p</i> -NPP	- <i>p</i> -nitrophenyl phosphate
P <sub>i</sub>	-inorganic phosphate
PP <sub>i</sub>	-inorganic pyrophosphate
RANK-L	-Receptor Activator for Nuclear Factor- $\kappa$ B Ligand
SCL	-synthetic cartilage lymph

SDS	-sodium dodecyl sulfate
SEM	-standard error of the mean
TES	-N-Tris(hydroxymethyl)methyl-2-aminoethane sulfonic acid
Tris	-Tris-(hydroxymethyl) aminomethane
TNAP	-tissue non-specific alkaline phosphatase
TRAP	-Tartrate-resistant acid phosphatase
v/v	-volume/volume
w/v	-weight/volume

## **CHAPTER I**

### **INTRODUCTION**

## **1. Bone Metabolism**

Bone is a dynamic organ, which consists of an abundant calcified extracellular matrix that makes up the skeleton. The skeleton can support, maintain and protect the vital tissue and organs in our bodies [1]. Bone is also a constantly changing tissue which carries out several metabolic functions, such as: mineral reservoir [2-4], cytokine-induced inflammation [5] resorption and formation of bone matrix. Bone cells and their progenitors control bone remodeling. The bone remodeling is a recycling process where the old bone tissue or damaged tissue is removed from the bone surface and the new bone matrix is deposited subsequently. Three consecutive phases participate in the cycle of remodeling process: resorption, where the bone is resorbed, then the trabecular bone is repaired and the accumulation of old matrix in microarchitecture changes is removed [6].

## **2. Bone Resorption and Formation**

In bone, there are three major cell types which are osteoclasts, osteoblasts and osteocytes. Bone resorption is generated by mature osteoclasts which require multiple sequential process [7-9], that consists in six steps: firstly, the mature osteoclast adheres to the bone matrix surface; then a special sealing zone is formed; the third step is the activations of the proton and chloride channels of osteoclasts, forming a local acidic environment in the bone resorption lacuna (sealing zone); the fourth step is the dissolution of old minerals by acidification; following by a skeletal organic matrix degradation and the last step is the migration of mature osteoclasts to another resorption site [10]. Bone formation is generated by osteoblasts [11] which are activated by osteoclasts once the bone resorption step was completed [12] (Fig. 1). Both bone resorption and formation are also regulated by osteocytes which includes osteoclastic resorption in the regulation of bone mass and architecture and osteoblastic mineralization to form primary new bone.

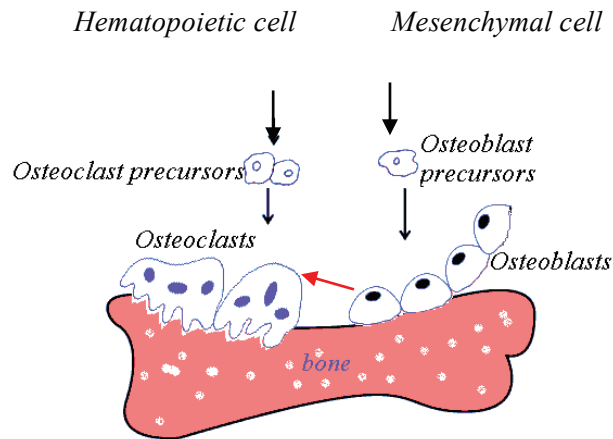


Figure 1. Actions of osteoblasts and osteoclasts during the resorption and formation of bone

### 3. Communications between osteoclast and osteoblast

Osteoblasts (Ob) derive from bone marrow stromal cells (BMSC) which are also known as mesenchymal stem cells (MSC). (Fig. 1). They are responsible for bone inorganic compound synthesis (mainly hydroxyapatite) and the organic matrix generation. In osteoblasts, parathyroid hormone receptor when stimulated by parathyroid hormone (PTH) activates the production of receptor activator of nuclear factor kappa-B ligand (RANKL). Osteoclasts are developed by fusion of monocytes that originate from hematopoietic stem cells. Hematopoietic cell precursors stimulated by macrophage colony stimulating factor (M-CSF) give rise to osteoclasts that express RANK receptor. The RANKL/RANK interaction (Fig.1 red arrow process ) stimulates the differentiation of osteoclasts so that they can resorb bone. Mature osteoclasts are large, multi-nuclear cells. Osteocytes are thought to be one if not the major bone cell type responsible for sensing mechanical strain and orchestrating signals of resorption and formation. Evidence suggests that the primary function of the osteocyte relates to the determination and maintenance of bone structure.

### 4. Cathepsin K is necessary for bone resorption by Osteoclast

In healthy skeletal bone, an equal balance of new bone matrix formation and old bone matrix resorption is achieved via the coordinated activity of bone-degrading osteoclasts and bone-forming osteoblasts [13,14]. To degrade bone, osteoclasts must first create a resorption pit. Osteoclasts do this by forming large arrays of multiple F-actin-rich cell-matrix adhesion structures, called podosomes, which create a basolateral sealing zone on the bone surface.

This allows the osteoclast to control bone degradation by the rapid assembly or disassembly of podosomes in response to intracellular signaling generated via the Rho family of GTPases<sup>10</sup> and Src family of kinases [15]. Once the resorption pit is formed, enzymes such as the cysteine protease, cathepsin K, are secreted to facilitate the localized degradation of the underlying bone; cathepsin K is the only mammalian protease having the ability to cleave the helical and non-helical type-I collagen fibers in mineralized bone [16]. Both the acidic microenvironment and activity of cathepsin K contribute to the bone resorption process. Cathepsin K exhibits about 60% amino acid sequence identity with cathepsin S but is distinct by its tissue expression profile and substrate specificity. Cathepsin K is predominantly found in osteoclasts. To lesser levels, it is also expressed in ovary, heart and skeletal muscle, lung, placenta, testis, small intestine and colon [17]. Cathepsins K are also expressed in hypertrophied chondrocytes. Everts et al. demonstrated that E64 and leupeptin, both inhibitors of papain-like cathepsins, were able to inhibit bone resorption in osteoclast cell assays [18] suggesting the involvement of cysteine protease in osteoclast-mediated bone resorption. Random sequence analyses of expressed sequence tag (EST) clones estimated that approximately 4% of the cDNA of an osteoclast derives a library encoded cathepsin K and that 98% of the total cysteine protease ESTs were cathepsin K [19]. The importance of cathepsin K in osteoclast-mediated resorption of the bone matrix provides a rationale for the design of inhibitors of cathepsin K as potential drugs for the treatment of diseases of excess bone remodeling such as osteoporosis.

## **5. Inhibition of Cathepsin K for the treatment of Osteoporosis and Osteoarthritis**

Osteoporosis, the sixth most common disease in the world is a socioeconomic threat [20, 21]. Osteoporosis is characterized by bone loss and microstructural deterioration that results in skeletal fragility and an increased risk in bone fractures. Detailed knowledge of bone biology [22] with molecular insights into the communication between bone-forming osteoblasts and bone-resorbing osteoclasts, as well as the signaling networks involved, has led to the identification of several therapeutic targets. Presently, a broad range of drug therapeutics is available to treat bone loss although none of them are able to completely prevent osteoporotic fractures. Besides hormone replacement therapy (HRT), common treatment regimes for osteoporosis include the use of bisphosphonates, calcitonin, calcium, and vitamin D supplements. All present pharmaceutical agents for the treatment of

osteoporosis have shortcomings in either their general efficacy, their mode of application, and various side effects. Thus the urge for more effective and safe anti-osteoporotic drugs remains high [23]. Osteoarthritis (OA) is much more prevalent and common in old age. Early signs of OA include progressive loss of proteoglycans, especially aggrecan, from articular cartilage, excessive damage to type II collagen, and general degeneration of the cartilage surface, resulting eventually in a loss of articular cartilage [23,24]. OA affects approximately 80% of people over the age of 65 but it is rare under 45. The number of people with OA is rising as the population ages whereas there is essentially no pharmaceutical intervention for OA available.

Not only the cysteine protease cathepsin K can also cleave the triple helix of types I and II collagens but cathepsin K is also capable of degrading other matrix molecules of hyaline cartilage, such as aggrecan and link protein 11 [25]. This would suggest that up regulation of cathepsin K might contribute to the degradation of cartilage. Therefore, the prevention of cartilage degradation by cathepsin K inhibition may represent a valid strategy for pharmacological intervention in OA [26].

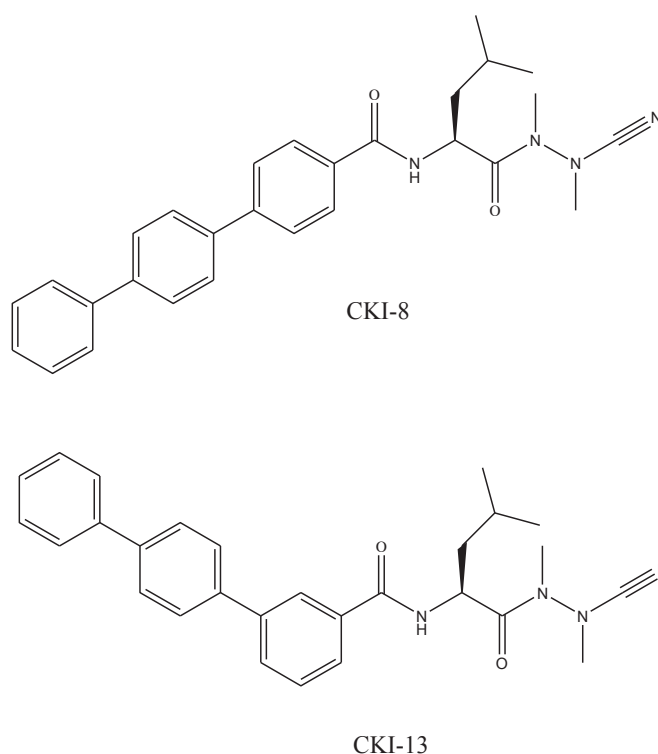
## **6. Cathepsin K inhibitors**

One of the most promising drug treatments for osteoporosis so far is based on the specific inhibition of the osteoclast protease cathepsin K (CatK) in order to slow down bone resorption [27,28]. CatK is a collagenase and the predominant papain-like cysteine protease expressed in osteoclasts, which has been recognized as an attractive target for antiresorptive osteoporosis therapy [28-30]. Considerable effort has been put into developing highly selective and orally applicable CatK inhibitors (**CKI**) [29]. Four **CKIs**, Balicatib, Relacatib, Odanacatib (ODN) and MIV-711 have been evaluated as possible drug therapies to prevent bone resorption [31, 32]: MIV-711 has been evaluated successfully in a phase I of clinical research for the treatment of osteoarthritis and other bone related disorders. Only ODN has presently reached phase three of clinical research [33, 34]. Although developed as antiresorptive agents, several compounds also show lysosomotropic effects [35], cutaneous adverse effects and anabolic activity [36], which are intrinsically related to the selectivity of inhibitors toward CatK. Therefore, alternative compounds having better selectivity toward CatK may complement the use of **CKIs** in bone resorption therapy. Typically, **CKIs** are mainly derived from peptides or peptidomimetic structures, which

generally contain electrophilic entities prone to covalently interact with the cysteine-thiol moiety in enzymes. With the rapid development of powerful and selective inhibitors for CatK, azapeptide nitriles have attracted much attention due to their extremely potent inhibition albeit with a relatively low selectivity [37-40].

Among these, proteolytically stable azadipeptide nitriles have been developed, [41] having picomolar  $K_i$  towards the therapeutically relevant cathepsins B, K, L and S with which they form reversible isothiosemicarbazide adducts [42,43]. Recently, we synthesized two series of candidate azanitrile inhibitors that were selected for their inhibition against human CatK activity *in vitro* [42,43]. One inhibitor (**CKI-13**,  $IC_{50} = 0.006 \text{ nM}$ ) from the first group, resulted in a picomolar  $K_i$  with remarkable selectivity over the cathepsins B and S (Scheme 1 and Table 1).

#### SCHEME 1



Chemical structures of cathepsin K inhibitors **CK-8** and **CK-13**

The other inhibitor (**CKI-8**,  $IC_{50} = 0.263 \text{ nM}$ , an isomer of **CKI-13**) (Scheme 1 and Table 1) from the second group, led to further improvement in the cathepsin K selectivity. These azanitriles inhibit cysteine proteases by forming a reversible thioimidate adduct resulting from the nucleophilic attack of a thiol on the carbon-nitrogen triple bond.

Table 1. The  $K_i$  values were calculated from the corresponding  $IC_{50}$  by using the equation  $K_i=IC_{50}/(1+[S]/K_m)$ .

Compounds	$K_i$ (nM)			
	Cat K	Cat B	Cat L	Cat S
CKI-8	0.124	0.692	0.262	1.54
CKI-13	0.0031	3.15	0.031	3.29

## 7. Biomarker of bone formation in Osteoblast: Alkaline phosphatases

The osteoblasts are enriched in tissue non-specific alkaline phosphatase (TNAP) which hydrolyzes inorganic pyrophosphate, an inhibitor of hydroxyapatite formation. Crystalline hydroxyapatite  $[Ca_{10}(PO_4)_6(OH)_2]$  is the major mineral component of bone inorganic matrix. Alkaline phosphatase (AP) (EC 3.1.3.1) catalyzes the hydrolysis of almost any phosphoesters to give inorganic phosphate and the corresponding alcohol [44]. There are four human isozymes, among them three are tissue specific : intestinal (IAP), placental (PLAP) and germ cell (GCAP) and one is tissue non-specific (TNAP). Osteoblasts and chondrocytes are cells which can mineralize and both are enriched in TNAP. TNAP activity is often used as a biochemical marker in bone [45-47]. TNAP is an ubiquitous enzyme expressed at high levels in bone, liver, and kidney [48]. Transgenic mice whose phenotypes show pathologic calcification strongly support the hypothesis that the level of extracellular pyrophosphate ( $ePP_i$ ), a TNAP substrate, regulates crystal deposition both physiologically and pathologically [49,50].  $ePP_i$  is an inhibitor of hydroxyapatite (HA) formation. Under physiological conditions HA is formed in bones, while under pathological conditions HA is accumulated in arteries (vascular calcification), in ligaments or tendons (ankylosing spondylitis) as well as in cartilage (osteoarthritis). There are three key enzymes that are central regulators of  $ePP_i$ , i.e. TNAP [51] which hydrolyzes  $ePP_i$ , the progressive ankylosis enzyme, (a  $PP_i$  transporter ANK) [52,53], contributing to the increase in  $ePP_i$  level, and the extracellular nucleotide pyrophosphatase/phosphodiesterase-1 (NPP1) which generates  $ePP_i$  from extracellular nucleotide triphosphates [54]. TNAP which hydrolyzes  $ePP_i$  is considered as an enzyme antagonistic to ANK and NPP1. The key role of TNAP in skeletal mineralization has been substantiated in the case of human hypophosphatasia, a rare heritable form of rickets, caused by mutations in the gene encoding TNAP which lead to defective TNAP activity and bone

formation [55,56]. High ePP<sub>i</sub> concentration persisting especially when TNAP activity is low, can inhibit HA formation leading to rickets or osteomalacia [55,56]. ePP<sub>i</sub> deficiency caused by the loss of NPP1 activity can lead to ectopic HA arterial calcification of the kind occurring in generalized arterial calcification of infancy (GACI) [57,58]. A loss of function ANK, causing ePP<sub>i</sub> deficiency, was described in the case of craniometaphyseal dysplasia, where excessive growth of craniofacial bones occurs [54]. High TNAP activity, leading to low ePP<sub>i</sub> concentration, as observed in the case of vascular calcification and in osteoarthritis cartilage, can lead to HA deposition in arteries or in cartilage respectively. Therefore, TNAP as well as ANK and NPP1 can be considered as attractive drug targets for the treatment of calcification disorders [59]. The search of inhibitors or activators of ANK, NPP1 or TNAP can lead to therapeutic treatment of mineralization disorders as well to novel molecules for determining their roles in ePP<sub>i</sub> homeostasis. So far, the screening of TNAP inhibitors has relied on the determination of the recombinant TNAP activity using para-nitrophenylphosphate (p-NPP) [60] as TNAP non-natural substrate. TNAP inhibitors selected under such conditions may act differently on the living cells. Therefore, there is a strong demand for flexible, fast and cost-effective strategies to select inhibitors with improved prospects for clinical success [61].

## **8. State of art of phosphatase activity assays**

Most of assays for measuring ePP<sub>i</sub> are based on coupled enzyme assays monitoring NADPH [62], NADH [63,64], luciferase [65-71] 2-amino-6-mercapto-7-methylpurine [72, 73] or luminol [74]. Additional controls are required to take into account competitive activities and to maintain saturated concentrations of substrates for optimal activity measurements. Direct colorimetric methods to measure hydrolytic activity of ePP<sub>i</sub> were recently developed. Malachite green to detect inorganic phosphate was successfully used as a fully automated high throughput screening assay for pyrophosphate and phosphate release from enzymes [75]. Zn (II) and Cd (II) coumarin-derivative complexes could serve as a turn on and turn off assay for monitoring pyrophosphate hydrolytic activity of alkaline phosphatase [76]. Pyrophosphate anion in an acidic acetonitrile-water solution form yellow  $[(P_2O_7)Mo_{18}O_{54}]^{4-}$  allowing its titration [77]. None of these methods measures protein content, P<sub>i</sub> or substrate concentrations simultaneously, allowing direct kinetic determinations in cells in a single assay.

So far, IR spectroscopy [78-80] is able to detect protein concentration, secondary structure and to measure enzymatic activity. It has been successfully employed to monitor

activities of alkaline phosphatase [81], amidase [82,83]  $\alpha$ -amylase [84,85], amyloglucosidase [86],  $\text{Ca}^{2+}$ ATPase [87-89], creatine kinase [90], diisopropylfluorophosphatase [91], b-fructofuranosidase [92, 93], fructose 1,6 biphosphatase [94], glucose oxidase [95], glutamic pyruvic transaminase [96], blactamase [97], oxalate decarboxylase [98], urease [99] and phopholipases [100-102]. IR can identify specific finger-like signatures in microbial cells [103-107] tumor cells [108-110] or in tissues [108] giving information on biochemical cell composition or changes induced by anti-tumor drugs in cells [111-122]. Combination of metabolic fingerprinting spectra obtained by infrared spectroscopy and multivariate statistical analyses [123-125] as well as infrared micro-spectroscopy to monitor cell biological processes of live or fixed cells have been employed successfully [126-128]. Activities of alkaline phosphatase in aqueous buffer [81] or in sera [130] have been determined by IR, suggesting the possibility of using this method for quantitative determination of a specific enzymatic activity in whole cells by IR in one single assay.

## **CHAPTER II**

### **AIMS**

## Context of the Ph D thesis

The Ph D thesis was directed under the Co-supervision of Prof. Yuqin WU (Jilin University) and of Dr. Saida MEBAREK and Prof. René BUCHET (University Lyon 1). Half part of my work was done at Jilin University, while the other half was performed at university Lyon 1. Due to specific regulations requested by the doctoral schools at Jilin University and of University Lyon 1 (Ecole Doctorale Interdisciplinaire Sciences et Santé EDISS), the whole Ph D thesis is written in Chinese and in English with a substantial French abstract. My Ph D thesis is centered on three distinct topics.

The first one is centered on the effects of azadipeptide nitrile cathepsin K inhibitors (**CKIs**) on bone formation mediated by osteoblasts and on bone resorption controlled by osteoclasts. I synthesized the cathepsin K inhibitors as it has been reported in the experimental part. However the organic synthesis has been published [42,43], therefore I did not include the organic synthesis of **CKIs** in the Result section.

The second part of my Ph D thesis is focused on the development of an alkaline phosphatase activity assay in matrix vesicles by infrared spectroscopy.

The third part is the extension of the infrared assay of the kinetics of phosphate-release from natural substrates in living cells. This allowed us to determine in a continuously manner the alkaline phosphatase activity by infrared spectroscopy under physiological condition and in cellular medium. This method could be used for screening inhibitors of alkaline phosphatase, a biological marker of mineral formation. Below are the detailed three specific aims which formed the basis of my thesis.

### 1. Effects of Cat K inhibitors on mineralization and bone resorption

In order to provide a proof of concept of the potential use of our **CKIs** [42,43] in drug treatments for osteoporosis, as well as to consolidate the efficiency/biological evaluation of these compounds, prior to preclinical trials, we compared the effects of two inhibitors, **CKI-8** and **CKI-13 (scheme 1)** with those of the commercial inhibitor **E64** on cell viability, osteoblast-induced mineralization and osteoclast-induced bone resorption.

The objective is to determine whether **CKIs** (**CKI-8** and **CKI-13**) can affect mineralization using osteoblast cells and to evaluate their bone resorption ability on osteoclasts. Cell viability assay is performed on osteoblasts and on osteoclasts to check the

toxicity of **CKIs** before mineralization and resorption treatment. The effect of **CKIs** on mineralization is evaluated on osteoblasts (human osteoblast-like Saos-2 cells and primary osteoblast from murine calvaria) which underwent the entire osteoblastic differentiation program from proliferation to mineralization. Mineralization is monitored by detecting calcium nodules with Alizarin Red-S and by measuring TNAP activity. Inhibition of Cat K in osteoclast-derived intracellular medium is evaluated by a gelatin zymography method, which could be used as a screening test of inhibitors before checking their effects on bone resorption. Bone resorption assay was assayed on the surface of an inorganic crystal coating surface (Corning Bone assay surface) and on bovine bone slices. Resorption pit area per osteoclast was measured to determine the effects of Cat K inhibitors. The overall findings of the regulating effect of cat K inhibitors were presented in Chapter IV (part I).

## **2. Development of a new Infrared assay to monitor pyrophosphate hydrolysis by Matrix Vesicles**

Tissue non specific alkaline phosphatase (TNAP) hydrolyses pyrophosphate ( $PP_i$ ) and is an inhibitor of hydroxyapatite (HA) formation. Inorganic phosphate ( $P_i$ )/ $PP_i$  ratio is a key factor determining the mineralization efficiency. A  $P_i/PP_i$  ratio greater than 140 leads to the formation of HA, while a ratio less than 70 inhibited completely HA formation. A  $P_i/PP_i$  ratio below 6 leads to the formation of calcium pyrophosphate dehydrate (CPPD), characteristic for CPPD pathological mineralization in osteoarthritis cartilage [130]. Therefore, a decrease in  $PP_i$  concentration, due to high TNAP activity, will induce HA mineralization.

Since TNAP as well as other enzymes were enriched in MVs implicated in the mineralization, the MVs will be used as a primary source of TNAP to test its activity. Our aim is to develop a direct determination of  $ePP_i$  hydrolytic activity in matrix vesicles under physiological conditions. Matrix vesicles (MV), secreted from hypertrophied chondrocytes, mature osteoblasts or mineral competent cells, are enriched in TNAP and thought to facilitate the first step of HA formation. Up to now, most of standard methods for measuring TNAP activity is based from the hydrolysis of colourless pNPP as a substrate at pH 10.4 leading to a colourful nitrophenolate. This part concerns the development of an infrared assay to determine directly the pyrophosphate hydrolysis by MVs that takes the advantage to use TNAP natural substrate,  $PP_i$ , under physiological pH. This IR assay served to test TNAP inhibitors under conditions optimal for physiological mineralization in MVs. The main findings were presented in Chapter IV (part II).

### **3. An infrared assay of the kinetics of phosphate-release from physiological substrates in living cells**

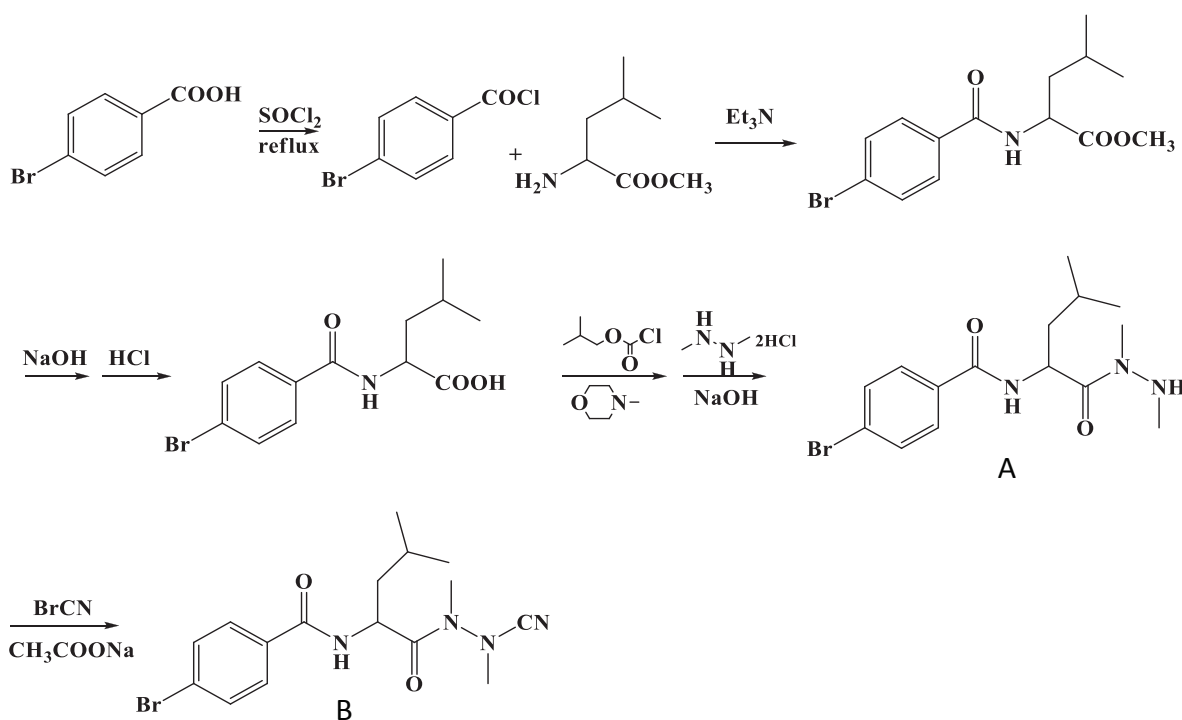
MVs are released from chondrocyte as well as from osteoblasts. Having demonstrated that the infrared assay can monitor phosphatase activity in MVs. Here, we developed a continuous infrared (IR) assay to determine phosphatase activity in Saos-2 cells and in primary osteoblasts from exogenous substrates such as  $PP_i$ , AMP, ADP, ATP, UTP,  $\beta$ -glycerophosphate or  $\alpha$ -D-glucose-1-phosphate and para-nitrophenylphosphate (pNPP). The IR assay can be employed as a cost-effective label-free approach to determine the phosphatase activity from extracellular physiological substrates in whole cells. It may serve to screen the phosphatase inhibitors in TNAP-enriched cells. An overview of the feasibility to determine the phosphatase activity in the different cellular models of TNAP-enriched is presented and discussed in Chapter IV (part III).

## **CHAPTER III**

### **MATERIALS AND METHODS**

## Organic synthesis:

The compounds CKI-8 and CKI-13 have been previously synthesized [42,43,131]. Here we present a short overview.



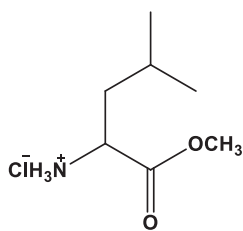
Scheme 2: Synthesis route for compounds A and B

### 4-bromobenzoyl chloride:



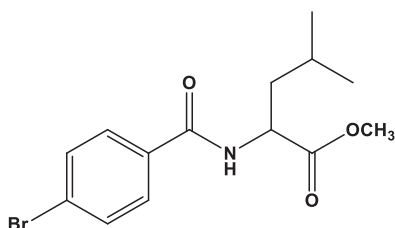
2.01 g 4-bromobenzoic acid (10 mmol) was added to a 50 mL round-bottomed flask equipped with a magnetic stir bar, 20 mL thionyl was then added. The mixture was stirred for 30 min, then it was heated at reflux for 60 min. After evaporation of the excessive thionyl, the solid residue was suspended in 30 mL cyclohexane for recrystallization. The mixture was heated at reflux for 30 min, then cooled slowly to room temperature and next to 0 °C in an ice bath. It was filtered through a fritted-glass funnel, the solid was washed with 15 mL cold cyclohexane and then dried under vacuum to afford 4-bromobenzoyl chloride as a white solid.

### L-leucine methyl ester hydrochloride:



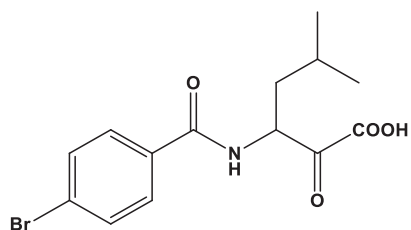
In an ice-bath, 5 mL thionyl was added drop wise under stirring to a 50 mL round-bottomed flask containing 30 mL anhydrous methanol. 10 min later 5 g L-leucine was added. After the mixture was stirred for 15 min in ice-bath, it was allowed to warm to room temperature and stirred for additional 30 min and then the mixture was heated at reflux for 60 min. The heated mixture was concentrated in a rotary evaporator to leave an oily residue, which was then suspended in 40 mL anhydrous ether. A white solid precipitated out and then was cooled to  $-20\text{ }^{\circ}\text{C}$  for 2 h, the mixture was filtered through a fritted-glass funnel and the solid was washed with 15 mL cold anhydrous ether and finally dried under vacuum to afford L-leucine methyl ester hydrochloride as a white solid.

#### **Methyl 2-(4-bromobenzamido)-4-methylpentanoate:**



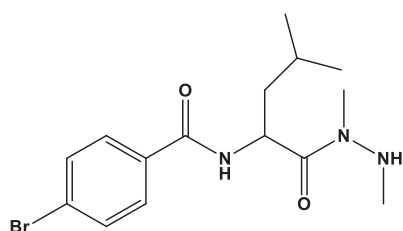
0.5 g sodium bicarbonate was dissolved in 20 mL water, and 1.82 g L-leucine methyl ester hydrochloride (10 mmol) was added under stirring. After 15 min, the solution was extracted with dichloromethane for four times (15 mL $\times$ 4). The combined organic layers were washed with H<sub>2</sub>O (2 $\times$ 15 mL), dried with Na<sub>2</sub>SO<sub>4</sub> and then concentrated in a rotary evaporator. 2.19 g 4-bromobenzoyl chloride (10 mmol) was added to the solution under ice-cooling and 1.40 mL anhydrous triethylamine was added drop wise. The mixture was stirred at  $0\text{ }^{\circ}\text{C}$  for 30 min, then it was allowed to warm to room temperature and stirred for additional 3 h. The mixture was washed with HCl (1 $\times$ 15 mL), saturated NaHCO<sub>3</sub> (1 $\times$ 15 mL), H<sub>2</sub>O (1 $\times$ 15 mL) and brine (1 $\times$ 15 mL) in turn. The solvent was dried by Na<sub>2</sub>SO<sub>4</sub> and then evaporated to obtain a white solid, then it was purified by column chromatography on silica gel with petroleum ether/ethyl acetate (1:1) as eluent to obtain methyl 2-(4-bromobenzamido)-4-methylpentanoate as white solid.

### 3-(4-bromobenzamido)-5-methyl-2-oxohexanoic acid:



3.42 g methyl 2-(4-bromobenzamido)-4-methylpentanoate (10 mmol) was dissolved in 15 mL THF, then 20 mL 1M NaOH was added under ice-cooling and then stirring was last for 3h. THF was removed in a rotary evaporator. The pH of the mixture was adjusted to 1-2, inducing a white solid precipitates. Then ethyl acetate was added to dissolve the precipitates, the organic layer was separated and the aqueous layer was extracted with ethyl acetate (15 mL×3). The combined organic phases were washed with brine twice (2×15 mL), then dried with Na<sub>2</sub>SO<sub>4</sub> and evaporated to obtain 3-(4-bromobenzamido)-5-methyl-2-oxohexanoic acid as a white solid.

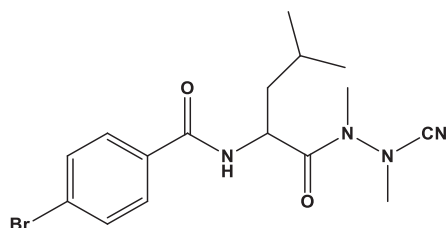
### 4-bromo-N-(1-(1, 2-dimethylhydrazinyl)-4-methyl-1-oxopentan-2-yl)benzamide:



3.56 g 3-(4-bromobenzamido)-5-methyl-2-oxohexanoic acid (10 mmol) was dissolved in THF (15 mL) and cooled to -25 °C. To the stirred solution, 1.11 mL N-methylmorpholine (10 mmol) and 1.32 mL isobutylchloroformate (10 mmol) were added consecutively. 2.66 g 1, 2-dimethylhydrazine dihydrochloride (20 mmol) was dissolved in 5 mL H<sub>2</sub>O, and 5 M NaOH (8 mL) was added under ice-cooling. When the precipitation of N-methylmorpholine hydrochloride occurred this solution was added to the reaction mixture. It was allowed to warm to room temperature within 30 min and stirred for additional 90 min. After evaporation of the solvent, the resulting aqueous residue was extracted with ethyl acetate (1×40 mL, 3×10 mL). The combined organic layers were washed with H<sub>2</sub>O (1×15 mL), saturated NaHCO<sub>3</sub> twice (2×15 mL), H<sub>2</sub>O (1×15 mL) and brine (1×15 mL) in turn. The solvent was dried with Na<sub>2</sub>SO<sub>4</sub> and evaporated to obtain colorless oil. It was purified by column chromatography on silica gel with petroleum ether/ethyl acetate (1:1) as eluent to obtain 4-bromo-N-(1-(1, 2-

dimethylhydrazinyl)-4-methyl-1-oxopentan-2-yl)benzamide as a colorless oil, which was then slowly solidified at room temperature.

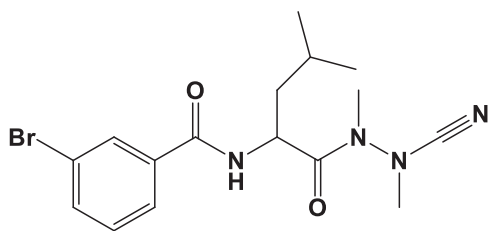
**4-bromo-N-(1-(2-cyano-1,2-dimethylhydrazinyl)-4-methyl-1-oxopentan-2-yl)benzamide**  
**(1)**



1.23 g sodium acetate (15 mmol) and 1.58 g cyanogen bromide (15 mmol) were added to a MeOH solution (20 mL) containing 1.78g (5 mmol) 4-bromo-N-(1-(1,2-dimethylhydrazinyl)-4-methyl-1-oxopentan-2-yl)benzamide. The mixture was stirred at room temperature for 5 h and then the solvent was removed under reduced pressure. The residue was suspended in 10 mL H<sub>2</sub>O, a pH of 1-2 was adjusted by using 10% KHSO<sub>4</sub>, and then it was extracted with ethyl acetate for three times (3×20 mL). The combined organic layers were washed with H<sub>2</sub>O (1×10 mL), sat. NaHCO<sub>3</sub> (2×10 mL) and brine (1×10 mL) in turn. The solvent was dried by Na<sub>2</sub>SO<sub>4</sub> and removed *in vacuo*. The oily residue was purified by column chromatography on silica gel using petroleum ether / ethyl acetate (2:1) as eluent. The obtained oil was dried in a desiccator at room temperature for several days to obtain 4-bromo-N-(1-(2-cyano-1,2-dimethylhydrazinyl)-4-methyl-1-oxopentan-2-yl)benzamide as a colorless solid.

<sup>1</sup>H NMR (500 MHz, CDCl<sub>3</sub>): δ 7.62 – 7.57 (m, 2H), 7.52 – 7.48 (m, 2H), 7.10 (d, J = 8.2 Hz, 1H), 5.30 – 5.23 (m, 1H), 3.37 (s, 3H), 3.26 (s, 3H), 1.88 – 1.80 (m, 1H), 1.78 – 1.58 (m, 2H), 1.04 (dd, J = 25.0, 6.6 Hz, 6H). <sup>13</sup>C NMR (500 MHz, CDCl<sub>3</sub>): δ 21.247, 23.264, 25.163, 30.576, 40.540, 40.958, 48.788, 113.515, 126.523, 128.734, 131.593, 166.747, 175.060. FT-IR (KBr, cm<sup>-1</sup>): 3268, 2960, 2936, 2872, 2222, 1708, 1660, 1590, 1542, 1482. MS (ESI) m/z: MH<sup>+</sup> 381.1, MNa<sup>+</sup> 402.9, MK<sup>+</sup> 418.9.

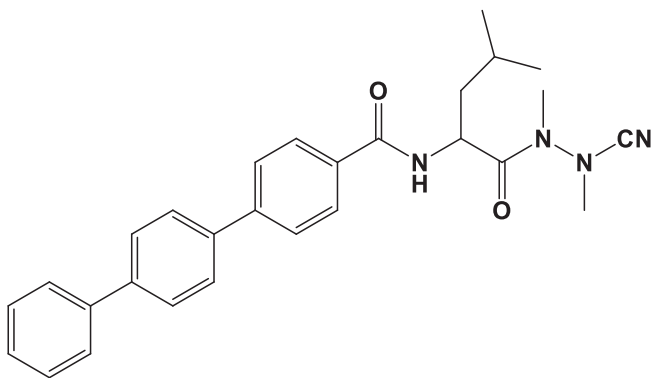
**3-bromo-N-(1-(2-cyano-1,2-dimethylhydrazinyl)-4-methyl-1-oxopentan-2-yl)benzamide**  
**(2)**



This compound was produced by using the similar procedures as for compound 1 but starting with 3-bromobenzoic acid instead of 4-bromobenzoic acid.

$^1\text{H}$  NMR (500 MHz, DMSO- $d_6$ ):  $\delta$  8.89 (d,  $J = 7.0$  Hz, 1H), 8.10 (s, 1H), 7.89 (d,  $J = 7.8$  Hz, 1H), 7.76 (d,  $J = 7.7$  Hz, 1H), 7.45 (t,  $J = 7.8$  Hz, 1H), 5.00 (s, 1H), 3.32 (d,  $J = 13.7$  Hz, 3H), 3.22 – 3.03 (m, 3H), 1.90 – 1.62 (m, 2H), 1.46 – 1.31 (m, 1H), 1.00 – 0.87 (m, 6H).  $^{13}\text{C}$  NMR (500 MHz,  $\text{CDCl}_3$ ):  $\delta$  21.287, 23.268, 25.133, 30.716, 40.527, 40.946, 48.727, 113.554, 122.501, 125.725, 129.914, 130.307, 134.513, 166.085, 175.362. FT-IR (KBr,  $\text{cm}^{-1}$ ): 3268, 2960, 2936, 2872, 2222, 1708, 1660, 1590, 1542, 1482. MS (ESI)  $m/z$ :  $\text{MH}^+$  381.1,  $\text{MNa}^+$  402.9,  $\text{MK}^+$  418.9.

**N-(1-(2-cyano-1,2-dimethylhydrazinyl)-4-methyl-1-oxopentan-2-yl)-4'-phenyl-biphenyl-4-carboxamide (CKI-8)**

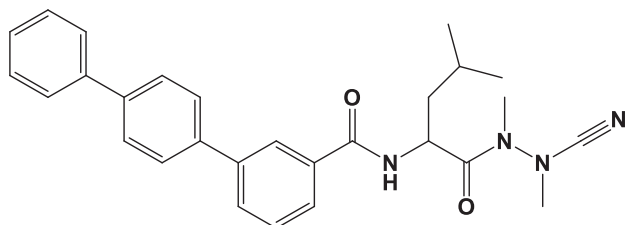


This compound was produced by using SUZUKI reaction in starting with compound 1 as maternal compound using biphenyl-4-ylboronic acid.

$^1\text{H}$  NMR (500 MHz,  $\text{CDCl}_3$ ):  $\delta$  7.91 (d,  $J = 8.1$  Hz, 2H), 7.76 – 7.71 (m, 6H), 7.67 (d,  $J = 7.5$  Hz, 2H), 7.50 (t,  $J = 7.5$  Hz, 2H), 7.41 (t,  $J = 7.3$  Hz, 1H), 6.61 (d,  $J = 8.4$  Hz, 1H), 5.38 (td,  $J = 10.0, 3.8$  Hz, 1H), 3.39 (s, 3H), 3.27 (s, 3H), 1.87 (s, 1H), 1.73 (ddd,  $J = 23.4, 21.8, 12.1$  Hz, 2H), 1.10 (dd,  $J = 28.6, 6.5$  Hz, 6H).  $^{13}\text{C}$  NMR (500 MHz,  $\text{CDCl}_3$ ):  $\delta$  21.502, 23.334, 25.167, 30.544, 41.051, 41.501, 48.265, 113.601, 127.083, 127.586, 127.667, 128.887, 132.200, 138.734, 140.454, 141.003, 144.187, 167.399, 174.617. FT-IR (KBr,  $\text{cm}^{-1}$ ): 3372,

2960, 2871, 2222, 1695, 1644, 1519, 1480, 1381. MS (ESI) m/z: MH<sup>+</sup> 455.5, MNa<sup>+</sup> 476.9, MK<sup>+</sup> 492.8.

**N-(1-(2-cyano-1,2-dimethylhydrazinyl)-4-methyl-1-oxopentan-2-yl)-4'-phenyl-biphenyl-3-carboxamide (CKI-13)**



This compound was produced by using the same procedure as for CKI-8 in starting with compound 2 as maternal compound using biphenyl-4-ylboronic acid.

<sup>1</sup>H NMR (500 MHz, CDCl<sub>3</sub>): δ 7.91 (d, J = 8.1 Hz, 2H), 7.76 – 7.71 (m, 6H), 7.67 (d, J = 7.5 Hz, 2H), 7.50 (t, J = 7.5 Hz, 2H), 7.41 (t, J = 7.3 Hz, 1H), 6.61 (d, J = 8.4 Hz, 1H), 5.39 (d, J = 6.5 Hz, 1H), 3.39 (s, 3H), 3.27 (s, 3H), 1.87 (s, 1H), 1.73 (ddd, J = 23.4, 21.8, 12.1 Hz, 2H), 1.10 (dd, J = 28.6, 6.5 Hz, 6H); <sup>13</sup>C NMR (500 MHz, CDCl<sub>3</sub>): δ 21.489, 23.337, 25.175, 30.554, 41.040, 41.414, 48.320, 113.162, 127.082, 127.585, 128.893, 132.182, 138.738, 140.452, 140.985, 144.160, 167.420, 174.670. FT-IR (KBr, cm<sup>-1</sup>): 3337, 2960, 2870, 2222, 1687, 1653, 1608, 1518, 1484; MS (ESI) m/z: MH<sup>+</sup> 455.5, MNa<sup>+</sup> 476.9, MK<sup>+</sup> 492.8.

## Cell cultures

All experiments were carried out according to the guidelines laid down by the French Ministère de l'Agriculture (n° 87-848) and the E.U. Council Directive for the Care and Use of Laboratory Animals of November 24th, 1986 (86/609/EEC). All efforts were made to minimize suffering. This study was specifically approved by the Committee on the Ethics of Animal Experiments of the INSA of Lyon CETIL (permit Number: 012012). The experiments were realized on euthanized animals (dislocation of cervical vertebra), which didn't require surgery and were not painful. Animal experiments were performed under the authorization n°69-266-0501 (INSA-Lyon, DDPP-SV, Direction Départementale de la Protection des Populations - Services Vétérinaires du Rhône), according to the guidelines laid down by the French Ministère de l'Agriculture (n° 87-848) and the E.U. Council Directive for the Care and

Use of Laboratory Animals of November 24th, 1986 (86/609/EEC). MLC (n°692661241), AG (n°69266332) and COS (n°69266257) hold special licenses to experiment on living vertebrates issued by the French Ministry of Agriculture and Veterinary Service Department. The preparation of primary cells were performed at INSA of Lyon, IMBL Building, 69100 Villeurbanne, France.

**1.** Primary osteoblast cells were enzymatically isolated from calvaria (frontal and parietal bones) of 5-6 day old mice (C57BL/6J strain). Calvaria were dissected aseptically and cells were isolated using sequential digestion at 37 °C with 0.05 % trypsin/ethylenediaminetetraacetic acid (EDTA) for 20 min and then with 0.8 U mL<sup>-1</sup> liberase for 20 min. The first two digestions were discarded, and the cells obtained after two digestions (each time incubated with 0.8 U mL<sup>-1</sup> liberase for 45 min) were collected, pooled and then filtered through a 100 µm-diameter-pore cell strainer. The cells were plated at a density of 100,000 cells/well in 12-well plates (Corning Inc) in Dulbecco modified Eagles medium (DMEM) containing 15% (mL/mL) fetal bovine serum (FBS), 100 U mL<sup>-1</sup> penicillin and 100 µg mL<sup>-1</sup> streptomycin, and 24 h later switched to DMEM containing 10 % FBS (mL/mL) supplemented with 50 g mL<sup>-1</sup> L-ascorbic acid (AA) for six days. They were then transferred to DMEM containing 10% FBS (mL/mL) supplemented with 50 g mL<sup>-1</sup> L-ascorbic acid (AA) [132, 133] with 0.1 % DMSO (mL/mL) and 7.5 mM β-glycerophosphate (β-GP) without (control) or with CKI at the indicated concentrations for one more week. AA and β-GP are two osteogenic factors commonly used to stimulate osteoblast differentiation and mineralization [132,133]. Cultures were maintained in a humidified atmosphere consisting of 95 % air and 5% CO<sub>2</sub> at 37 °C. Primary cell cultures were used without passage. Primary osteoblasts as prepared were used for the mineralization (calcium nodule detection) and TNAP activity assays.

**2.** Human osteosarcoma Saos-2 cells (ATCC HTB-85) were cultured in so-called growth medium consisting of Dulbecco modified Eagles medium DMEM (ATCC) supplemented with 100 U mL<sup>-1</sup> penicillin, 100 g mL<sup>-1</sup> streptomycin (both from Sigma) and 10 % FBS (mL/mL); Gibco), at 37 °C, in an atmosphere of 5 % CO<sub>2</sub> and 95% air. For the MTT test (3-(4,5-dimethylthiazol-2-yl)-2,5-diphenyltetrazolium bromide), Saos-2 cells were plated in 96-well culture plates at a cell density of 10,000 cells/well in growth medium supplemented with 0.1 % DMSO (mL/mL) , 50 µg mL<sup>-1</sup> AA and 7.5 mM β-GP for three days without (control) or with CKI at the indicated concentrations. For mineralization (calcium nodule detection) and TNAP assays, Saos-2 cells were plated in 12-well culture plates at a cell density of 100,000

cells/well in growth medium supplemented with 0.1 % DMSO (mL/mL) , 50  $\mu\text{g mL}^{-1}$  AA and 7.5 mM  $\beta$ -GP for eight days without (control) or with CKI at the indicated concentrations.

3. The transformed murine monocytic cell line RAW 264.7 (ATCC, Manassas, VA, USA) was cultured at 37 °C in 5 % CO<sub>2</sub> atmosphere in DMEM supplemented with 10 %FBS (mL/mL) and antibiotics (100 U mL<sup>-1</sup> penicillin and 100  $\mu\text{g mL}^{-1}$  streptomycin), so-called growth medium. For MTT tests, cells were plated in a 96-well plate at a density of 10,000 cells/well in growth medium containing 0.1 % DMSO (mL/mL), 20ng mL<sup>-1</sup> recombinant mouse receptor-activator of NF- $\kappa$ B ligand (mRANK-L), without (control) or with CKI at the indicated concentrations for three days. mRANK-L was produced in our facility (PAP; SFR Biosciences). For the conditioned medium used for zymography, cells were plated in a 6-well plate at a density of 350,000 cells/well in growth medium containing 20 ng mL<sup>-1</sup> mRANK-L for five days.

4. Primary osteoclasts from bone marrow cultures from posterior limbs were collected from 7-9 week-old mice (C57BL/6J strain). Cell suspensions were prepared by flushing bone marrow cells using complete medium ( $\alpha$ -MEM) (Invitrogen, Cergy Pontoise, France) supplemented with 10% FBS (mL/mL), 100 U mL<sup>-1</sup> penicillin, 100  $\mu\text{g mL}^{-1}$  streptomycin and 2 mM L-glutamine (Invitrogen)). Mononuclear cells isolated using lymphocyte separation medium (EuroBio, Courtaboeuf, France) were seeded at 37° C and 5 % CO<sub>2</sub> in complete  $\alpha$ -MEM medium supplemented with 30 ng mL<sup>-1</sup> mRANKL and 25 ng mL<sup>-1</sup> recombinant mouse macrophage-colony stimulating factor produced in our facility (PAP; SFR Biosciences), so-called differentiation medium. Bone marrow mononuclear cells from mice, were seeded at 350,000 cells/well, in 6-well plates, with a change of medium every second day, over five days. Once the cells were mature, they were ready for the MTT and bone resorption assays. For the MTT assay, mature cells were detached from the plastic plates using PBS with 25 mM EDTA. They were plated at a density of 10,000 cells/well in 96-well plates in differentiation medium containing 0.1 % DMSO (mL/mL) without (control) and with CKI at the indicated concentrations for three days.

### **Cell viability assay**

The viability of cultured cells (Saos-2 or RAW 264.7 cell lines or osteoclast primary cells) was measured using the MTT colorimetric assay (Roche Diagnostics, Meylan, France)

as described previously [134]. Briefly, cells were prepared as described above. Then the MTT labeling reagent ( $0.5 \text{ mg mL}^{-1}$  final concentration) was added to each well. The cells were further incubated for 4 h. 100  $\mu\text{l}$  of solubilization solution (10 % SDS g:mL in 0.01M HCl) were then added and plates were allowed to stand overnight at 37 °C in a humidified atmosphere. The absorbance was measured at 550 and 690 nm wavelengths using a Tecan Infinite M200 (Salzburg, Austria) micro-titer plate reader. Cell viability was directly related to the difference in absorbance measured at 550 and 690 nm. Results were normalized relative to their respective controls (without inhibitors) taken as 100. For each inhibitor/cell combination, three distinct sample pools were analyzed in a triplicate manner ( $n = 9$ ).

### **Calcium nodule detection**

Cell layers (Saos-2 cells or primary osteoblasts isolated from mouse calvaria) were washed with phosphate-buffered saline (PBS) (PAA) and stained with 0.5 % (g/mL) Alizarin Red-S (AR-S) (Sigma) in PBS (pH 5.0) for 30 min at room temperature. After washing four times with PBS to remove free calcium ions, cell cultures were destained with 3.6 % (g/mL) cetylpyridinium chloride (Sigma) in PBS pH 7.0 for 60 min at room temperature. The AR-S concentration was determined by measuring the absorbance at 562 nm [135].

### **Tissue-nonspecific alkaline phosphatase activity assay**

To determine tissue-nonspecific alkaline phosphatase (TNAP) activity, cells (Saos-2 cells or primary osteoblasts isolated from mouse calvaria) cultured in 6-well plates were harvested in 0.2 % (g/mL) Nonidet P-40 and disrupted by sonication. The homogenate was centrifuged at 1,500 g for 5 min, and TNAP activity in the supernatant was determined by measuring the absorbance at 405 nm in buffer (pH 10.4) containing A-M-P [136]. In the same lysates, the protein content was determined using a bicinchoninic acid (BCA) assay (Pierce) or Bradford (see below). Results are shown as  $\mu\text{mol para-nitrophenolphosphate (pNPP) min}^{-1} \text{mg protein}^{-1}$ .

### **Zymography of cathepsin K in cell lysates**

Zymography was performed as reported [137]. Briefly, a cell extraction buffer (20 mM Tris-HCl pH 7.5, 5 mM ethylene glycol tetraacetic acid (EGTA), 150 mM NaCl, 20 mM  $\beta$ -glycerol phosphate, 10 mM NaF, 1 mM sodium orthovanadate, 1 % (mL:mL) Triton X-100, and 0.1 % (mL:mL) Tween 20) was added to the cells (RAW 264.7 and primary mouse osteoclasts). Then lysates were collected and cleared. They contained CatK in extracellular medium and in cells. Protein concentrations were determined using the bicinchoninic acid (BCA) assay (Pierce). Five times (5 $\times$ ) no reducing loading buffer (0.05 % (g/mL) bromophenol blue, 10 % (g/mL) sodium dodecyl sulfate (SDS), 1.5 M Tris, and 50 % (mL/mL) glycerol) was added to all samples prior to loading. Equal amounts of protein were resolved by 12.5% SDS-polyacrylamide gels containing 0.2 % (g/mL) gelatin, a CatK substrate, at 4 °C. Gels were removed and washed in 65 mM Tris buffer (pH 7.4) with 20 % (mL/mL) glycerol for 10 min. The washing was repeated twice for 10 min each time. Gels were then incubated for 30 min at room temperature in activity buffer containing 100 mM sodium phosphate buffer pH 6.0, 1 mM EDTA and 2 mM dithiothreitol (DTT). Then this activity buffer was exchanged for fresh activity buffer containing 0.1% DMSO (mL/mL) without (control) or with CKI at the indicated concentrations for 24 h incubation at 37 °C. The gels were rinsed twice with deionized water and were incubated for 1 h in Coomassie stain (10 % mL/mL acetic acid, 25 % mL/mL isopropanol, and 4.5 % mL/mL Coomassie blue) to label the gelatin. This was followed by destaining (10 % mL/mL isopropanol and 10 % mL/mL acetic acid). Gels were scanned using a Canon scanner. Densitometry was performed using Image J software (developed by the National Institutes of Health), and the IC<sub>50</sub> values for **CKI-8** and **CKI-13** inhibition on human catK were calculated based on the results of gelatin zymography.

### **TRAP staining of RAW 264.7 cells and osteoclast primary cells**

To confirm the generation of multinucleated osteoclast cells, the cultured monocytic cell line RAW 264.7 cells and also osteoclast primary cells were stained for TRAP using the TRAP-staining kit (Sigma-Aldrich), according to the manufacturer's instructions. TRAP-positive multinucleated (3 or more nuclei) osteoclasts were visualized by light microscopy and photographed. Each osteoclast formation assay was performed independently at least 3 times.

## Resorption pit assay

Assessment of bone resorption per single osteoclast (resorption index) was performed as described [138]. Briefly, osteoclasts (RAW 264.7 cells and primary mouse osteoclasts), after 5 days of differentiation (see above for details), were detached from plastic plates using PBS 25 mM EDTA and replated on bovine bone slices at a density of 50,000 cells/well in 96-well plates or on a 96-well Corning Osteo Assay Surface plate at a density of 30,000 cells/well. They were treated during the entire experiment with 30 ng mL<sup>-1</sup> mRANKL and M-CSF at 25 ng mL<sup>-1</sup>, in the presence or absence of **CKI-8** and **CKI-13**. After 48 h, mature cell numbers were first determined by staining cells for TRAP using a leukocyte acid phosphatase kit. The cells were removed with water from the Osteo Corning plates and from the bone surface, then stained with 5 % (g/mL) silver nitrate solution to determine bone resorption. In the case of the bovine bone slices, osteoclasts were scraped from the slices using cotton buds, and slices were stained for 3 min with a 1 % (g/mL) toluidine solution. Images were acquired using a widefield microscope with side illumination, followed by quantitative analysis of the resorption area using Image J software 1.44p (NIH, USA). The results for each bone slice were expressed as the ratio of the area of resorption to the number of mature osteoclasts, and were normalized relative to their respective controls (without inhibitors), taken as 100 (corresponding to 3914 μm<sup>2</sup>/ osteoclast). For each inhibitor in the cells three distinct sample pools were analyzed in a duplicate manner (n = 6).

## Preparation of Matrix Vesicles

Matrix vesicles (MVs) were prepared according to Wuthier's methods [139]. Femurs from twenty 17-day-chicken embryos were taken. Slices (1-3 mm thick) of growth plates and epiphyseal cartilage were cut. They were washed five times in synthetic cartilage lymph (SCL) buffer containing 1.42 mM NaH<sub>2</sub>PO<sub>4</sub>·H<sub>2</sub>O, 1.83 mM NaHCO<sub>3</sub>, 12.7 mM KCl, 0.57 mM MgCl<sub>2</sub>, 5.55 mM D-glucose, 63.5 mM sucrose, 16.5 mM TES, 100 mM NaCl, 0.57 mM Na<sub>2</sub>SO<sub>4</sub>, pH 7.4. The slices were incubated at 37 °C for 180 min by mixing continuously in SCL buffer containing 200-500 units g<sup>-1</sup> tissue of type I collagenase from *Clostridium histolyticum* (Sigma) and 1 mM CaCl<sub>2</sub>·H<sub>2</sub>O. Then, it was filtered through a nylon filter. The filtrate was centrifuged at 600 g for 15 min at 4 °C. After the first centrifugation the debris

were discarded and the supernatant was centrifuged at 20 000 g for 20 min at 4 °C. A second centrifugation at 80 000g for 60 min at 4°C was then performed. The supernatant was discarded and the pellet was gently washed with 1 mL Tris HCL (100 mM, pH 8.0) containing 5 μM ZnCl<sub>2</sub> and 5 mM MgCl<sub>2</sub>. Washing medium was discarded and the intact pellet (around 0.05 mL) was suspended in 0-2 mL Tris HCL (100 mM, pH 8.0) containing 5 μM ZnCl<sub>2</sub> and 5 mM MgCl<sub>2</sub> (called throughout buffer A). The protein concentration in MVs was determined by Bradfords [140] was in the range of 0.2 to 8 mg MV protein mL<sup>-1</sup>. MVs were freshly prepared for the IR measurements.

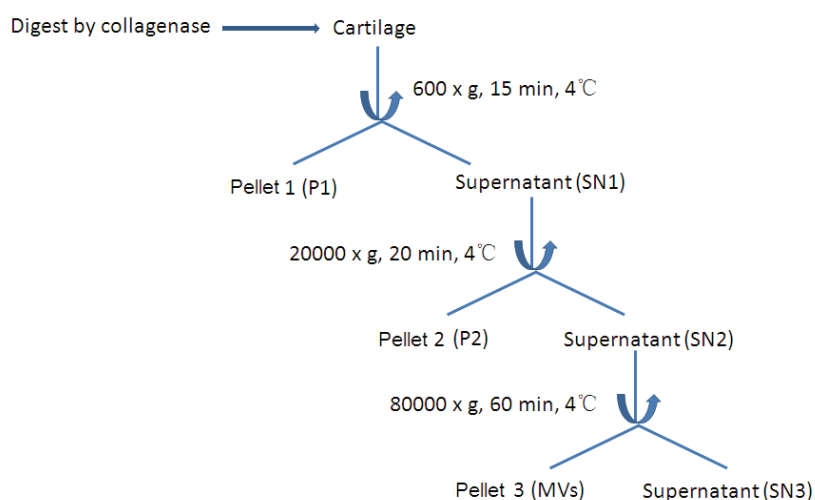


Figure 2. Steps of differential centrifugations for the in purification of matrix vesicles (MVs)

## SDS-PAGE Analysis

Proteins of each fraction were separated on 12 % (w:v) SDS-polyacrylamide gels [141]. Composition of the SDS-polyacrylamide gels are indicated in Table 2.

Table 2. Composition of gel electrophoresis

	Separated gel 12 %	Concentrated gel
Acrylamide 40%	1.5 mL	0.16 mL
Tris HCl pH=8.8	1.88 mL	
Tris HCl pH=6.8		0.2 mL
SDS 10%	50 μL	16 μL
H <sub>2</sub> O	1.54 mL	1.21mL
APS 10%	25 μL	20 μL
TEMED	2.5 μL	4 μL

## **Mineralization assay**

MVs provide a favorable environment for mineralization in the presence of calcium ions and phosphate ions by enrichment in alkaline phosphatase. UV-spectrophotometer was employed for real time measurement of mineral formation in MVs with the synthetic cartilage lymph (SCL) medium. [142,143]. The composition of SCL buffer pH=7.8 was 1.42 mM  $\text{NaH}_2\text{PO}_4 \cdot \text{H}_2\text{O}$ , 1.83 mM  $\text{NaHCO}_3$ , 12.7 mM KCl, 0.57 mM  $\text{MgCl}_2$ , 5.55 mM D-glucose, 63.5 mM succrose, 16.5 mM TES, 100mM NaCl, 0.57 mM  $\text{Na}_2\text{SO}_4$ . Three cuvettes with 1 mL solutions were prepared each containing 500  $\mu\text{L}$  of synthetic cartilage lymph (SCL).

One contains MVs (10  $\mu\text{L}$ ) with 2 mM  $\text{CaCl}_2$  and 3.42 mM  $\text{NaH}_2\text{PO}_4$  final concentrations, the second contains 2 mM  $\text{CaCl}_2$  and 3.42 mM  $\text{NaH}_2\text{PO}_4$  final concentrations without MVs and the third contains MVs at the same concentration but without  $\text{CaCl}_2$  and  $\text{NaH}_2\text{PO}_4$ . Mineralization is followed by measuring the turbidity at 340 nm at 37 ° C overnight by UV spectrophotometer.

## **Determination of protein concentration**

The protein content was determined using a Bradford assay [140]. Enzyme units are  $\mu\text{mol}$  of *p*-nitrophenolate released per min per mg of proteins. The amount of protein in the different fractions was determined by the Bradford method. This is a colorimetric method based on the adsorption of Coomassie blue R250 to the side chains of basic amino acid residues and hydrophobic proteins, forming a complex having a color absorption maximum at 595 nm. The absorbance change is proportional to the amount of dye fixed and therefore the amount of protein in the sample. To determine the amounts of protein in the different fractions, a reference range is made using increasing amounts of protein of known concentration, bovine serum albumin BSA 5 $\mu\text{g}/\mu\text{L}$  ( 0, 2, 4, 6, 8, 10, 15 mg). In parallel, 5  $\mu\text{L}$  of each fraction were prepared. Bradford reagent ( 200  $\mu\text{L}$ ) is added last at the same time in all tubes containing equal volumes of 800  $\mu\text{L}$  after adding water.

## **Infrared Spectra**

IR data were acquired with a Thermo Scientific Nicolet iS10 spectrometer equipped with a DTGS detector. The IR spectra were recorded with a thermostated cell kept at 37°C with

256 interferograms at  $4\text{ cm}^{-1}$  resolution each and Fourier transformed. During data acquisition, the spectrometer was continuously purged with dry filtered air (Balston regenerating desiccant dryer, model 75-45 12 VDC). At least three independent measurements have been performed to determine the nature of minerals and to obtain kinetics parameters.

### Identification of Mineral Complexes by Infrared Spectroscopy

From the mineralization assay, the formed minerals were centrifuged and washed two times with water, then dried under  $\text{N}_2$ . Dry material (0.5 mg) was put on a diamond ATR support. The infrared spectra were measured by the means of Thermo Scientific Nicolet iS10 spectrometer as stated above.

### Protein determination by infrared spectroscopy

To determine protein concentration, we measured the intensity of the amide I and II bands in the infrared spectra (Fig.3) [144].

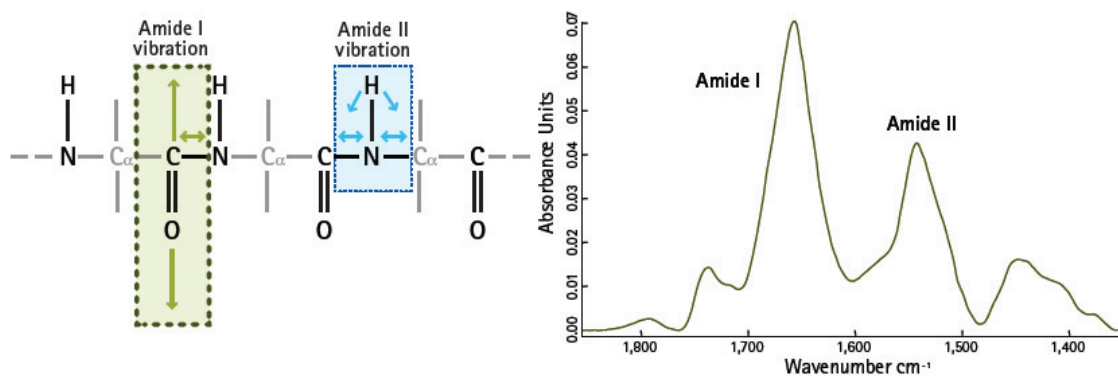


Figure 3. Part of the infrared spectrum indicating Amide I and Amide II bands of proteins in cells.

The IR spectra were recorded with a thermostated IR cell kept at  $37\text{ }^\circ\text{C}$  with 128 interferograms at  $4\text{ cm}^{-1}$  resolution each and then Fourier transformed. All measurements were performed by taking  $3\text{ }\mu\text{L}$  of sample solution, deposited between two  $\text{BaF}_2$  windows of a demountable thermostated cell (model Harrick) separated with a  $6\text{ }\mu\text{m}$ . A series of five concentrations of BSA from  $5\text{ mg mL}^{-1}$  to  $20\text{ mg mL}^{-1}$  served to as a calibration curve for

protein determination. Final protein concentrations in cells were determined directly by measuring the intensity of the amide-II band at  $1550\text{ cm}^{-1}$  using  $\epsilon_{\text{amide II}} = 3.6\text{ mg}^{-1}\text{ ml cm}^{-1}$ .

### **Phosphatase activity determination of matrix vesicles by infrared spectroscopy**

To start the enzymatic reaction, an aliquot of freshly prepared  $0.2$  to  $8\text{ mg MV mL}^{-1}$  was taken and mixed with the reaction mixture containing stock solution of  $100\text{ mM PP}_i$  in aqueous buffer  $100\text{ mM Tris-HCl}$ ,  $\text{pH } 8.0$ ,  $5\text{ }\mu\text{M de ZnCl}_2$  and  $5\text{ mM MgCl}_2$  so that final  $\text{PP}_i$  concentration was  $40$ - $60\text{ mM}$ . Final protein concentration in MVs was  $0.250$  to  $4\text{ mg MV protein mL}^{-1}$ . Three  $\mu\text{L}$  of reaction mixture containing MVs was taken and deposited between two ZnSe windows of a demountable thermostated cell (model Harrick) separated with a  $12\text{ }\mu\text{m}$  (for activity measurements) or with a  $6\text{ }\mu\text{m}$  spacer (for protein determination and activity measurements). Protein concentration was measured with the amide-II band using  $\epsilon_{\text{amideII}} = 3.6\text{ mg}^{-1}\text{ ml cm}^{-1}$ .  $\text{PP}_i$  band located at  $1107\text{ cm}^{-1}$  (Molar absorption coefficient =  $2158 \pm 211\text{ M}^{-1}\cdot\text{cm}^{-1}$ ) and  $\text{P}_i$  bands located at  $1076\text{ cm}^{-1}$  (Molar absorption coefficient =  $1346 \pm 116\text{ M}^{-1}\cdot\text{cm}^{-1}$ ) and at  $990\text{ cm}^{-1}$  (Molar absorption coefficient =  $493 \pm 49\text{ M}^{-1}\cdot\text{cm}^{-1}$ ) served to measure the substrate and the product concentrations. IR data were acquired with a Thermo Scientific Nicolet iS10 spectrometer equipped with a DTGS detector as specified above.

### **Phosphatase activity determination of osteoblasts by infrared spectroscopy**

To start the enzymatic reaction, an aliquot of either Saos-2 cells ( $6$  to  $28\text{ mg protein mL}^{-1}$ ) or primary osteoblast ( $20$  to  $45\text{ mg protein mL}^{-1}$ ) was taken and mixed with the reaction medium containing  $40$ - $80\text{ mM final PP}_i$  or one of other substrates (AMP, ADP, ATP, UTP, G-1-P,  $\beta$ -GP and  $p$ -NPP),  $5\text{ mM MgCl}_2$  and  $5\text{ }\mu\text{M ZnCl}_2$  in either DMEM (10% FBS) and  $100\text{ mM Tris-HCl}$  buffer  $\text{pH}= 7.8$ . Three  $\mu\text{L}$  of the reaction mixture containing either Saos-2 cells or primary osteoblast cells were taken and deposited between two BaF<sub>2</sub> windows of a demountable thermostated cell (model Harrick) separated with a  $12\text{ }\mu\text{m}$  (for IR spectra of substrates) or  $6\text{ }\mu\text{m}$  (for IR spectra of cells with substrates) Teflon spacer. Tissue non-specific alkaline phosphatase activity was assayed at  $37\text{ }^\circ\text{C}$  by recording absorbance from  $1300$  to  $900\text{ cm}^{-1}$  wavenumbers. Protein concentration was measured with the amide-II band using  $\epsilon_{\text{amide II}} = 3.6\text{ mg}^{-1}\text{ ml cm}^{-1}$ .  $\text{PP}_i$  band located at  $1107\text{ cm}^{-1}$  (Molar absorption coefficient =  $2158 \pm 211\text{ M}^{-1}\cdot\text{cm}^{-1}$ ) and  $\text{P}_i$  bands located at  $1076\text{ cm}^{-1}$  (Molar absorption coefficient =  $1346 \pm 116\text{ M}^{-1}\cdot\text{cm}^{-1}$ )

$^1.\text{cm}^{-1}$ ) and at  $990\text{ cm}^{-1}$  (Molar absorption coefficient =  $493 \pm 49\text{ M}^{-1}.\text{cm}^{-1}$ ) served to measure the substrate and the product concentrations. IR data were acquired with a Thermo Scientific Nicolet iS10 spectrometer equipped with a DTGS detector as specified above.

### **Statistics**

All data are presented as mean values  $\pm$  SEM (standard error of the mean). Differences between groups were assessed using the Mann-Whitney test, depending on their normal distribution. Results were considered statistically significant at p-values  $<0.05$  indicated by (\*) while  $p < 0.01$  is indicated by (\*\*) in all figures.

**CHAPTER IV**  
**RESULTS and DISCUSSION**

# 1 Effects of Azanitrile Cathepsin K Inhibitors on Mineralization and Bone Resorption

## Cytotoxicity of CKI-8 and CKI-13 on cells (colorimetric MTT assay for cell viability)

The cytotoxicity of **CKI-8** and **CKI-13** (Scheme 1) were tested on three distinct types of cells: human osteoblast-like Saos-2, the mouse monocyte cell line RAW 264.7 and the mature mouse primary osteoclast cells, using a MTT assay [134]. These tests were performed after the cells had been incubated without (control) or with the compounds for 3 days. **CKI-8** and **CKI-13** were not toxic in the concentration range of 0.1 to 1000 nM on osteoblast-like Saos-2 cells (Fig. 4a) and on RAW 264.7 cells (Fig. 4b).

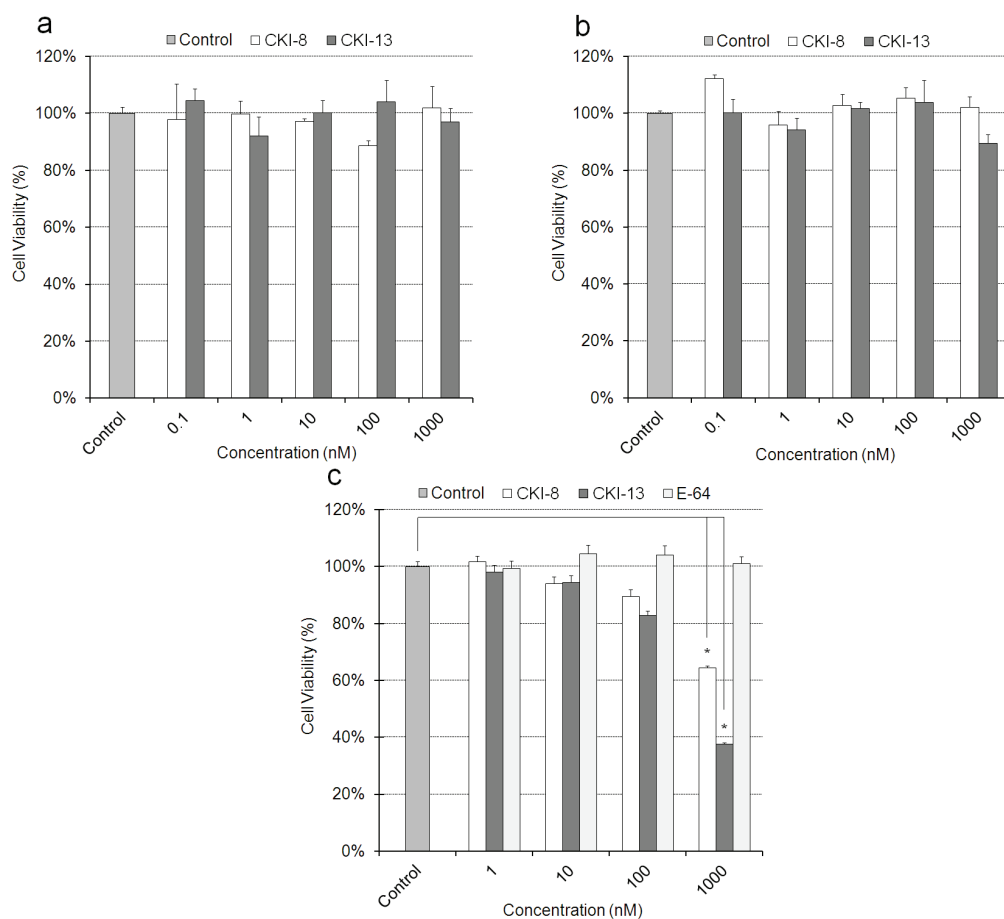


Figure 4. The two catK inhibitors are not cytotoxic. MTT test of **CKI-8** and **CKI-13** on **a)** osteoblast-like Saos-2 cells, **b)** RAW 264.7 and **c)** mature osteoclasts, respectively, at the indicated concentrations. After 3-day incubations with **CKI-8** and **CKI-13**, the compounds did not induce any significant toxicity on Saos-2 and RAW 264.7 cells up to 1000 nM, while they were not toxic on mature osteoclasts up to 100 nM. For comparison, commercial **E64** inhibitor was not toxic in primary osteoclast cells up to 1000 nM. Results are expressed as

percentage of control containing DMSO 0.1% (mL/mL) without inhibitor. DMSO 0.1 % (mL/mL) has no effect on cell toxicity. The experiments were repeated three times in triplicate for each inhibitor (n=9).

On mature mouse primary osteoclasts, there was no toxicity up to 100nM, while at 1000 nM, less than 40-60 % cells were viable (Fig. 4c). On the other hand, the commercial inhibitor **E64** was not toxic throughout this concentration range (Fig. 4c). The addition of 0.1 % (mL/mL) DMSO used to solubilize the inhibitors did not affect cell toxicity.

### **Differentiation and mineralization of osteoblast-like Saos-2 cells and primary mouse calvarial osteoblasts**

To check whether **CKI-8** and **CKI-13** could inhibit the mineralization process, human Saos-2 cells and mouse primary osteoblasts were selected as cell models to monitor mineralization. To stimulate mineralization, AA and  $\beta$ -GP, as osteogenic factors, were added [132,133,135]. The extent of AR-S staining was measured to quantify calcium nodules (Fig. 5a and b). As reported earlier [134], mineralization induced by Saos-2 cells was strongly enhanced by the combined addition of AA and  $\beta$ -GP in the cell cultures (Fig. 5b). We determined the effects of the inhibitors **CKI-8** and **CK-13** on the mineralization process induced by Saos-2 cells after stimulation (Fig 5c and d) and on primary osteoblasts (Fig 5e and f). As shown by AR-S staining, **CKI-13** significantly inhibited mineralization with Saos-2 cells at 10 and 100 nM concentrations to around 60 % of control, while **CKI-8** did not inhibit significantly, although there were slight variations (Fig. 5c). We then measured the effect of **CKI-8** and **CKI-13** on the activity of tissue-non-specific alkaline phosphatase (TNAP), a mineralization marker [136], in cells. **CKI-13** reduced TNAP activity significantly on Saos-2 cells at 1000 nM to 80 % of control (Fig. 5d), suggesting that **CKI-13** can slow down TNAP activity and mineralization. We determined the effects of both **CKI-8** and **CK-13** at concentrations ranging from 100 to 1000 nM in primary osteoblasts. AR-S staining did not indicate any significant effect of either **CKI-8** or **CK-13** on mineralization induced by primary cells (Fig. 5e). However, TNAP activity decreased from 100% (control) to 58 % of control using 100 nM **CK-13** (Fig. 5f). In contrast, **CKI-8** did not inhibit TNAP significantly, consistent with the AR-S staining results. In all cases, the addition of 0.1 % (v/v) DMSO to solubilize the inhibitors did not affect calcium nodule formation and TNAP activity. **CKI-13** could inhibit TNAP activity slightly in murine osteoblasts, as well as in human Saos-2 cells accompanied by a decrease in mineralization in murine osteoblasts but not in human Saos-2 cells.

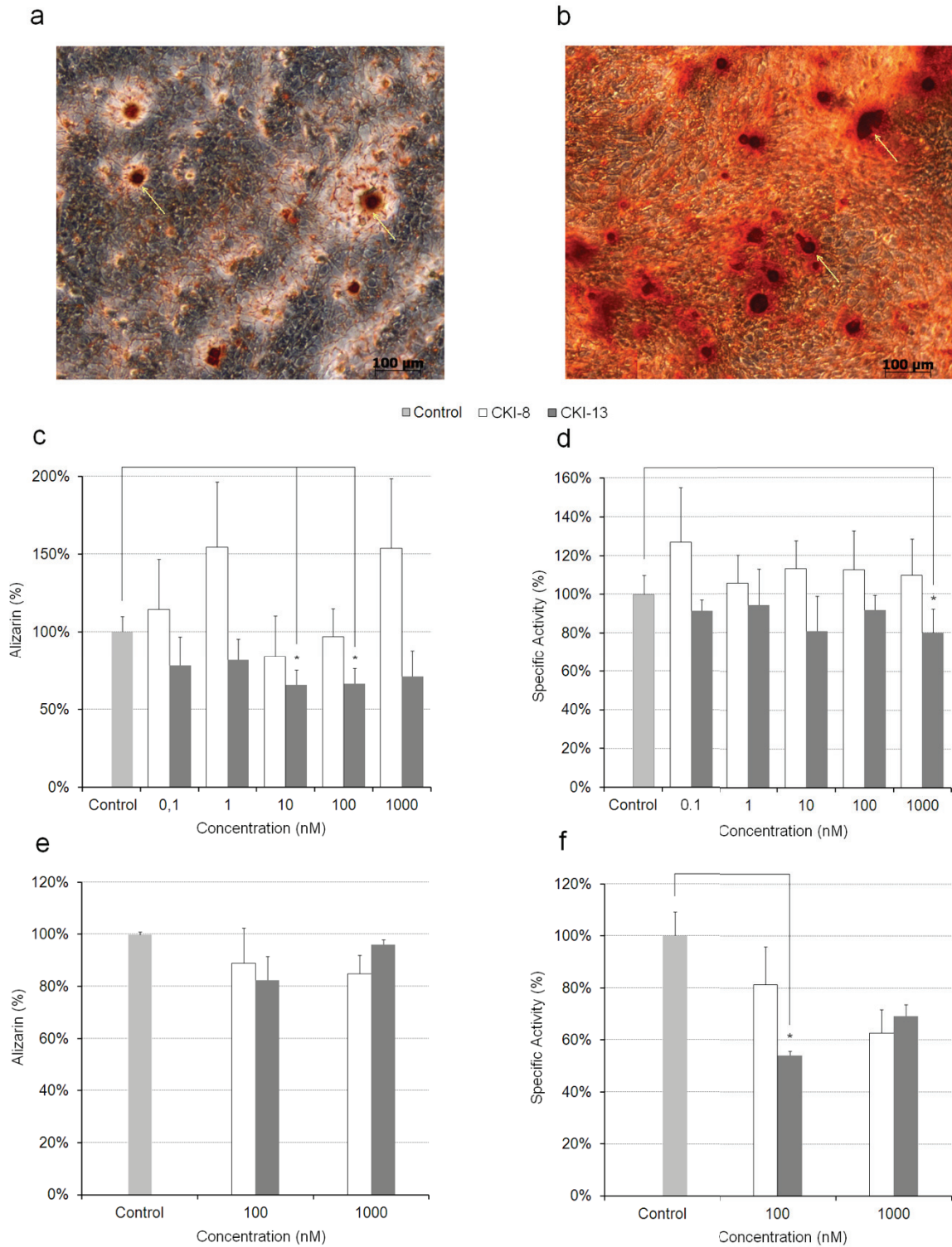


Figure 5. Effect of the two catK inhibitors on osteoblast-mediated mineralization. Saos-2 cells were incubated for 6 days without ((a) non-stimulated) or with 50  $\mu\text{g ml}^{-1}$  AA and 7.5 mM  $\beta\text{-GP}$  ((b) stimulated). Both sets of cells were stained with AR-S to detect the calcium nodules (the nodules are shown with a white arrow) and then were photographed. Effects of **CKI-8** and **CKI-13** on the mineralization process induced by osteoblast-like Saos-2 cells and primary osteoblasts as monitored c and e) by AR-S staining and by d and f) TNAP activity at

the indicated concentrations. Results are expressed as percentage of control containing DMSO 0.1% (mL/mL) without inhibitor. DMSO 0.1 % (mL/mL) has no effects on AR-S staining nor on TNAP activity. The experiments were repeated three times in triplicate for each inhibitor (n=9).

### **Gelatin zymography assay on cathepsin K activity in RAW 264.7 cells**

As **CKI-8** and **CKI-13** inhibited human recombinant CatK *in vitro* [43], we wanted to verify whether they could inhibit mouse CatK from RAW 264.7 and from primary murine mature osteoclasts since we are using these cells. Recombinant human CatK was used as a control (600 ng) and as a protein marker in zymography. Cellular proteins (300 ng) including CatK were extracted from RAW 264.7 cells or primary murine mature osteoclasts. Recombinant CatK and extracted cell proteins were then loaded onto 12.5% SDS-polyacrylamide gels containing 0.2 % (g/mL) gelatin at 4 °C for zymography. Human CatK (Fig. 6a, left lanes) migrated at the same position as CatK in RAW 264.7 cell extracts on the zymography gel (Fig. 6a, right lanes). Gels were then pre-incubated with **CKI-8** (Fig. 6a, top lanes) and **CKI-13** (Fig. 6a, bottom lanes), respectively, at concentration ranging from 5 to 1000 nM. At 1000 nM, both inhibitors were able to completely block the gelatinolytic activity of human CatK (Fig. 6a, left lanes) or mouse CatK (Fig. 6a, right lanes). We also observed a slight inhibition of gelatinolytic activity of CatK in extracts of primary osteoclasts (Fig. 6b), albeit less pronounced than observed for RAW 264.7 cells or human CatK (Fig. 6a). From the results of gelatin zymography, it is possible to calculate the apparent  $IC_{50}$  of inhibition of **CKI-8** and **CKI-13** by human CatK (Fig. 6c and d). A value of  $IC_{50} = 29 \pm 11$  nM was obtained for **CKI-13**, and a value of  $IC_{50} = 51 \pm 20$  nM was obtained for **CKI-8**. The addition of 0.1 % (mL/mL) DMSO used to solubilize the inhibitors did not affect the inhibition. These  $IC_{50}$  values were higher than those reported from *in vitro* enzymatic assays based on a synthetic dipeptide containing fluorescent labeling [43]. On the other hand, the  $IC_{50}$  of **CKI-13** is lower than that of **CKI-8**, being consistent with a previous *in vitro* report [42].

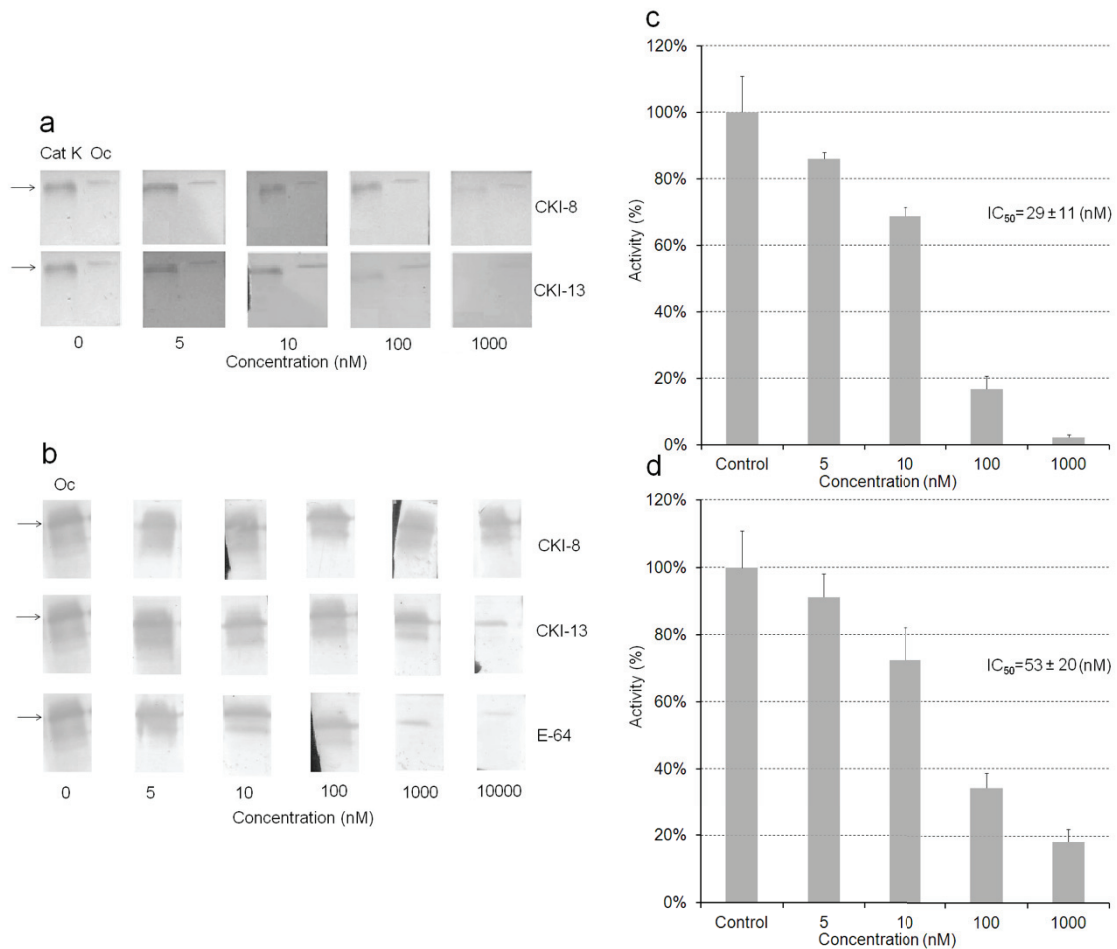


Figure 6. Gelatin zymography assay on catK activity. **(a)** Left lanes: Human recombinant catK (CatK) as positive control and right lanes: CatK extracted from RAW264.7 cells (OC), was loaded for gelatin zymography and incubated overnight in active buffer of 0.1 M sodium phosphate, pH 6.0, 1 mM EDTA and 2 mM DTT with **CKI-8** and **CKI-13** at the indicated concentrations. **(b)** CatK (OC) extracted from primary osteoclasts was loaded for gelatin zymography and incubated overnight in the active buffer of 0.1 M sodium phosphate buffer, pH 6.0, 1 mM EDTA 0.1 % DMSO (mL/mL) and 2 mM DTT without inhibitors (Control) and with **CKI-8**, **CKI-13** and E64 at the indicated concentrations. DMSO 0.1 % (mL/mL) has no effect on CatK activity. **(c)**  $IC_{50}$  of **CKI-13** and **(d)** **CKI-8** as determined by zymography (twice repeated) using human CatK.

## Assessment of bone resorption index on bone model matrix

### 1. Osteo corning plate assay

Osteoclastogenesis was induced using osteoclasts from murine bone marrow on Osteo Assay plates mimicking the bone surface, as well as on bovine bone slices. Typical mineralized matrix resorption by primary osteoclasts on Osteo Assay plates are shown,

incubated in the absence (Fig. 7a) or presence of 100 nM **CKI-13** (Fig. 7b) for 48 hours. Incubation with **CKI-13** at 100 nM significantly decreased resorption of this mineralized surface. The effects of CKI on resorption on Osteo Assay plates were quantified by comparing the resorption index in the control sample with 0.1 % DMSO (mL/mL) with that obtained by osteoclasts in the presence of **CKI-8** and **CKI-13** in 0.1 % DMSO (mL/mL). The presence or absence of DMSO at concentrations of up to 0.1 % (mL/mL) did not affect the resorption index on Osteo Assay plates by primary osteoclasts. **CKI-13** at 100 nM decreased significantly the resorption index of primary osteoclasts (Fig. 7c), while the commercial inhibitor **E64** and **CKI-8** did not (Fig. 7c). **CKI-8**, **CKI-13** and **E64** at 10 nM tend to increase the resorption. This is probably due to an acidic secretion by osteoclast, dissolving hydroxyapatite crystals. The Corning Osteo Assay surface does not contain any protein and consists of an inorganic crystalline calcium phosphate, mostly hydroxyapatite as probed by infrared spectroscopy (Fig. 7d) coated on a polystyrene plate [145].

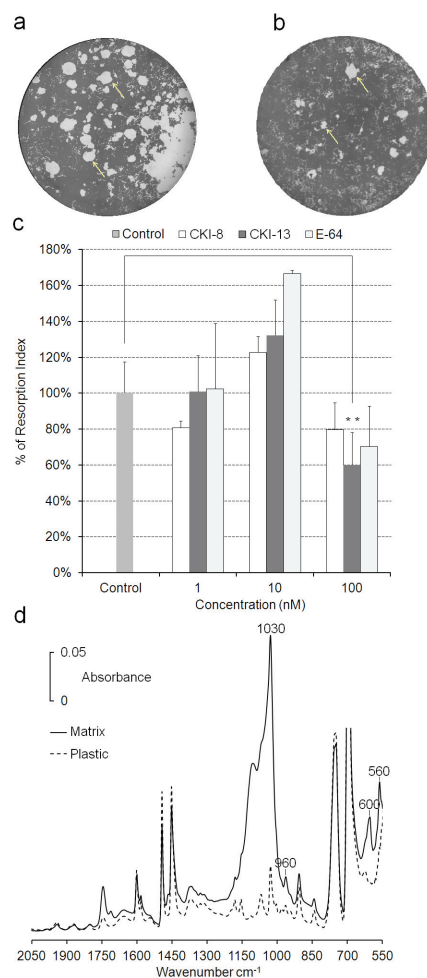


Figure 7. Resorption activity of osteoclasts derived from murine bone marrow on osteo assay plates mimicking bone surface. Osteoclast incubated in the **(a)** absence and **(b)** presence of 100 nM **CKI-13**. **(c)** Resorption index of osteoclasts on Osteo Assay plates. Resorption index of primary osteoclasts with **CKI-8**, **CKI-13** and **E-64**, respectively. Results are expressed as percentage of control containing DMSO 0.1% (mL/mL) without inhibitor. DMSO 0.1 % (mL/mL) has no effect on the resorption activity. The experiments were repeated in triplicate for each inhibitor (n=6). **(d)** The composition of osteoassay plate was identified by infrared spectroscopy. The infrared spectrum exhibited four peaks at 1030  $\text{cm}^{-1}$ , 960  $\text{cm}^{-1}$ , 600  $\text{cm}^{-1}$  and 560  $\text{cm}^{-1}$ , corresponding to the peaks of HA.

## 2. Bovine bone slice assay

Since **E64**, **CKI-8** and **CKI-13** are inhibitors of CatK acting on collagen, we needed to confirm their anti-resorption properties on bone slices. Furthermore, there are differences in the way that osteoclasts act on the hydrated mineral interspaced with extracellular matrix proteins, as in bovine bone slices, compared with dissolving a continuous microcrystalline surface, as in Corning Osteo Assay plate. Therefore we evaluated the effects of **CKI-8** and **CKI-13** on osteoclast resorbing bovine bone slices. The results showed that **CKI-13** at 10 and 100 nM, while **CKI-8** and **E64** both at 100nM decreased resorption significantly by primary osteoclasts on bovine bone slices (Fig. 8a). Moreover, the resorption lacunae on bovine bone slices in the presence of **CKI-8** (Fig. 8d) and **CKI-13** (Fig. 8e) were clearly smaller than the control (Fig. 8b) or the **E64**-treated bone slices (Fig. 8c). Significant difference in the mean area of resorption pits was observed between **CKI-8**, **CKI-13** and **E64** at 100nM (Fig. 8f). These differences in pit morphology could be due to **CKI-8** and **CKI-13** slowing down osteoclast spreading or motility.

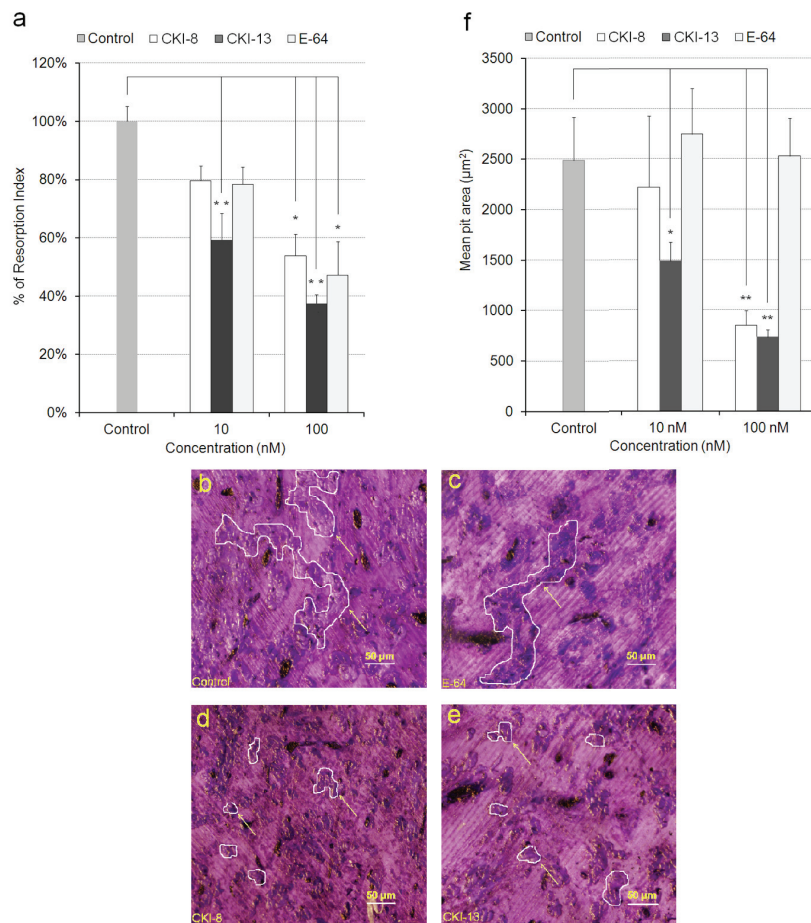


Figure 8. Resorption activity of osteoclasts derived from primary osteoclasts on bovine bone slices. **a)** Resorption index of primary osteoclasts with 0.1 % (mL/mL) DMSO not treated (control) or treated with following inhibitors: **E-64**, **CKI-8** and **CKI-13**. 0.1 % (mL/mL) DMSO has no effect on the resorption activity **b-e)** Typical bone resorbed surfaces by primary osteoclasts without and with CKIs, as revealed by three-min toluidine blue staining. Pits are delineated with white contours and yellow arrows. They were formed by osteoclasts resorbing on bovine bone plates without inhibitors (**b**), with **E-64** (**c**), with **CKI-8** (**d**) and with **CKI-13** (**e**) at 100nM. Smaller pits were observed in the presence of **CKI-8** (**d**) and with **CKI-13** (**e**) as compared with those without inhibitors (**b**) and with **E-64** (**c**). Quantitative analysis of mean pit area ( $\mu\text{m}^2$ ) on bovine bone slices without and with inhibitors at 100nM (**f**).

## DISCUSSION

We report the properties of a series of cathepsin K, B, L and S inhibitors, among these **CKI-13** having an  $\text{IC}_{50} = 0.006$  nM and being highly selective for CatK over B and S (~1000-fold) [43]. As these inhibitors were selective under *in vitro* conditions using human recombinant CatK as a target enzyme, zymography was used to ascertain their inhibition properties on mouse CatK. Both **CKI-8** and **CKI-13** inhibited CatK in extracts of mouse

monocyte-derived macrophage RAW 264.7 cells and from primary osteoclasts from mouse calvaria at higher concentrations than expected from *in vitro values* [43]. The IC<sub>50</sub> values determined from zymography of **CKI-8** ( $51 \pm 20$  nM) and of **CKI-13** ( $29 \pm 11$  nM) were higher than those of **CKI-8** ( $0.263$  nM) and **CKI-13** ( $0.006$  nM) acting on human CatK determined using the colorimetric method on dipeptides containing fluorophore [43]. This discrepancy is probably due to the nature of the substrate: dipeptides and gelatin are different in size and structure, affecting their accessibility to the active site of catK, as well as the inhibitor's binding site. Alternatively gel zymography can over estimate the apparent IC<sub>50</sub> due to the long exposure of inhibitors in the gel since the inhibitors may not stop completely the gelatinolytic activity.

To validate the feasibility of the possible therapeutic use of the candidate inhibitors prior to preclinical trials, we tested their toxicities, their effects on the mineralization process induced by osteoblasts and their influence on resorption mediated by osteoclasts. **CKI-8** and **CKI-13** showed no toxicity up to 1000 nM on osteoblast-like Saos-2 cells and on osteoclast RAW 264.7 cells. However, they were toxic when their concentrations exceeded 100 nM in primary osteoclasts. This suggested that the maximum concentration in cells without producing any cytotoxicity was around 100 nM for the candidate molecules. **CKIs** cell treatments were further verified for a possible side effect on osteoblast-induced mineralization. Neither **CKI-8** nor **CKI-13** affected the mineralization process induced by primary osteoblasts from mouse calvaria although a slight inhibition of TNAP activity by **CKI-13** was observed. **CKI-13** slowed down significantly the mineralization process induced by the Saos-2 cell line, as well as inhibiting slightly the TNAP activity. The different effects on mineralization of **CKI-13** on both types of cells are probably due to their distinct maturation times, as well as their mouse vs human origin.

The anti-resorption property of **CKI-8** and **CKI-13** was evaluated on Corning Osteo Assay plates at non-toxic concentration up to 100 nM for **CKI-13**. **CKI-13** inhibited the resorption activity of primary osteoclasts on the Corning Osteo Assay plate, in contrast to **CKI-8** and **E-64** which did not. The Corning Osteo Assay plate consisting mostly of hydroxyapatite coated onto polystyrene plate, indicated that **CKI-13** may interact with other targets than CatK. The increase in bone resorption observed at around 10 nM inhibitor concentrations (**CKI-8**, **CK-13** and **E-64**) is probably caused by an acidic secretion of osteoclasts unrelated to the Cat-K inhibition property of CKIs, dissolving the hydroxyapatite coated on the Osteo Assay plate.

Bone resorption on bovine slices decreased significantly at 10 nM **CKI-13**, while 100 nM **CKI-8** and 100 nM of the commercial inhibitor **E64** were necessary to significantly decrease bone resorption. **CKI-8** and **CKI-13** treatments produced smaller pits when compared with the larger pits induced by **E64** treatment (**Fig. 8b**), suggesting that **CKI-8** and **CKI-13** might affect the mobility of osteoclasts in addition to their osteoclast resorption activity. Possible targets of **CKI-8** and **CKI-13** are F-actin and other proteins involved in osteoclast podosome dynamics [146]. Although the findings look promising, especially the bone-resorption property of **CKI-13**, further work is needed to ascertain the feasibility of using CatK inhibitors to treat bone resorption diseases, since their side effects on TNAP activity may impair their therapeutic potential, especially for **CKI-13**.

## 2 Direct determination of pyrophosphate hydrolysis in Matrix Vesicles by Infrared Spectroscopy

### Characterization of matrix vesicles

MVs were isolated from femurs of 17-day-old chicken embryos. To check the purity of matrix vesicles, we analyzed the SDS-PAGE of the distinct fractions during differential centrifugation (Fig. 2) After a first centrifugation at 600 x g to discard cellular debris, pellet 1 (P1) was extracted, then the supernatant 1 (SN1) was subjected to a second centrifugation at 20 000 x g where pellet 2 (P2) was extracted, supernatant 2 (SN2) was subjected to a third centrifugation at 80 000 x g to obtain supernatant 3 (SN3) and MVs in pellet 3 (P3). P1, P2, SN1, SN3 and P3 were analyzed by SDS-PAGE (Fig. 9). MVs are enriched in three bands with apparent molecular masses of 45, 37, and 31 kDa (Fig. 9), consistent with the finding of Wu et al. [139].

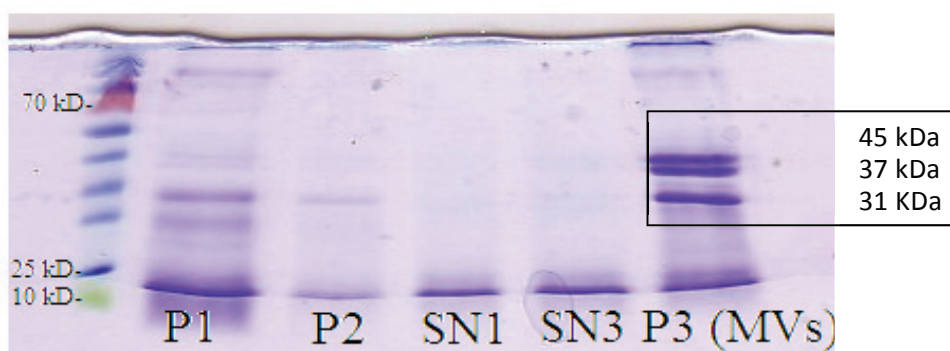


Figure 9. SDS-PAGE of matrix vesicles. (A) Protein profiles analyzed by 12 % SDS- PAGE followed by Coomassie brilliant blue staining of intact pellet 1 (P1); pellet 2 (P2); supernatant (SN1); supernatant 3 (SN3); pellet 3 (MVs).

Since TNAP is a marker of mineralization process, we determined its activity in different fractions P1, P2, SN1, SN3 and P3 during differential centrifugation (Fig. 10). The specific activity of pellet 3 in the TNAP is 19.61 U/mg at pH 10.4 (Table 3), which is more than two times higher in other chondrocyte membranes. The results indicated an enriched amount of TNAP characteristic of MVs.

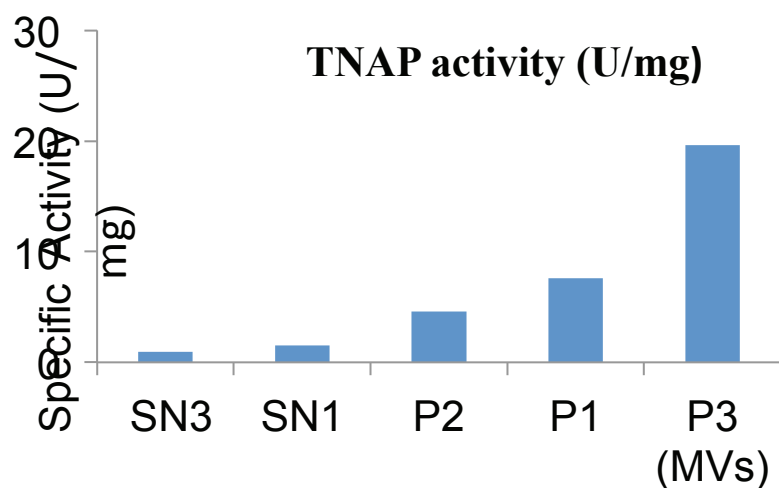


Figure 10. Specific activity of the different fractions in TNAP measured during hydrolysis of p-NPP at pH 10.4.

Fractions	Protein Concentration ( $\mu\text{g}/\mu\text{L}$ )	Total Activity (U/mL)	Specific Activity (U/mg)
Pellet 1	0.5	3.8	7.6
Supernatant 1 (SN1)	0.52	0.804	1.55
Pellet 2 (P2)	0.18	0.83	4.59
Supernatant 3 (SN3)	0.3	0.28	0.93
Pellet 3 (P3:MVs)	3.41	66.89	<b>19.61</b>

Table 3. Enzymatic activity of TNAP in the different fractions during the hydrolysis of p-NPP.

The ability of isolated MVs to induce mineral formation was monitored by light scattering at 340 nm. MVs in the SCL mineralization medium containing 2mM  $\text{Ca}^{2+}$  (total concentration) and 3.42mM  $\text{P}_i$  (total concentration) induced mineralization after a lag period of about 6 h when  $\text{P}_i$  and  $\text{Ca}^{2+}$  accumulated within MVs. The absorbance at 340 nm increased rapidly after 6 h, indicating the formation of calcium-Pi complexes. The maximum value was reached after an 8-h incubation (Fig 11. full line). In the medium containing only the SCL buffer with 2 mM  $\text{Ca}^{2+}$  and 3.42 mM  $\text{P}_i$  without MVs (Fig. 11 dots line), there were less mineral formation than in SCL medium under the same conditions with MVs. In the mineralization medium containing MVs without ions, the changes in turbidity were almost negligible over a 16-h incubation time (Figure 11. small dots line). This indicates that MVs are able to initiate

mineral formation under the ionic microenvironment .

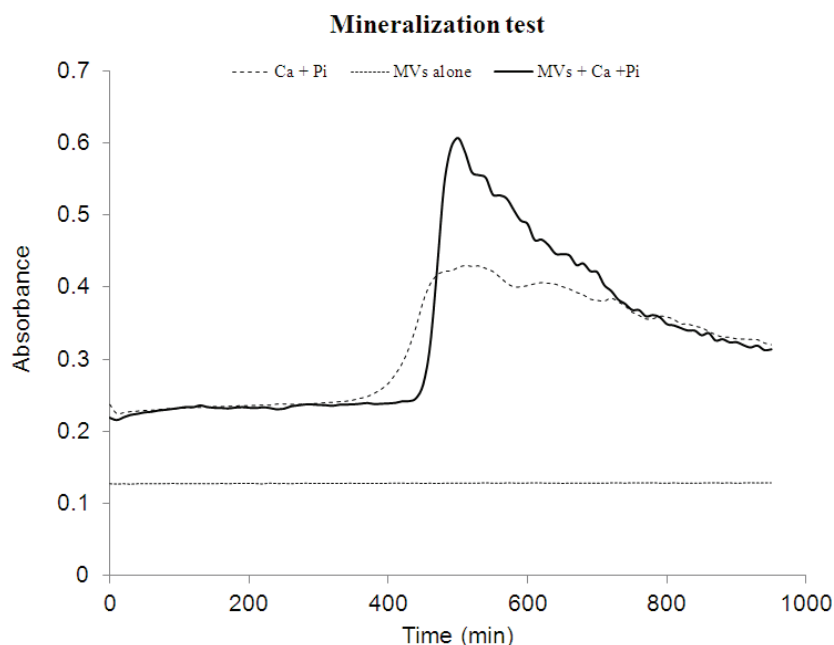


Figure 11. Mineralization induced by MVs: mineralization in SCL containing 2 mM  $\text{Ca}^{2+}$ , 3.42 mM  $\text{P}_i$ , and 10 $\mu\text{g}$  of protein/ml MVs. (dots line): control of mineralization in SCL containing 2mM  $\text{Ca}^{2+}$  and 3.42mM  $\text{P}_i$ , but without MV;(small dots line): control of mineralization in SCL containing MVs only without ions; (full line): mineralization-process containing MVs with 2 mM  $\text{Ca}^{2+}$ , 3.42 mM  $\text{P}_i$ . The mineral formation was assessed by light scattering at 340 nm.

Minerals formed in the presence of MVs were analyzed by IR spectroscopy and compared with IR spectra of HA. The mineral formed under the same conditions for the turbidity measurements were determined by IR assay (Fig. 12). The positions of bands in the infrared spectrum at 1090  $\text{cm}^{-1}$ , 1020  $\text{cm}^{-1}$ , 962  $\text{cm}^{-1}$ , 633  $\text{cm}^{-1}$ , and 602  $\text{cm}^{-1}$  (Figure 12. HA), corresponding to mineral formed in the MVs, matched almost exactly the positions of bands in the infrared spectrum of HA (Fig. 12. MVs), indicating the ability of MVs to produce HA. Minor variations around 1020  $\text{cm}^{-1}$  are associated to the presence of MVs membrane phospholipids. These results confirmed that MVs are functional and able to produce HA.

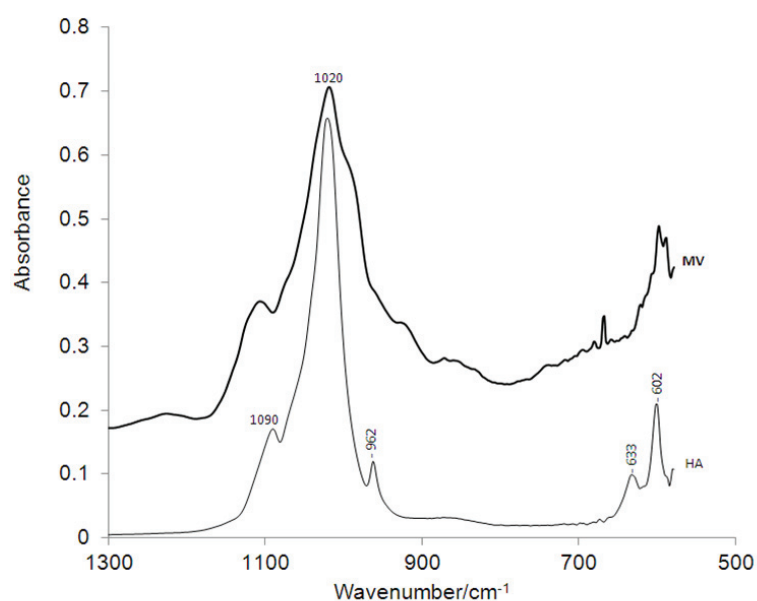


Figure 12. Infrared spectra of mineral deposits by MVs and pure HA. MVs were incubated at 37 °C in mineralization buffer for 8 hours, then the minerals formed were collected, washed and analyzed by infrared spectroscopy. Infrared spectrum of hydroxyapatite as control (HA); Infrared spectrum of minerals formed by matrix vesicles (MV). Infrared spectra of minerals indicated that the minerals formed by MVs were hydroxyapatite. (Typical infrared spectra averaged with two independent measurements).

Having demonstrated that P3 contains enriched amount of MVs as revealed by SDS-PAGE (Fig. 9) and by TNAP activity (Fig. 10) in addition to their functional property as indicated by turbidity measurements (Fig. 11) and their ability to form HA as shown by infrared spectroscopy (Fig. 12), P3 sample served as a source of MVs.

### Development of an IR assay to determine TNAP enzymatic activity in MVs

Up to now, TNAP activity is measured at non-physiological alkaline pH (10.4) using a non-natural substrate para-nitrophenyl phosphate (*p*-NPP). To screen inhibitors, it is necessary to develop an assay using natural substrates in turbid medium at physiological pH. Another problem often encountered with our types of inhibitors is that they contain aromatic groups which can interfere with the band absorption of nitrophenolate rendering the determination of TNAP activity difficult by using colorimetric method. Therefore we developed an infrared (IR) assay that may solve the problems encountered with the hydrolysis of *p*-NPP. IR spectroscopy will allow the use of a natural substrate pyrophosphate (PP<sub>i</sub>) at physiological pH 8. In addition the activity measurement will not be affected by colored or turbid medium. Hydrolysis of PP<sub>i</sub> by TNAP released inorganic phosphate (P<sub>i</sub>) [44]. The IR spectrum of HPO<sub>3</sub><sup>2-</sup> anion in

aqueous buffer containing 50 mM Tris-HCl, pH 8.0, 5  $\mu$ M ZnCl<sub>2</sub> and 5 mM MgCl<sub>2</sub> indicates two bands at around 1076 and 990 cm<sup>-1</sup> (**Fig. 13**) that are assigned respectively to asymmetric stretching and symmetric stretching vibrations [147]. The position of the phosphate bands is sensitive to their ionic environment as in the case of nucleotides [148] or phospholipids [149].

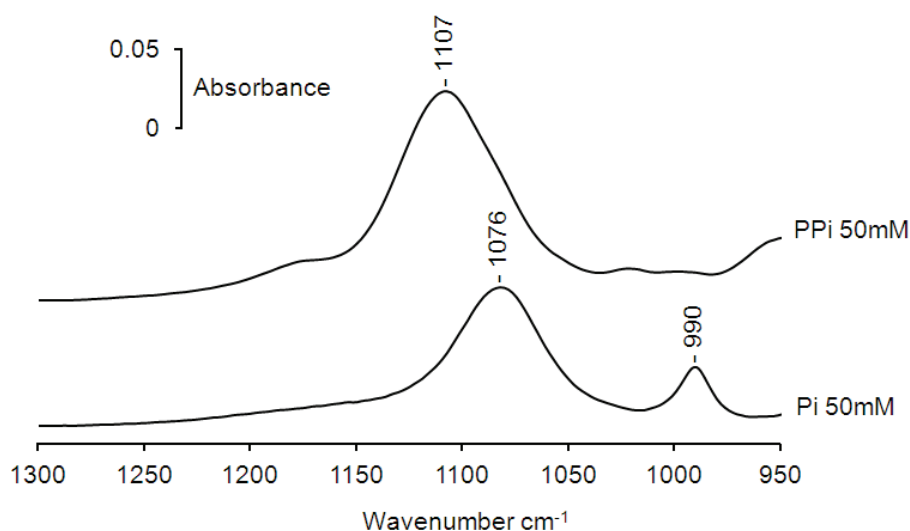


Figure 13. Infrared spectra of 50 mM inorganic phosphate (bottom trace) and of 50 mM pyrophosphate (top trace) in aqueous buffer 50 mM Tris-HCL, pH 8.0, 5  $\mu$ M ZnCl<sub>2</sub> and 5 mM MgCl<sub>2</sub>.

The IR spectrum of 50 mM PP<sub>i</sub> shows one band located at around 1107 cm<sup>-1</sup> (Fig. 13). The IR spectra of P<sub>i</sub> and of PP<sub>i</sub> present sufficient differences in band shapes and positions (Fig. 13) to be used for analytical application. To illustrate the potential of the enzymatic assay, we measured the hydrolytic activity of MVs towards PP<sub>i</sub> in reaction medium containing 5  $\mu$ M ZnCl<sub>2</sub> and 5 mM MgCl<sub>2</sub>, 100 mM Tris-HCL, pH 8.0. IR spectra of MVs in reaction medium after 5 min and after 60 min (Fig. 14a) incubation time at 37°C have been recorded. As a control IR spectra of MVs in reaction medium without PP<sub>i</sub> have been measured after 5 min and after 60 min indicating no changes (data not shown). The 1300 - 900 cm<sup>-1</sup> wavenumber ranges was selected to reveal the PP<sub>i</sub> hydrolysis (Fig. 14 a).

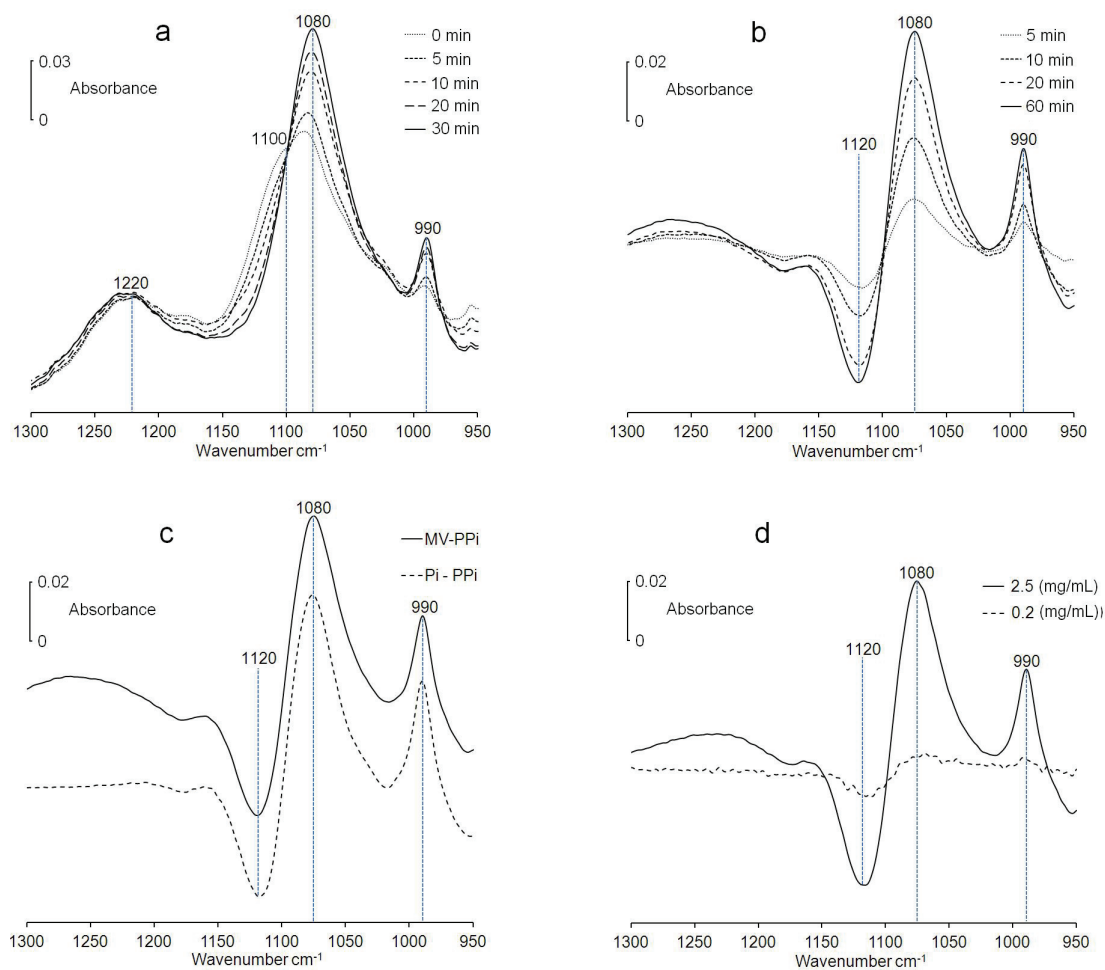


Figure 14. Phosphatase activity in matrix vesicles as determined by infrared spectroscopy. (a) Kinetic recording of 50 mM  $\text{PP}_i$  hydrolysis by 2 mg MV protein  $\text{mL}^{-1}$  in medium containing 5 mM  $\text{MgCl}_2$ , 5  $\mu\text{M}$   $\text{ZnCl}_2$  and 100 mM Tris-HCL, pH 8.0 (buffer A) at 37 °C. Successive infrared spectra were measured at the indicated times. (b) Difference IR spectra of MVs with  $\text{PP}_i$  (spectrum recorded at the indicated time minus that recorded immediately). Significant variation in the intensity of absorption bands of  $\text{PP}_i$  located at 1120-1100  $\text{cm}^{-1}$  as well as other variations attributed to  $\text{P}_i$  at 1075-1080  $\text{cm}^{-1}$  and 990  $\text{cm}^{-1}$  were observed. (c) Expected IR difference spectrum of product and substrate ( $2 \times \text{P}_i$  minus  $\text{PP}_i$ ) (dashed line). IR difference spectrum of the hydrolysis of 50 mM  $\text{PP}_i$  by 2.5 mg MV protein  $\text{mL}^{-1}$  in buffer A (spectrum recorded at 60 min minus spectrum recorded immediately) (Full line) (d) Sensitivity of the infrared assay to determine the hydrolysis of 50 mM  $\text{PP}_i$  by 2.5 mg MV protein  $\text{mL}^{-1}$  (full line) and by 0.2 mg MV protein  $\text{mL}^{-1}$  (dashed line) as shown by their difference spectrum respectively (spectrum of MVs with 50 mM  $\text{PP}_i$  recorded at 30 min minus spectrum recorded immediately).

The IR spectra of MVs in the reactive medium did not indicate any changes in the 4000-1400  $\text{cm}^{-1}$  region of the IR spectrum. In the 1400-900- $\text{cm}^{-1}$  range, the IR spectral changes are dominated by the hydrolysis of  $\text{PP}_i$  by MVs due to the relative large amount of  $\text{PP}_i$  (Fig. 14a). The absorbance decrease of  $\text{PP}_i$  band at 1100-1107  $\text{cm}^{-1}$  (Fig. 14a) is associated to a decrease

of  $PP_i$ , while the increase of the  $1076\text{-}1080\text{-cm}^{-1}$  and  $990\text{-cm}^{-1}$  bands signaled the apparition of  $P_i$ . This is better seen on the difference spectra of MVs with  $PP_i$  (Fig. 14b) (spectrum recorded at the indicated time minus that recorded immediately). The negative band at  $1100\text{-}1120\text{ cm}^{-1}$  and the two positive bands located at  $1076\text{-}1080\text{cm}^{-1}$  and  $990\text{-cm}^{-1}$  bands indicated the hydrolysis of  $PP_i$ . This was confirmed by calculating the difference spectra corresponded to the hydrolysis (spectrum of two  $P_i$  minus spectrum  $PP_i$  since one molecule  $PP_i$  gives to two molecules of  $P_i$ ) (Fig. 14c, dashed line). The IR difference spectrum of MVs in reactive medium containing  $PP_i$  (Spectrum of sample incubated for 60 min minus spectrum of sample incubated for 5 min) (Fig. 14c, full line) is identical to that of the calculated difference (Fig. 14c, dashed line). This confirms that the IR changes are solely related to the hydrolysis of  $PP_i$  by MVs. The limit to detect significant infrared changes of the hydrolysis of  $PP_i$  was estimated to be around  $0.2\text{ mg MV-proteins mL}^{-1}$  (Fig. 14d, dashed line). For comparison, the hydrolysis of  $PP_i$  by  $2.5\text{ mg MV-proteins mL}^{-1}$  induced about ten times larger infrared changes (Fig. 14d, full line). At  $0.2\text{ mg mL}^{-1}$  MV protein, only faint bands not much more intensive than the noise signal are detected (Figure 14. d, dashed line), while at  $2.5\text{ mg mL}^{-1}$  MVs protein, the IR bands indicating disappearance of  $PP_i$  and appearance of  $P_i$  are well resolved (Figure 14. d, full line).

We selected the  $PP_i$  band (located at  $1100\text{-}1120\text{ cm}^{-1}$ ) and the two  $P_i$  bands (located at  $1076\text{-}1080\text{-cm}^{-1}$  and  $990\text{-cm}^{-1}$ ) to determine the hydrolytic activity of  $PP_i$  by MVs (Fig. 15).

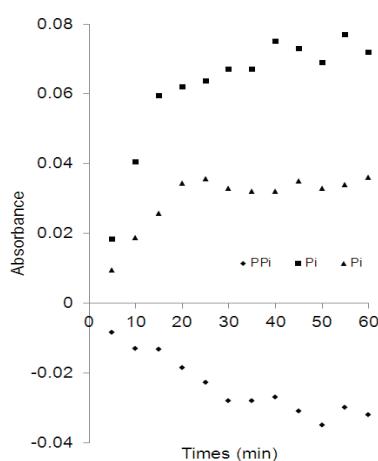


Figure 15. Absorbance changes during  $PP_i$  hydrolysis by MVs of  $PP_i$  band located at  $1107\text{ cm}^{-1}$  (bottom trace, Molar absorption coefficient =  $2158 \pm 211\text{ M}^{-1}\cdot\text{cm}^{-1}$ ) and of the two  $P_i$  bands located at  $1076\text{-}1080\text{-cm}^{-1}$  and  $990\text{-cm}^{-1}$  (top traces, Molar absorption coefficients of  $1215 \pm 131\text{ M}^{-1}\cdot\text{cm}^{-1}$  and  $443 \pm 50\text{ M}^{-1}\cdot\text{cm}^{-1}$  respectively).

We can determine the concentration changes during  $PP_i$  hydrolysis by MVs and determine

activity of PP<sub>i</sub> hydrolysis by MVs. Using the 1107 cm<sup>-1</sup> bands we calculated an activity of around 1.367-1.83 μmole mg<sup>-1</sup> min<sup>-1</sup> for MV-protein concentration range of 1 to 2.5 mg mL<sup>-1</sup> (Table 4).

Table 4. Specific activities of TNAP in the different concentration of MVs

MVs mg/mL	Specific Activity U/mg
1	1.484
1.5	1.368
2	1.566
2.5	1.83

For comparison, the TNAP activity of MVs determined at pH 10.4 using the p-NPP as a substrate, amounted to 30 ± 10 μmole mg<sup>-1</sup> min<sup>-1</sup>. This is consistent with the reported values for alkaline phosphatase extracted from HeLa Ch cells, having a PP<sub>i</sub> hydrolytic activity at pH 8.5 about 26 to 30 times smaller than the pNPP hydrolytic activity at pH 10.4 [150].

To test if the hydrolysis of PP<sub>i</sub> is specifically associated to TNAP, we incubated the reactive medium containing MVs and 50 mM PP<sub>i</sub> with 5 mM levamisole, a TNAP specific inhibitor. Addition of levamisole induced a smaller slope in the absorbance changes at 1107 cm<sup>-1</sup> (Figure 16.a red symbols), at 990 cm<sup>-1</sup> (Figure 16. b red symbols) and at 1076 cm<sup>-1</sup> (Figure 16. c, red symbols) as compared with the control sample without levamisole (Figure 16. blue symbols). We observed a significant inhibition of PP<sub>i</sub> hydrolysis in the presence of 5 mM levamisole from 1132 ± 370 nmol min<sup>-1</sup> mg<sup>-1</sup> (without levamisole) to 343 ± 112 nmol min<sup>-1</sup> mg<sup>-1</sup> (with 5 mM Levamisole) confirming that TNAP is to a large extent responsible for PP<sub>i</sub> hydrolysis.

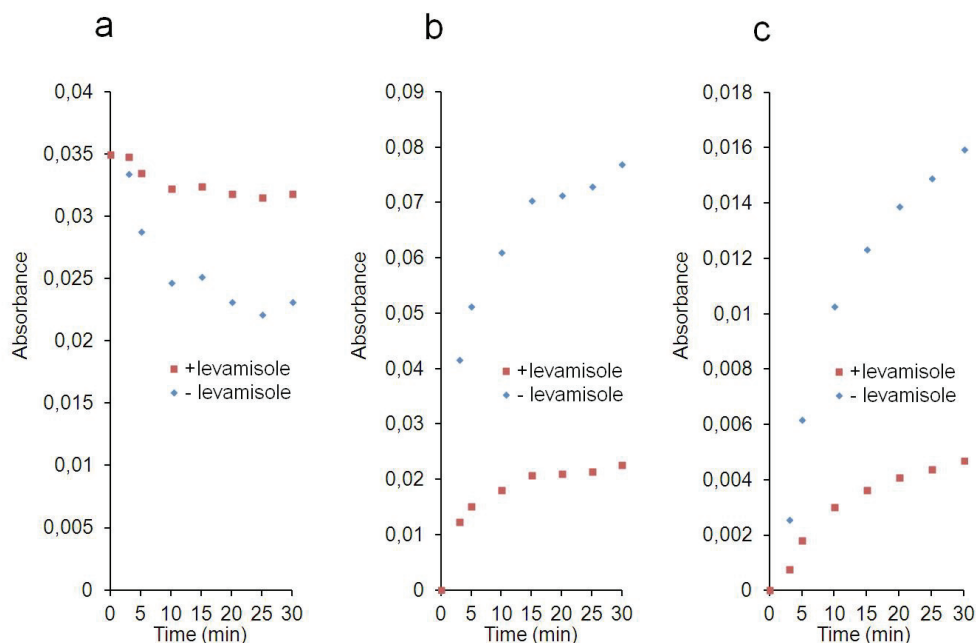


Figure 16. **a)** Absorption changes of  $PP_i$  band at  $1107\text{ cm}^{-1}$ ; **b)** Absorption changes of  $P_i$  peak at  $990\text{ cm}^{-1}$ ; Absorption changes of  $P_i$  band at  $1076\text{ cm}^{-1}$  during  $PP_i$  hydrolysis by  $2\text{ mg mL}^{-1}$  MVs in buffer A at  $37\text{ }^\circ\text{C}$  in the absence (blue symbols) or presence (red symbols) of  $5\text{ mM}$  levamisole.

## DISCUSSION

It has been recognized that IR spectroscopy in combination with the appropriate multivariate analysis has considerable potential as a metabolic fingerprinting tool for the diagnosis of disease or dysfunction [124,125] and can assess biochemical changes of cells exposed to various inhibitors such as cardiotoxic glycoside inhibitor ouabain [120, 122], tyrosine inhibitor imatinib [151] or AKT kinase inhibitor [152]. It is quite rare to find an infrared assay to monitor directly one specific activity in the extracellular vesicles, cells or tissues which can be used to screen inhibitors. In this work, we purified matrix vesicles derived from chicken embryo chondrocytes and we verified their characteristics. They are able to initiate mineralization and they have a high activity in TNAP. Matrix vesicles were selected as model of extracellular vesicles due to their high alkaline phosphatase activity. In addition, inhibitors of TNAP may serve as a drug therapy to cure vascular calcification. The TNAP highly expressed in mineralized tissues, and essential for the mineralization of the bone, is an important therapeutic target for the treatment of pathological calcifications. Diseases associated with calcifications belong to a large family of diseases that can be caused not only in skeletal tissues but also in non-skeletal tissues such as vascular calcification

tissues.

The aim of our work was to develop an assay of the enzymatic activity in the hydrolysis of TNAP as  $PP_i$  a natural substrate for MVs activity assay. We demonstrate the feasibility of the infrared assay by measuring the TNAP activity in MVs that was around  $1.4 \mu\text{mol min}^{-1} \text{mg}^{-1}$ , while we observed a significant inhibition of  $PP_i$  hydrolysis in the presence of 5 mM levamisole (a TNAP inhibitor) from  $343 \pm 112 \text{ nmol min}^{-1} \text{mg}^{-1}$  confirming that the pyrophosphatase activity originated mostly from TNAP. The main advantages of the IR assay lie in the possibility to determine directly in situ hydrolytic activity of TNAP and to obtain  $IC_{50}$  of inhibitors using natural substrates in an almost continuous manner at physiological pH. In this respect, IR is insensitive to light scattering effects caused by the turbidity of the samples and relatively large concentrations of protein can be employed. However, for the IR assay, this technique presents some limitations related to the accuracy of determination of the base line but also in the thickness of the spacer. We estimated that the sensitivity based on a 30-min assay is around  $0.2 \text{ mg cell proteins mL}^{-1}$  in a 5-10  $\mu\text{L}$  sample containing 50 mM  $PP_i$ . Lower protein concentration could be used with longer incubation times. The other limitation concerns the minimal amount of  $P_i$  or  $PP_i$  concentrations which should be at least around 1 mM to be reliably detected.

### 3. An infrared assay of the kinetics of phosphate-release from physiological substrates in living cells

#### Infrared spectra of different substrates

Having demonstrated that the hydrolysis of pyrophosphate in matrix vesicles can be measured by infrared spectroscopy, we wanted to explore if other types of substrates could serve to determine a phosphatase activity. IR spectra of 50 mM phosphatase substrates: AMP, ADP, ATP, UTP, glucose-1-phosphate (G-1-P),  $\beta$ -glycerophosphate ( $\beta$ -GP), *p*-nitrophenylphosphate (*p*-NPP), PP<sub>i</sub> and Pi in buffer A (100 mM Tris-HCl, pH 8.0, 5  $\mu$ M ZnCl<sub>2</sub> and 5 mM MgCl<sub>2</sub>) recorded at 37 °C present sufficient differences in band shapes and positions (Fig. 17) to be used for analytical application.

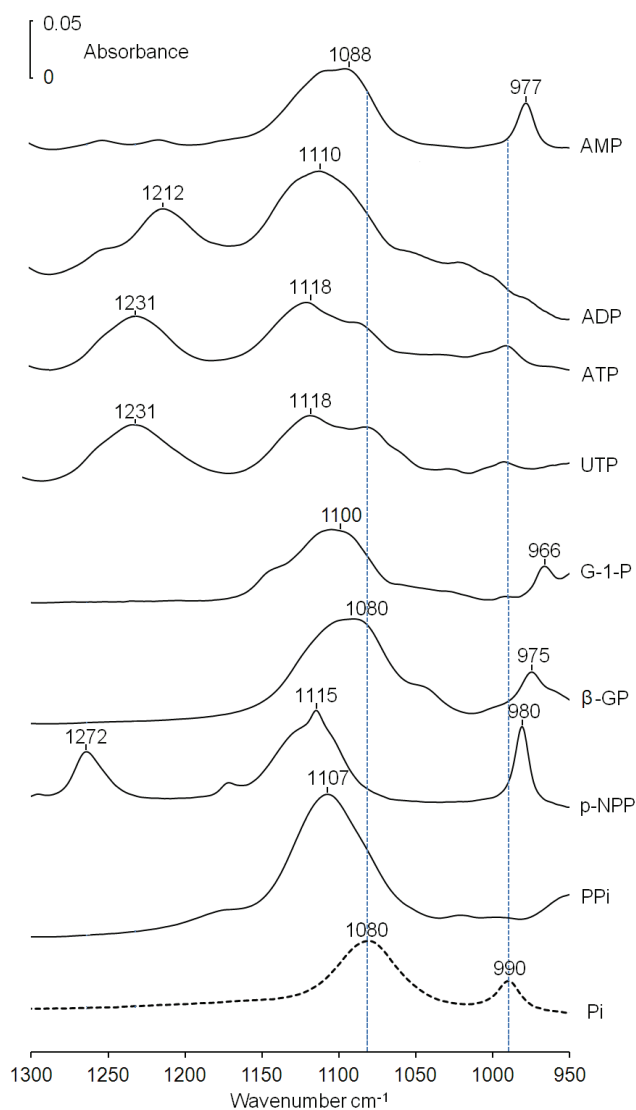


Figure 17. IR spectra of 50 mM of different physiological substrates and 50 mM P<sub>i</sub> in aqueous buffer containing 100 mM Tris-HCl, pH 8.0, 5 mM MgCl<sub>2</sub> and 5  $\mu$ M ZnCl<sub>2</sub>.

To determine the molar absorption coefficient, we used the Beer-Lambert law :  $A = \varepsilon \cdot l \cdot C$ .

Where  $A$  is the absorbance,  $\varepsilon$  is the molar absorption coefficient ( $M^{-1} \text{ cm}^{-1}$ ),  $l$  is the path length (cm), and  $C$  is the protein concentration (M). Table 5 contained the values of molar absorption coefficients for  $P_i$  ( $\varepsilon_{P_i} = 1346 \pm 116 M^{-1} \cdot \text{cm}^{-1}$  for the  $1076\text{-cm}^{-1}$  band and  $\varepsilon_{P_i} = 493 \pm 49 M^{-1} \cdot \text{cm}^{-1}$  for the  $990 \text{ cm}^{-1}$  band) and for other substrates: AMP, ADP, ATP, UTP, glucose-1-phosphate (G-1-P),  $\beta$ -glycerophosphate ( $\beta$ -GP),  $p$ -nitrophenylphosphate ( $p$ -NPP),  $PP_i$ .

Table 5. Molar absorbance of different physiological substrates.  $\varepsilon$  value= mean  $\pm$  mean deviation and the results were based on three independent measurements.

Substrates	Band position $\text{cm}^{-1}$	Molar Absorbance $L \cdot \text{mol}^{-1} \cdot \text{cm}^{-1}$	Substrates	Band position $\text{cm}^{-1}$	Molar Absorbance $L \cdot \text{mol}^{-1} \cdot \text{cm}^{-1}$
AMP	1088	$1034 \pm 133$	$\beta$ -GP	1086	$1219 \pm 154$
	977	$476 \pm 48$		975	$294 \pm 27$
ADP	1212	$456 \pm 56$	G-1-P	1100	$1063 \pm 18$
	1110	$1450 \pm 61$		966	$355 \pm 70$
ATP	1231	$1032 \pm 84$	$p$ -NPP	1115	$1389 \pm 55$
	1118	$1150 \pm 128$		980	$1012 \pm 81$
UTP	1231	$842 \pm 62$	$PP_i$	1107	$2158 \pm 211$
	1118	$903 \pm 81$			

### Determination of protein concentration

The determination of protein concentration by infrared spectra was performed using NIST-certified BSA solution in buffer A. A series of five dilutions (in triplicates) spanning the range from 5 mg/mL to 20 mg/mL served to obtain an accurate calibration curve (Fig. 18). We obtained a mean molar absorption coefficient of the amide-II band:  $\varepsilon_{\text{amide II}} = 3.6 \text{ mg}^{-1} \text{ ml cm}^{-1}$ .

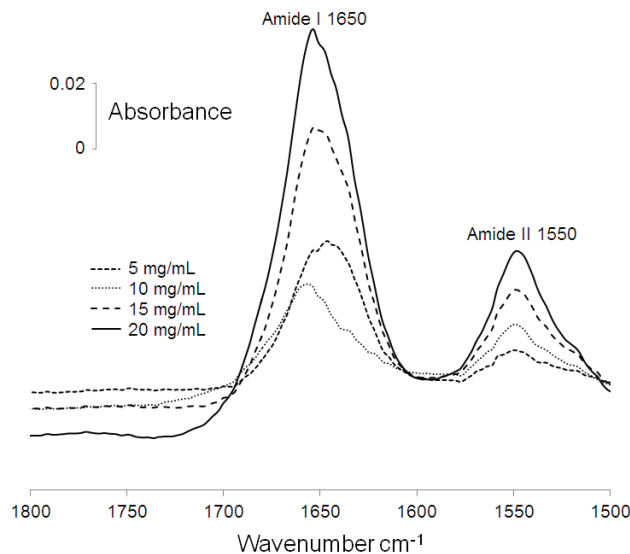


Figure 18. Infrared spectra of BSA solution in buffer A that served to determine molar absorption coefficient of the amide-II band at  $1550\text{ cm}^{-1}$

The amide-I band intensity is slightly affected by the intensity of water band (especially at low protein concentration) due to the subtraction factor for the water band (Fig.18). Therefore the amide-II band served to determine the protein concentration since this band is outside the absorption of water band.

### IR assay to determine TNAP enzymatic activity in Saos-2 cells

To illustrate the potential of the IR assay in assessing phosphatase activity in cells, we selected human osteoblast-like Saos-2 cells which are known for their high TNAP activity. These cells express the entire osteoblastic differentiation program from proliferation to mineralization [153], produce a collagenous extracellular matrix [154] and spontaneously release mineralization-competent MVs [155]. We measured IR spectrum immediately (3 min dead time) after mixing Saos-2 cells with 50 mM substrate such as AMP, ADP, ATP, UTP,  $\alpha$ -D-glucose 1-phosphate (G-1-P),  $\beta$ -glycerophosphate ( $\beta$ -GP), pNPP and  $\text{PP}_i$  in aqueous Buffer A (Fig. 19 full lines). After 30 min-incubation in the infrared cell at  $37^\circ\text{C}$ , a second IR spectrum was measured (Fig. 19 dashed lines).

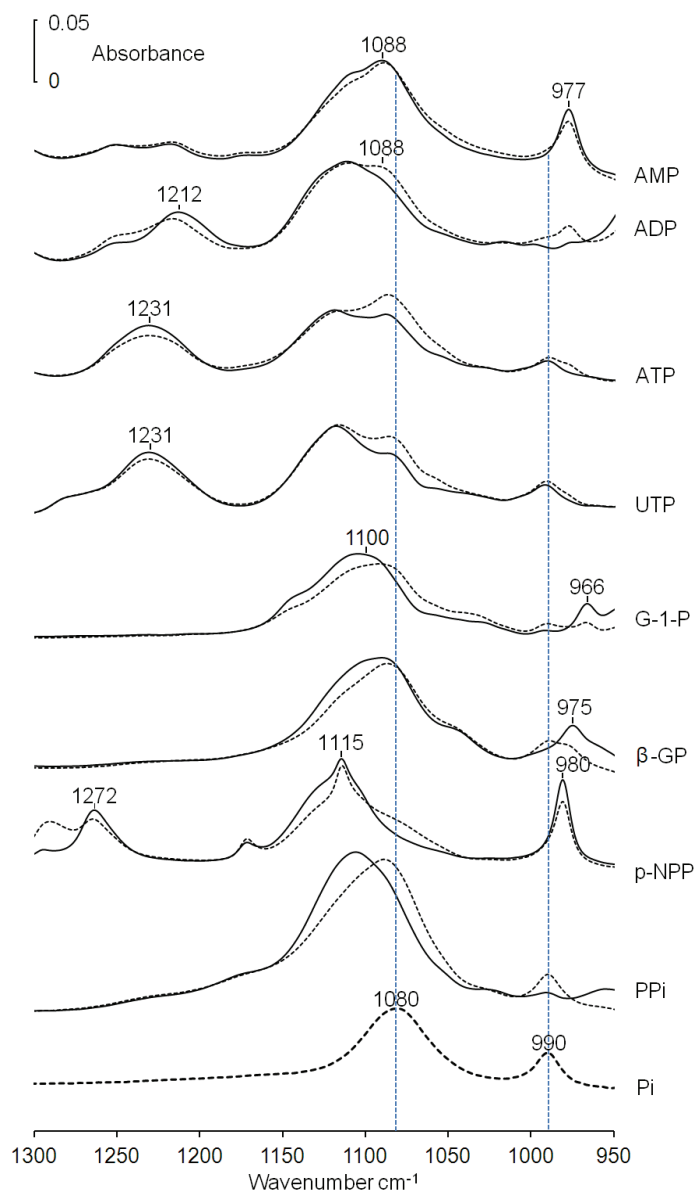


Figure 19. IR spectra of 50 mM substrate (one among the substrates: AMP, ADP, ATP, UTP, G-1-P, b-GP, *p*NPP, PP<sub>i</sub>) in buffer A with Saos-2 cells, recorded immediately after mixing the substrate with cells (full lines) and after 30 min (dashed lines) at 37 °C. The bottom trace indicated the IR spectrum of 50 mM P<sub>i</sub>, the product of the hydrolysis of substrate. Vertical lines served to guide the eye to evidence P<sub>i</sub> formation.

The bottom trace shows the spectrum of 50 mM P<sub>i</sub> indicating the positions of the two 1080 and 990 cm<sup>-1</sup> bands (vertical blue dashed lines). The IR spectrum of buffer A was deduced from the IR spectra of Saos-2 cells with substrate. In all cases (with AMP, ADP, ATP, UTP, G-1P, β-GP), *p*NPP or PP<sub>i</sub>), the intensity of either one or both P<sub>i</sub> bands at 1076-1080 and 990 cm<sup>-1</sup> increased or the intensity of the substrate decreased, indicating the phosphatase activity in the whole cells (Fig. 19). It was clearly observed in the successive difference spectra (spectrum measured at the indicated time minus that measured immediately after mixing 50 mM substrate with Saos-2 cells) (Figure. 20). Negative peaks indicated the disappearance of the substrate while positive peaks at 1076-1080 and 990 cm<sup>-1</sup> illustrated the formation of a hydrolytic product, namely P<sub>i</sub> (Figure. 20). The hydrolysis of ATP, UTP and ADP in the Saos-2 cells produced P<sub>i</sub>

(positive 1088-1080  $\text{cm}^{-1}$  and 990- $\text{cm}^{-1}$  bands) and AMP (positive 977  $\text{cm}^{-1}$  band), however it was not possible to ascertain the formation of  $\text{PP}_i$  since there were no significant positive 1107- $\text{cm}^{-1}$   $\text{PP}_i$  band. We also observed hydrolysis of G-1P,  $\beta$ -GP and  $p$ NPP and  $\text{PP}_i$  in Saos-2 cells indicating a broad phosphatase activity.

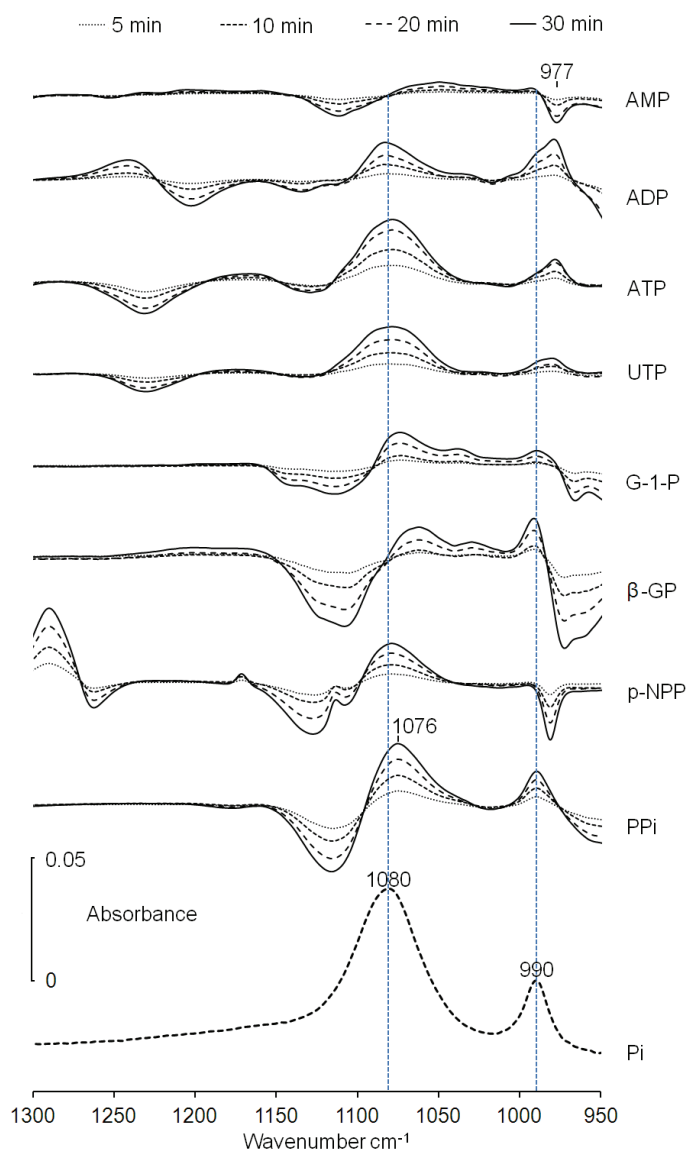


Figure 20. Successive difference spectra of Saos-2 cells with 50 mM substrate (AMP, ADP, ATP, UTP, G-1P,  $\beta$ -GP,  $p$ -NPP,  $\text{PP}_i$  and  $\text{P}_i$ ) in buffer A (spectrum measured after a given time minus that measured immediately after mixing the substrate with cells) at 37°C determined at 5, 10, 20 and 30 min. The negative intensities indicated the decline of substrate concentration while the positive intensities of the 1076-1080 and the 990  $\text{cm}^{-1}$  bands indicated the appearance of  $\text{P}_i$ . The bottom trace shows the spectrum of 50 mM  $\text{P}_i$  to indicate the positions of the two 1080 and 990  $\text{cm}^{-1}$  bands (vertical blue dashed lines).

The feasibility to monitor a phosphatase activity by Saos-2 cells in buffer A was verified. Now, we want to demonstrate the possibility to determine protein concentration using the amide-II band so that we could determine a specific phosphatase activity in one single assay. That is to determine protein concentration in cells and the phosphatase activity simultaneously. Typical IR spectra of 50 mM  $\text{PP}_i$  with Saos-2 cells in buffer A (Fig. 21) immediately and after mixing 30 min incubation (full trace) indicated the decrease of the 1100  $\text{cm}^{-1}$  band of  $\text{PP}_i$  and the increase of the 1080  $\text{cm}^{-1}$  band of  $\text{P}_i$ , confirming the presence of pyrophosphatase activity. Furthermore, the

1550  $\text{cm}^{-1}$  protein band (amide-II band) allowed us to determine directly protein concentration using  $\epsilon = 3.6 \text{ mg}^{-1}\text{mL cm}^{-1}$ .

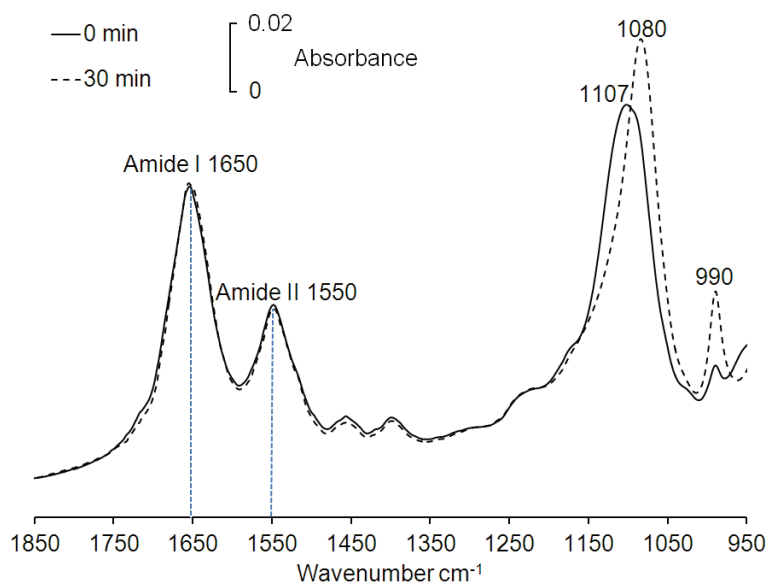


Figure 21. IR spectra of Saos-2 cells ( $12 \text{ mg}$  of Saos-2-cell protein  $\text{mL}^{-1}$ ) with  $50 \text{ mM}$   $\text{PP}_i$  in buffer A recorded immediately after mixing the substrate with cells (full line) and after  $30 \text{ min}$  incubation at  $37 \text{ }^\circ\text{C}$  (dashed line).

The absorbance changes of  $1120\text{-}1100 \text{ cm}^{-1}$  band of  $\text{PP}_i$  and the  $990 \text{ cm}^{-1}$  band of  $\text{P}_i$  served to determine the pyrophosphatase activity (Table 6). We obtained an apparent specific phosphatase activity in Saos-2 cells of around  $116 \pm 113 \text{ nmol min}^{-1} \text{ mg}^{-1}$  (Table 6). This compares well with the pyrophosphatase activity of  $130 \text{ nmol min}^{-1} \text{ mg}^{-1}$  in mammalian HeLa cells at pH 8.5 as assayed by the modified method of Fiske and Subbarow [150]. Quantitative determinations were also obtained for AMP, G-1-P,  $\beta$ -GP,  $p$ -NPP using both  $\text{P}_i$  bands at  $990$  and  $1070\text{-}1080 \text{ cm}^{-1}$  (Table 6). The substrate bands were also used to determine enzyme specific activity, as in the case of AMP ( $977 \text{ cm}^{-1}$ ),  $p$ -NPP ( $980 \text{ cm}^{-1}$ ) and  $\text{PP}_i$  ( $1107 \text{ cm}^{-1}$ ) (Table 6). Specific activities determined either from  $\text{P}_i$  or from substrate-bands were identical within experimental errors except for G-1-P and  $\beta$ -GP due to strong band overlapping.

Table 6. Specific of phosphatase activity ( $\text{nmol mg}^{-1} \text{min}^{-1}$ ) of different substrates in Saos-2 cells as determined by using phosphate bands ( $990$  and  $1080\text{-}1070 \text{ cm}^{-1}$ ) and other substrates bands.

Substrates	Band position $\text{cm}^{-1}$	Molar Absorbance $\text{L} \cdot \text{mol}^{-1} \cdot \text{cm}^{-1}$	Specific activity $\text{nmol} \cdot \text{mg}^{-1} \cdot \text{min}^{-1}$	Average $\text{nmol} \cdot \text{mg}^{-1} \cdot \text{min}^{-1}$
AMP	977-AMP	$476 \pm 48$	$66 \pm 4$	$58 \pm 4$
	990- $\text{P}_i$	$443 \pm 50$	$42 \pm 7$	
$\alpha$ -G-1-P	966-G-1-P	$355 \pm 70$	$171 \pm 28$	$100 \pm 12$
	990- $\text{P}_i$	$443 \pm 50$	$84 \pm 9$	
	1080- $\text{P}_i$	$1215 \pm 131$	$45 \pm 8$	
$\beta$ -GP	975- $\beta$ -GP	$294 \pm 27$	$181 \pm 9$	$100 \pm 3$
	990- $\text{P}_i$	$443 \pm 50$	$97 \pm 2$	
$p$ -NPP	1080- $\text{P}_i$	$1215 \pm 131$	$22 \pm 1$	$121 \pm 3$
	980- $p$ NPP	$1210 \pm 81$	$108 \pm 3$	
$\text{PP}_i$	1107- $\text{PP}_i$	$1258 \pm 21$	$116 \pm 22$	$118 \pm 5$
	990- $\text{P}_i$	$443 \pm 50$	$127 \pm 12$	
	1080- $\text{P}_i$	$1215 \pm 131$	$110 \pm 4$	

Buffer A has the disadvantage of inducing cell aggregation after several hours incubation but its absorption in the  $1200\text{-}1000 \text{ cm}^{-1}$  (Fig. 22) region is lower than that of DMEM (cellular medium) and its composition can be controlled.

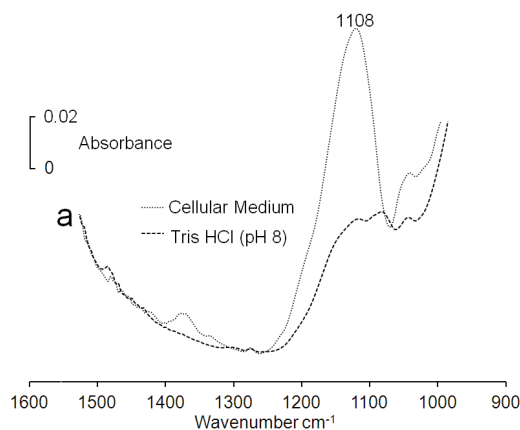


Figure 22. IR spectrum of tris buffer A and IR spectrum of DMEM.

We tested the possibility to determine a specific activity of Saos-2 cells in the cellular medium DMEM. IR spectra of Saos-2 cells (28 mg of Saos-2-cell protein mL<sup>-1</sup> with 50 mM PP<sub>i</sub> in DMEM (Fig. 23a) recorded immediately after mixing the substrate with cells (dashed line) and after 30 min incubation at 37 °C (full line). The spectrum of DMEM was deduced from the spectra of Saos-2 cells. Infrared spectra indicated both the decrease of the 1100-cm<sup>-1</sup> band of PP<sub>i</sub> and the increase of the 1076-1080-cm<sup>-1</sup> band of P<sub>i</sub>, confirming the presence of a pyrophosphatase activity (Fig. 23a). Furthermore, the 1550-cm<sup>-1</sup> protein band allowed us to determine directly protein concentration using  $\epsilon = 3.6 \text{ mg}^{-1}\text{mL cm}^{-1}$ .

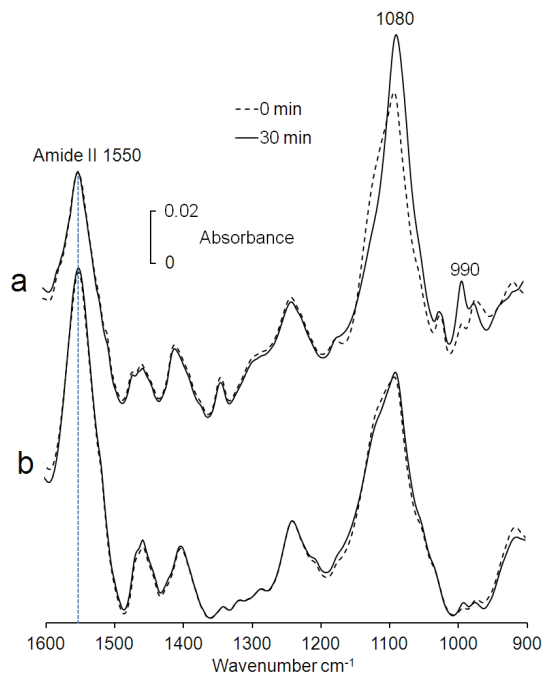


Figure 23. a) IR spectra of Saos-2 cells (28 mg of Saos-2-cell protein mL<sup>-1</sup> with 50 mM PP<sub>i</sub> in DMEM recorded immediately after mixing the substrate with cells (dashed line) and after 30 min incubation at 37 °C (full line). The spectrum of DMEM was deduced from the spectra of Saos-2-cells. b) IR spectra of primary osteoblast cells (45 mg of cell protein mL<sup>-1</sup>) in buffer A with 50 mM PP<sub>i</sub> recorded immediately after mixing PP<sub>i</sub> with cells (dashed line) and after 30 min incubation at 37 °C (full line). The spectrum of buffer A was deduced from the spectra of osteoblasts.

Saos-2 osteoblast-like cells were selected due to their high TNAP activity, making it easier to monitor phosphatase activity in DMEM. Saos-2 cells are cell lines which are easier to cultivate but which are less good models than primary cells. Therefore, primary osteoblasts from mouse calvaria (45 mg of cell protein mL<sup>-1</sup>) were tested for their phosphatase activities. They exhibited also a pyrophosphatase activity both in buffer A (Fig. 23b) and in DMEM (not shown) but it were much lower than those in Saos-2 cells. This was confirmed qualitatively by the magnitude of the difference in IR spectra (spectrum measured after 30 min or the indicated time minus that

measured immediately after mixing  $PP_i$  with cells) recorded for Saos-2 cells in buffer A (Fig. 24A) and in DMEM medium (Fig. 24B) which were higher than that those of primary osteoblasts in buffer A (Fig. 24C) and in DMEM (Fig. 24D) respectively. Infrared spectra indicated both of the disappearance of the 1100-1120- $cm^{-1}$  band of  $PP_i$  and the appearance of the 1076-1080- $cm^{-1}$  and 990- $cm^{-1}$  bands of  $P_i$ , confirming the presence of a pyrophosphatase activity.

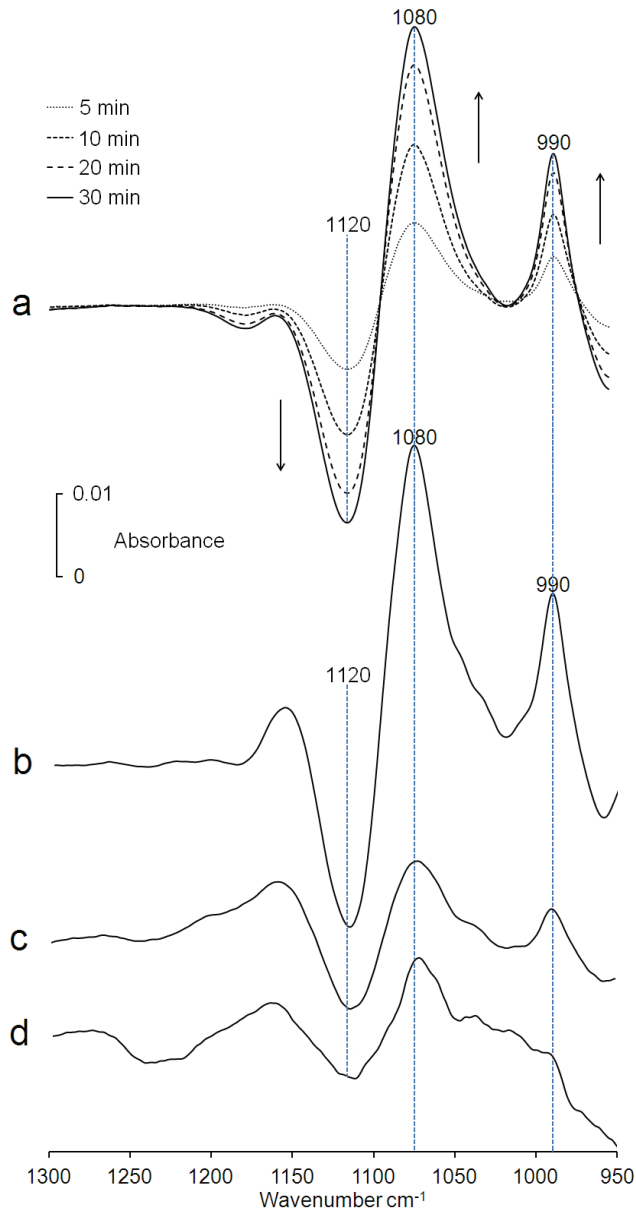


Figure 24. Infrared difference spectra of 50 mM  $PP_i$  in Saos-2 cells or in primary cells measured immediately and after the indicated time. a) Successive IR difference spectra of Saos-2 cells (12 mg of Saos-2-cell protein  $mL^{-1}$ ) in buffer A with 50 mM  $PP_i$  at 37 °C from 5 min to 30 min (spectrum recorded after the indicated time minus spectrum recorded immediately after mixing substrate with cells). b) IR difference spectrum of Saos-2 cells (28 mg of cell protein  $mL^{-1}$ ) with 50 mM  $PP_i$  in DMEM medium at 37 °C (spectrum recorded after 30 min minus spectrum recorded immediately after mixing substrate with cells). c) IR difference spectrum of primary osteoblast cells (45 mg of cell protein  $mL^{-1}$ ) with 50 mM  $PP_i$  in buffer A at 37 °C (spectrum recorded after 30 min minus spectrum recorded immediately after mixing substrate with cells). d) IR difference spectrum of primary osteoblast cells (220 mg of cell protein  $mL^{-1}$ ) with 50 mM  $PP_i$  in DMEM at 37 °C. (spectrum recorded after 30 min minus spectrum recorded immediately after mixing substrate with cells).

The kinetic parameters are easily obtained from IR spectra. The absorbance changes of the 1120-1100- $cm^{-1}$  band of  $PP_i$  (Fig. 25a) and the 990  $cm^{-1}$  band of  $P_i$  (Fig. 25b) served to determine the pyrophosphatase activity and the amide-II band allowed us to determine protein concentration.

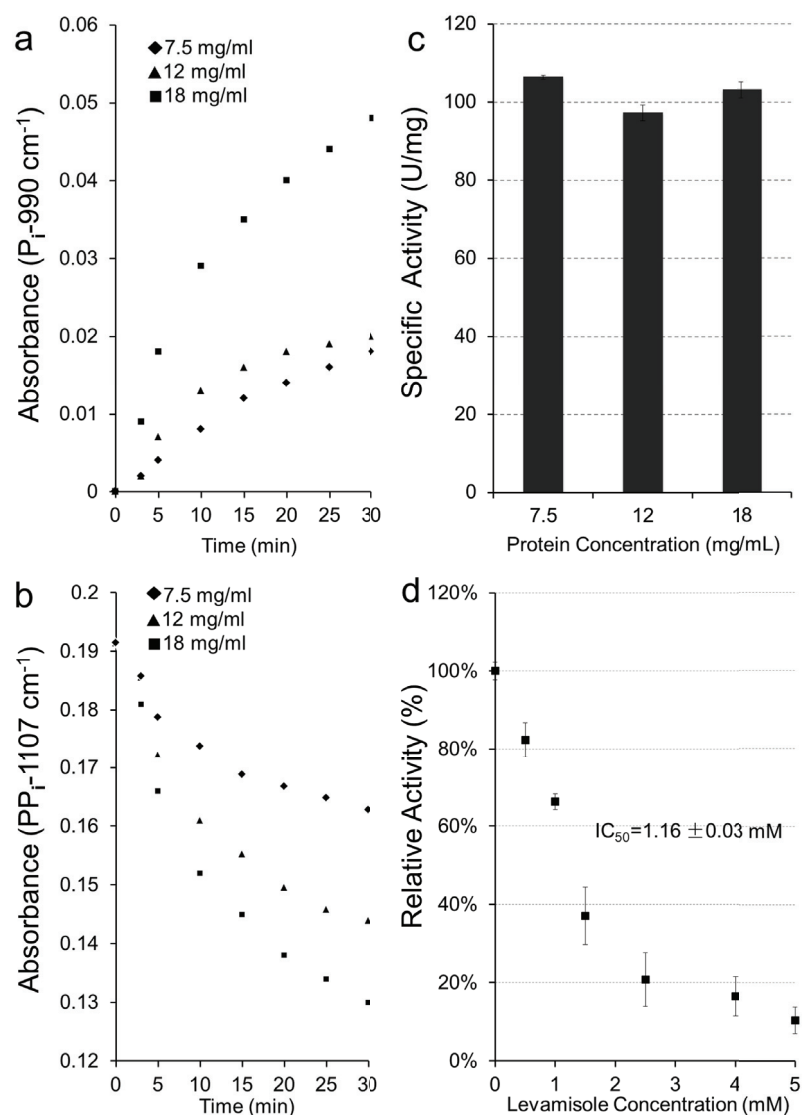


Fig. 25 a) Absorption of PP<sub>i</sub> in 1120-1100 cm<sup>-1</sup> region as a function of incubation time and of Saos-2 cell protein concentration (from 7.5 to 18 mg mL<sup>-1</sup>). b) Absorption of 990 cm<sup>-1</sup> band of P<sub>i</sub> as a function of incubation time and of Saos-2 cell protein concentration. c) Specific activity of PP<sub>i</sub> hydrolysis by Saos-2 cells at three concentrations from 7.5, 12 and 18 mg mL<sup>-1</sup>. One enzyme unit (1 U) is expressed as 1 nmol hydrolyzed PP<sub>i</sub> per min at 37 °C. d) Determination of IC<sub>50</sub> of levamisole by measuring inhibition of PP<sub>i</sub> hydrolysis by Saos-2 cells.

As expected, increasing the amount of Saos-2 cells, from 7.5 mg mL<sup>-1</sup>, 12 mg mL<sup>-1</sup> to 18 mg mL<sup>-1</sup> as determined by the amide-II protein band, increased the pyrophosphatase activity (expressed as nmol min<sup>-1</sup>) but the specific activity remained at the level of 116 ± 13 nmol min<sup>-1</sup> mg<sup>-1</sup> as expected (Fig. 25c). To check if the pyrophosphatase activity originates from TNAP-enriched cells, levamisole (a TNAP inhibitor) was added to the medium. At the concentrations of 5 mM (Fig. 25d), levamisole almost completely inhibited the PP<sub>i</sub> hydrolysis by Saos-2 cells (IC<sub>50</sub> = 1.16 ± 0.03 mM), suggesting TNAP contributed mostly to the pyrophosphatase activity of

Saos-2 cells. The  $IC_{50}$  value of  $1.16 \pm 0.03$  mM is comparable with the reported concentration of 1 mM levamisole that blocked calcification in cultures of aortas from uremic rats [156].

## DISCUSSION

Enzymes, which release phosphate ( $P_i$ ), are among one of the most diverse sets of proteins with respect to the reactions they catalyze [157]. Among the enzymes having a phosphatase activity and releasing  $P_i$ , tissue non-specific alkaline phosphatase (TNAP) performs indispensable, multisystemic functions in humans [48,158].

TNAP is thus today recognized as an attractive drug target for the treatment of vascular calcification. [59,60]. The screening of TNAP inhibitors has relied on the determination of the recombinant TNAP activity at alkaline pH using para-nitrophenylphosphate ( $p$ -NPP). A 1,000-fold more sensitive and 10-fold faster than the  $p$ -NPP assay has been developed with  $p$ -NPP dioxetane-based substrate as TNAP substrate and with recombinant TNAP [61]. However, TNAP inhibitors selected under such conditions may act differently on the living cells. Therefore, there is a strong demand for flexible, fast and cost-effective strategies to select inhibitors with improved prospects for clinical success [159].

Here we demonstrated the ability of IR spectroscopy to directly determine *in situ* a phosphatase activity in osteoblasts using natural substrates without any labeling. We showed the ability of IR spectroscopy to directly determine simultaneously protein concentration and the phosphatase activity in in matrix vesicles as well in cultured osteoblasts using physiological substrates such as AMP, ADP, ATP, UTP, and  $PP_i$ . The method has been validated for osteoblasts (Saos-2 cells and primary osteoblasts) and chondrocyte-derived matrix vesicles which are all TNAP enriched. This approach could be extended to determine any type of phosphatase activity in other cells. It may serve as a metabolomics tool to characterize any types of phosphatase activities and to screen the phosphatase inhibitors in cells.

**CHAPTER V**  
**CONCLUDING REMARKS**

## 1. Effects of Cathepsin K inhibitors on bone resorption and mineralization

In China we developed a series of Cathepsin K, B, L and S inhibitors [42, 43]. The best is **CKI-13** having an  $IC_{50} = 0.006$  nM and is highly selective over Cathepsin B and S (~1000-fold). I synthesized several inhibitors including **CKI-8** and **CKI-13** in China. In France, I examined the effects of these inhibitors on mineralization using human Saos-2 osteoblast-like cells and murine primary calvaria cells. Survival MTT tests on Saos-2 osteoblast-like, RAW264.7 cell and murine primary osteoclast have been performed in the presence of the inhibitors. The alizarin red staining and TNAP activity assay were performed to check the possible effects of inhibitors on mineralization. In addition, a gelatin zymography method was optimized to observe the effects of inhibitors on cathepsin K activity in osteoclasts-derived extracellular medium, which would be served as a screening test of inhibitors before checking their effects on bone resorption. Bone resorption by RAW 264.7 cells and osteoclast primary cells were performed on the surface of an inorganic crystal coating surface (Corning Bone assay surface) and on bovine bone slices. Resorption pit area per osteoclast was measured to determine the effects of Cat K inhibitors. Taken together, the overall findings indicate that both **CKI-8** and **CKI-13** can inhibit cathepsin K in cellular medium at the non-toxicity concentration ranges and can inhibit bone resorption, validating the proof of concept of the possible therapeutic use of the small molecules as cathepsin K inhibitors.

At this stage, several points need to be considered. 1) **CKI-13** slowed down significantly the mineralization process induced by the Saos-2 cell line, as well as inhibiting slightly the TNAP activity, while it did not affect the mineralization process in primary cell lines. This indicates that further work is needed to optimize chemical structures to obtain the best candidate molecules having strong inhibition of bone resorption and having no effects on the mineralization. 2) We observed that our **CKI-8** and **CKI-13** treatments produced smaller pits when compared with the larger pits induced by **E64** treatment. This is an important observation since this suggests that **CKI-8** and **CKI-13** can slow down the mobility of osteoclasts. Actually we do not know how these inhibitors can slow down the mobility of osteoclasts. 3) So far, all of our biological assays were performed on *in vitro* cellular models. Preclinical trials on animal models are a necessity to validate the proof of concept of the use of cathepsin-K inhibitors as a drug treatment to cure osteoporosis.

## 2. Development of an IR assay to detect TNAP activity in matrix vesicles and living cells

One of the main problems for drug screening is that the small molecules selected during the drug screening tests fail often to pass the preclinical and clinical trials. This is not surprising considering the fact that most of the drug screening process use labeled substrates, which often are not natural substrates, sometimes under non physiological conditions and the tests are performed on recombinant enzymes and not on cells or tissues.

Therefore there is a necessity to develop cost-effective drug screening tests, which can mimic as well as possible the drug target in a biological system.

The main advantages of the IR assay lie in the possibility to determine directly in situ hydrolytic activity of phosphatase and to obtain  $IC_{50}$  of inhibitors using natural substrates in an almost continuous manner at physiological pH and in a single assay (determination of protein concentration and enzymatic activity in one single measurement). In addition, we demonstrated that the IR assay could monitor a phosphatase activity in matrix vesicles and in the whole cells in cellular medium close to physiological conditions.

The main disadvantages of the IR assay lie in its low sensitivity, experimental errors can be as large than 20 % due to a difficulty to control the thickness of the cell, although ATR could solve partly this problem. There is a limit in detection, which is around 1 mM of substrate (phosphate compounds). It is not possible to determine reliably the concentration of substrate or product below this concentration. However, the IR assay is well adapted to determine  $V_{max}$  as a kinetic parameter due to saturate concentrations of substrate or  $IC_{50}$ . Another problem is the sample-to-sample reproducibility; especially when the cells have variable activities and maturation degrees. This necessitates to prepare the same types of cells under the same conditions for screening the small molecules, which limitates the numbers of molecules to be tested.

Nevertheless, despite these difficulties, the IR assay can serve as a metabolic tool to evaluate the phosphatase activity in the cells.

## REFERENCES

- [1] Buckwalter JA, Cooper RR. Bone structure and function. *Instr Course Lect.* 1987 36: 27-28.
- [2] Szollar SM, Martin EM, Sartoris DJ, Parthemore JG, Deftos LJ. Bone mineral density and indexes of bone metabolism in spinal cord injury. *Am J Phys Med Rehabil.* 1998 77: 28-35.
- [3] Kon E, Filardo G, Roffi A, Di Martino A, Hamdan M, De Pasqual L, Merli ML, Marcacci M. Bone regeneration with mesenchymal stem cells. *Clin Cases Miner Bone Metab.* 2012 9: 24-27.
- [4] Hu MI, Lu H, Gagel RF. Cancer therapies and bone health. *Curr Rheumatol Rep.* 2010 12: 177-85
- [5] Grant SFA, Ralston SH (1997) Genes and osteoporosis. *Endocrinology.* 1997 8: 232–239
- [6] Hadjidakis DJ, Androulakis II. Bone remodeling. *Ann NY Acad Sci.* 2006 1092: 385-96.
- [7] Väänänen HK, Zhao H, Mulari M, Halleen JM. The cell biology of osteoclast function, *J Cell Sci.* 2000 113: 377–381.
- [8] Boyle WJ, Simonet WS, Lacey DL. Osteoclast differentiation and activation, *Nature.* 2003 423: 337–342.
- [9] Li Z, Kong K, Qi W. Osteoclast and its roles in calcium metabolism and bone development and remodeling. *Biochem Biophys Res Commun.* 2006 343: 345–350.
- [10] Ahn H, Kim JM, Lee K, Kim H, Jeong D. Extracellular acidosis accelerates bone resorption by enhancing osteoclast survival, adhesion, and migration. *Biochem Biophys Res Commun.* 2012 418: 144–148.
- [11] Baylink DJ, Finkelman RD, Mohan S. Growth factors to stimulate bone formation. *J Bone Miner Res.* 1993 8: 565–572.
- [12] Clarke B. Normal bone anatomy and physiology. *Clin J Am Soc Nephrol.* 2008 3: S131–S139
- [13] Sturge J, Caley MP, Waxman J. Bone metastasis in prostate cancer: emerging therapeutic strategies. *Nat Rev Clinical Oncology.* 2011 8: 357-369.

- [14] Zaidi M. Skeletal remodeling in health and disease. *Nat Med.* 2007 13: 791–801.
- [15] Heckel T, Czupalla C, Expirto Santo AI, Anitei M, Arantzazu Sanchez-Fernandez M, Mosch K, Krause E, Hoflack B. Src-dependent repression of ARF6 is required to maintain podosome-rich sealing zones in bone-digesting osteoclasts. *Proc Natl Acad Sci.* 2009 106: 1451–1456.
- [16] Garnero P, Borel O, Byrjalsen I, Ferreras M, Drake FH, McQueney MS, Foged NT, Delmas PD, Delaissé JM. The collagenolytic activity of cathepsin K is unique among mammalian proteinases. *J Biol Chem.* 1998 273: 32347–32352.
- [17] Brömme D, Okamoto K. Human cathepsin O2, a novel cysteine protease highly expressed in osteoclastomas and ovary molecular cloning, sequencing and tissue distribution. *Biol Chem Hoppe-Seyler.* 1995 376: 379-384.
- [18] Everts V, Beertsen W, Schröder R. Effects of proteinase inhibitors leupeptin and e-64 on osteoclastic bone resorption. *Calcif Tissue Int.* 1988 43: 172-178.
- [19] Drake FH, Dodds RA, James IE, Connor JR, Debouck C, Richardson S, Lee-Rykaczewski E, Coleman L, Rieman D, Barthlow R, Hastings G, Gowen M. Cathepsin K, but not cathepsins B, L, or S, is abundantly expressed in human osteoclasts. *J Biol Chem.* 1996 271: 12511-12516.
- [20] Rachner TD, Khosla S, Hofbauer LC. Osteoporosis: now and the future, *Lancet.* 2011 377: 1276-1287.
- [21] Novack DV, Faccio R. Osteoclast motility: putting the brakes on bone resorption, *Ageing Res Rev.* 2011 10: 54-61.
- [22] Rousselle AV, Heymann D. Osteoclastic acidification pathways during bone resorption, *Bone.* 2002 30: 533-540.
- [23] Yasuda Y, Kaleta J, Brömme D. The role of cathepsins in osteoporosis and arthritis: Rationale for the design of new therapies. *Advanced Drug Delivery Reviews.* 2005 57: 973-993.
- [24] Felson DT, Neogi T. Osteoarthritis: is it a disease of cartilage or of bone? *Arthritis Rheum.* 2004 50: 341-344.

- [25] Dejica VM, Mort JS, Lavery S, Percival MD, Antoniou J, Zukor DJ, Poole AR. Cleavage of Type II Collagen by Cathepsin K in Human Osteoarthritic Cartilage. *American Journal of Pathology*. 2008 173: 161-169.
- [26] Connor JR, LePage C, Swift BA, Yamashita D, Bendele AM, Maul D, Kumar S. Protective effects of a cathepsin K inhibitor, SB-553484, in the canine partial medial meniscectomy model of osteoarthritis. *Osteoarthritis and Cartilage*. 2009 17: 1236-43.
- [27] Garnero P, Delmas PD. New developments in biochemical markers for osteoporosis. *Calcif Tissue Int*. 1996 59: 2-9.
- [28] Stoch SA, Wagner JA. Cathepsin K inhibitors: a novel target for osteoporosis therapy, *Clin Pharmacol. Ther*. 2008 83: 172-176.
- [29] Boonen S, Rosenberg E, Claessens F, Vanderschueren D, Papapoulos S. Inhibition of cathepsin K for treatment of osteoporosis. *Curr Osteoporos Rep*. 2012 10: 73-79.
- [30] Kim MK, Kim HD, Park JH, Lim JI, Yang JS, Kwak WY, Sung SY, Kim HJ, Kim SH, Lee CH, Shim JY, Bae MH, Shin YA, Huh Y, Han TD, Chong W, Choi H, Ahn BN, Yang SO, Son MH. An orally active cathepsin K inhibitor, furan-2-carboxylic acid, 1-{1-[4-fluoro-2-(2-oxo-pyrrolidin-1-yl)-phenyl]-3-oxo-piperidin-4-ylcarbamoyl}-cyclohexyl)-amide (OST-4077), inhibits osteoclast activity in vitro and bone loss in ovariectomized rats. *J Pharmacol Exp. Ther*. 2006 318: 555-562.
- [31] Bone HG, McClung MR, Roux C, Recker RR, Eisman JA, Verbruggen N, Hustad CM, DaSilva C, Santora AC, Ince BA. Odanacatib, a cathepsin-K inhibitor for osteoporosis: a two-year study in postmenopausal women with low bone density. *J Bone Miner Res*. 2010 25: 937-947.
- [32] Stoch SA, Zajic S, Stone JA, Miller DL, van Bortel L, Lasseter KC, Pramanik B, Cilissen C, Liu Q, Liu L, Scott BB, Panebianco D, Ding Y, Gottesdiener K, Wagner JA. Odanacatib, a selective cathepsin K inhibitor to treat osteoporosis: safety, tolerability, pharmacokinetics and pharmacodynamics--results from single oral dose studies in healthy volunteers. *Br J Clin Pharmacol*. 2013 75: 1240-1254.
- [33] Delbeck M, Geerts A, Golz S, Meier H, Mondritzki T, Trubel H, Patent Application. A1 WO. 2012 2012: 156311.

- [34] Nakamura T, Shiraki M, Fukunaga M, Tomomitsu T, Santora AC, Tsai R, Fujimoto G, Nakagomi M, Tsubouchi H, Rosenberg E, Uchida S. Effect of the cathepsin K inhibitor odanacatib administered once weekly on bone mineral density in Japanese patients with osteoporosis--a double-blind, randomized, dose-finding study. *Osteoporos Int.* 2014 25:367-376.
- [35] Fuller K, Lindstrom E, Edlund M, Henderson I, Grabowska U, Szewczyk KA, Moss R, Samuelsson B, Chambers TJ. The resorptive apparatus of osteoclasts supports lysosomotropism and increases potency of basic versus non-basic inhibitors of cathepsin K. *Bone.* 2010 46: 1400-1407.
- [36] Chambers TJ, Tobias JH. Are cathepsin k inhibitors just another class of anti-resorptives?, *J Clin Endocrinol Metab.* 2013 98: 4329-4331.
- [37] Loh Y, Shi H, Hu M, Yao SQ. "Click" synthesis of small molecule-peptide conjugates for organelle-specific delivery and inhibition of lysosomal cysteine proteases. *Chem. Commun.* 2010 46: 8407-8409.
- [38] Yang PY, Wang M, Li L, Wu H, He CY, Yao SQ. Design, synthesis and biological evaluation of potent azadipeptide nitrile inhibitors and activity-based probes as promising anti-*Trypanosoma brucei* agents. *Chemistry.* 2012 18: 6528-6541.
- [39] Frizler M, Lohr F, Lülldorff M, Gütschow M. Facing the gem-dialkyl effect in enzyme inhibitor design: preparation of homocycloleucine-based azadipeptide nitriles. *Chemistry.* 2011 17: 11419-11423.
- [40] Löser R, Frizler M, Schilling K, Gütschow M. Azadipeptide nitriles: highly potent and proteolytically stable inhibitors of papain-like cysteine proteases, *Angew Chem Int Ed Engl.* 2008 47: 4331-4334.
- [41] Frizler M, Lohr F, Furtmann N, Kläs J, Gütschow M. Structural optimization of azadipeptide nitriles strongly increases association rates and allows the development of selective cathepsin inhibitors. *J Med Chem.* 2011 54: 396-400.
- [42] Ren XF, Li HW, Fang X, Wu Y, Wang L, Zou S. Highly selective azadipeptide nitrile inhibitors for cathepsin K: design, synthesis and activity assays. *Org Biomol Chem.* 2013 11: 1143-1148.

- [43] Yuan XY, Fu DY, Ren XF, Fang X, Wang L, Zou S, Wu Y. Highly selective aza-nitrile inhibitors for cathepsin K, structural optimization and molecular modeling. *Org Biomol Chem*. 2013 11: 5847-5852.
- [44] Ferney HN. Mammalian alkaline phosphatases *The Enzymes*, Boyer Paul D, ed. Third Edition, Chapter 4. Hydrolysis; other C-N bonds; phosphate esters. Academic Press, NY 1971: 17-447.
- [45] Balcerzak M, Hamade E, Zhang L, Pikula S, Azzar G, Radisson J, Bandorowicz-Pikula J, Buchet R. The roles of annexins and alkaline phosphatase in mineralization process. *Acta Biochimica Polonica*. 2003 50: 1019-1038.
- [46] Risteli L, Risteli J. Biochemical markers of bone metabolism. *Ann Med*. 1993 25: 385-393.
- [47] Garnero P, Delmas PD. New developments in biochemical markers for osteoporosis. *Calcif Tissue Int*. 1996 59: 2-9.
- [48] Millan JL. Mammalian alkaline phosphatases. *From Biology to Applications in Medicine and Biotechnology* (Wiley-VCH Verlag, Germany). 2012.
- [49] Hessle L, Johnson KA, Anderson HC, Narisawa S, Sali A, Goding JW, Terkeltaub R, Millan JL. Tissue non-specific alkaline phosphatase and plasma cell membrane glycoprotein-1 are central antagonistic regulators of bone mineralization. *Proc Natl Acad Sci*. 2002, 99: 9445-9449.
- [50] Harmey D, Hessle L, Narisawa S, Johnson KA, Terkeltaub R, Millán JL. Concerted regulation of inorganic pyrophosphate and osteopontin by Akp2, Ennp1 and Ank. *Am J Pathol*. 2004 164: 1199-1209.
- [51] Gollub EE, Boesze-Battaglia K. The role of alkaline phosphatase in mineralization. *Curr Opin Orthopaed*. 2007 18: 444-448.
- [52] Wang W, Xu J, Du B, Kirsch T. Role of the progressive ankylosis gene (ank) in cartilage mineralization. *Mol Cell Biol*. 2005 18: 181-186.
- [53] Zaka R, Williams CJ. Role of the progressive ankylosis gene in cartilage mineralization. *Curr Opin Rheumatol*. 2006 18: 181-186.

- [54] Richette P, Bardin T, Doherty M. An update on the epidemiology of calcium pyrophosphate dihydrate crystal deposition disease. *Rheumatology*. 2009 48: 711-715.
- [55] Mornet E. Hypophosphatasia. *Best Pract Res Clin Rheumatol*. 2008 22: 113-127.
- [56] Whyte MP. Hypophosphatasia and the role of alkaline phosphatase in skeletal mineralization. *Endocrinol Rev*. 1994 15: 439-461.
- [57] Rutsch F, Ruf N, Vaingankar S, Toliat MR, Suk A, Höhne W, Schauer G, Lehman M, Roscioli T, Schnabel D, Epplen JT, Knisely A, Superti-Furga A, McGill J, Filippone M, Sinaiko AR, Valance H, Hinrichs B, Smith W, Ferre M, Terkeltaub R, Nürnberg P. Mutations in ENPP1 are associated with “idiopathic” infantile arterial calcification. *Nat Genet*. 2003 34: 379-381.
- [58] Ruf N, Uhlenberg B, Terkeltaub R, Nürnberg P, Rutsch F. The mutational spectrum of ENPP1 as arising after the analysis of 23 unrelated patients with generalized arterial calcification of infancy (GACI). *Human Mutation*. 2005 25: 98.
- [59] Mebarek S, Hamade E, Thouverey C, Bandorowicz-Pikula J, Pikula S, Magne D, Buchet R. Ankylosing spondylitis, late osteoarthritis, vascular calcification, chondrocalcinosis and pseudo gout: toward a possible drug therapy. *Curr Med Chem*. 2011 18: 2196-203.
- [60] Dahl R, Sergienko EA, Su Y, Mostofi YS, Yang L, Simao AM, Narisawa S, Brown B, Mangravita-Novo A, Vicchiarelli M, Smith LH, O'Neill WC, Millán JL, Cosford ND. Discovery and validation of a series of aryl sulfonamides as selective inhibitors of tissue-nonspecific alkaline phosphatase (TNAP). *J Med Chem*. 2009 52: 6919-6925.
- [61] Sergienko EA, Millán JL. High-throughput screening of tissue-nonspecific alkaline phosphatase for identification of effectors with diverse modes of action. *Nat Protoc*. 2010 8: 1431-1439.
- [62] Lust G, Seegmiller JE. A rapid, enzymatic assay for measurement of inorganic pyrophosphate in biological samples. *Clin Chim Acta*. 1976 66: 241-249.
- [63] Cook GA, O'Brien WE, Wood HG, King MT, Veech RL. A rapid, enzymatic assay for the measurement of inorganic pyrophosphate in animal tissues. *Anal Biochem*. 1978 91: 557-65.

- [64] Sakasegawa S, Hayashi J, Ikura Y, Ueda S, Imamura S, Kumazawa T, Nishimura A, Ohshima T, Sakuraba H. Colorimetric inorganic pyrophosphate assay using a double cycling enzymatic method. *Anal Biochem.* 2011 416:61-66.
- [65] Nyrén P, Lundin A. Enzymatic method for continuous monitoring of inorganic pyrophosphate synthesis. *Anal Biochem.* 1985 151: 504-509.
- [66] Nyrén P. Enzymatic method for continuous monitoring of DNA polymerase activity. *Anal Biochem.* 1987 167: 235-238.
- [67] Nyrén P, Pettersson B, Uhlén M. Solid phase DNA minisequencing by an enzymatic luminometric inorganic pyrophosphate detection assay. *Anal Biochem.* 1993 208: 171-175.
- [68] Nyrén P, Edwin V. Inorganic pyrophosphatase-based detection systems. I. Detection and enumeration of cells. *Anal Biochem.* 1994 220: 39-45.
- [69] Nyrén P, Edwin V. Inorganic pyrophosphatase-based detection systems. II. Detection and quantification of cell lysis and cell-lysing activity. *Anal Biochem.* 1994 220: 46-52.
- [70] Ronaghi M, Karamohamed S, Pettersson B, Uhlén M, Nyrén P. Real-time DNA sequencing using detection of pyrophosphate release. *Anal Biochem.* 1996 242: 84-89.
- [71] Marques SM, Peralta F, Esteves da Silva JC. Optimized chromatographic and bioluminescent methods for inorganic pyrophosphate based on its conversion to ATP by firefly luciferase. *Talanta.* 2009 77: 1497-503.
- [72] Webb MR. A continuous spectrometric assay for inorganic phosphate and for measuring phosphate release kinetics in biological systems. *Proc Natl Acad Sci.* 1992 89: 4884-4887.
- [73] Upson RH, Haugland RP, Malekzadeh MN, Haugland RP. A spectrophotometric method to measure enzymatic activity in reactions that generate inorganic pyrophosphate. *Anal Biochem.* 1996 243: 41-45.
- [74] Jansson, V; Jansson, K. Enzymatic chemiluminescence assay for inorganic pyrophosphate. *Anal Biochem.* 2002 304: 135-137.
- [75] Pegan SD, Tian Y, Sershon V, Mesecar AD. A Universal, Fully Automated High Throughput Screening Assay for Pyrophosphate and Phosphate Release from Enzymatic Reactions. *Comb Chem High Throughput Screen.* 2010 13: 27-38.

- [76] Das P, Bhattacharya S, Mishra S, Das A. Zn(II) and Cd(II)-based complexes for probing the enzymatic hydrolysis of Na<sub>4</sub>P<sub>2</sub>O<sub>7</sub> by alkaline phosphatase in physiological conditions. *Chem Commun (Camb)*. 2011 47: 8118-8120.
- [77] Katano H, Tanaka R, Maruyama C, Hamano Y. Assay of enzymes forming AMP+PPi by the pyrophosphate determination based on the formation of 18-molybdopyrophosphate. *Anal Biochem*. 2012 421: 308-312.
- [78] Jencks WP. Infrared measurements in aqueous media. *Methods Enzymol*. 1963 6: 914-928.
- [79] Goormaghtigh E, Cabiaux V, Ruyschaert J.M. Secondary structure and dosage of soluble and membrane proteins by a reflection. *European Journal of Biochemistry*. 1990 193: 409-420.
- [80] Kumar S, Barth A. Following enzyme activity with infrared spectroscopy. *Sensors*. 2010 10: 2626-2637.
- [81] Wong PT, Armstrong DW. FTIR spectroscopic kinetic analysis of alkaline phosphatase under hyperbaric manipulation. *Biochim Biophys Acta*. 1992 1159: 237-242.
- [82] Pacheco R, Serralheiro ML, Karmali A, Haris PI. Measuring enzymatic activity of a recombinant amidase using Fourier transform infrared spectroscopy. *Anal Biochem*. 2003 322: 208-214.
- [83] Pacheco R, Karmali A, Serralheiro ML, Haris PI. Application of Fourier transform infrared spectroscopy for monitoring hydrolysis and synthesis reactions catalyzed by a recombinant amidase. *Anal Biochem*. 2005 346: 49-58.
- [84] Schindler R, Lendl B, Kellner R. Simultaneous determination of  $\alpha$ -amylase and amylogucosidase activities using flow injection analysis with Fourier transform infrared spectroscopic detection and partial least-squares data treatment. *Anal Chim Acta* .1998 366: 35-43.
- [85] Krieg P, Lendl B, Vonach R, Kellner R. Determination of alpha-amylase activity using Fourier transform infrared spectroscopy. *Anal Bioanal Chem*. 1996 356: 504-507.
- [86] Schindler R, and Lendl B. Simultaneous determination of enzyme activities by FTIR-spectroscopy in a one-step assay. *Anal Chim Acta*. 1999 391: 19-28.

- [87] Barth A, Mäntele W, Kreutz W. Infrared spectroscopic signals arising from ligand binding and conformational changes in the catalytic cycle of sarcoplasmic reticulum calcium ATPase. *Biochim Biophys Acta*. 1991 1057: 115-123.
- [88] Barth A, Kreutz W, Mäntele W. Molecular changes in the sarcoplasmic reticulum calcium ATPase during catalytic activity. A Fourier transform infrared (FTIR) study using photolysis of caged ATP to trigger the reaction cycle. *FEBS Lett*. 1990 277: 147-150.
- [89] Thoenges D, Barth A. Direct measurement of enzyme activity with infrared spectroscopy. *J Biomol Screen*. 2002 7: 353-357.
- [90] Raimbault C, Clottes E, Leydier C, Vial C, Buchet R. ADP-binding and ATP-binding sites in native and proteinase-K-digested creatine kinase, probed by reaction-induced difference infrared spectroscopy. *Eur J Biochem*. 1997 247: 1197-1208.
- [91] Gáb J, Melzer M, Kehe K, Richardt A, Blum MM. Quantification of hydrolysis of toxic organophosphates and organophosphonates by diisopropyl fluorophosphatase from *Loligo vulgaris* by in situ Fourier transform infrared spectroscopy. *Anal Biochem*. 2009 385: 187-193.
- [92] Cadet F, Pin FW, Rouch C, Robert C, Baret P. Enzyme kinetics by mid-infrared spectroscopy: beta-fructosidase study by a one-step assay. *Biochim Biophys Acta*. 1995 1246: 142-150.
- [93] Schindler R, Thannh LH, Lendl B, Kellner R. Determination of enzyme kinetics and chemometric evaluation of reaction products by FTIR spectroscopy on the example of  $\beta$ -fructofuranosidase. *Vib Spectrosc*. 1998 16: 127-135.
- [94] López-Sánchez M, Ayora-Cañada MJ, Molina-Díaz A, Siam M, Huber W, Quintás G, Armenta S, Lendl B. Determination of enzyme activity inhibition by FTIR spectroscopy on the example of fructose biphosphatase. *Anal Bioanal Chem*. 2009 394: 2137-2144.
- [95] Karmali K, Karmali A, Teixeira A, Curto MJ. Assay for glucose oxidase from *Aspergillus niger* and *Penicillium amagasakiense* by Fourier transform infrared spectroscopy. *Anal Biochemistry*. 2004 333: 320-327.

- [96] Wright W, Vanderkooi JM. Use of IR absorption of the carboxyl group of amino acids and their metabolites to determine pKs, to study proteins, and to monitor enzymatic activity. *Biospectroscopy*. 1997 3: 457-467.
- [97] Fisher J, Belasco JG, Khosla S, Knowles JR. beta-Lactamase proceeds via an acyl-enzyme intermediate. Interaction of the Escherichia coli RTEM enzyme with cefoxitin. *Biochemistry*. 1980 19: 2895-2901.
- [98] Muthusamy M, Burrell MR, Thorneley RN, Bornemann S. Real-time monitoring of the oxalate decarboxylase reaction and probing hydron exchange in the product, formate, using fourier transform infrared spectroscopy. *Biochemistry*. 2006 45: 10667-10773.
- [99] Karmali K, Karmali A, Teixeira A, Curto MJ. The use of Fourier transform infrared spectroscopy to assay for urease from *Pseudomonas aeruginosa* and *Canavalia ensiformis*. *Anal Biochem*. 2004 331: 115-121.
- [100] Estrela-Lopis I, Brezesinski G, Möhwald H. Dipalmitoyl-phosphatidylcholine phospholipase D interactions investigated with polarization-modulated infrared reflection absorption spectroscopy. *Biophys J*. 2001 80: 749-754.
- [101] Yamamoto I, Konto A, Handa T, Miyajima K. Regulation of phospholipase D activity by neutral lipids in egg-yolk phosphatidylcholine small unilamellar vesicles and by calcium ion in aqueous medium. *Biochim Biophys Acta*. 1995 1233: 21-26.
- [102] Do ID, Buchet R, Pikula S, Abousalham A, Mebarek S. Direct determination of phospholipase D activity by infrared spectroscopy. *Anal Biochem*. 2012 430:32-38.
- [103] Bosch A, Prieto C, Serra DO, Martina P, Stämmbler M, Naumann D, Schmitt J, Yantorno O. Type-IV pili spectroscopic markers: applications in the quantification of piliation levels in *Moraxella bovis* cells by a FT-IR ANN-based model. *J Biophotonics*. 2010 3: 522-533.
- [104] Naumann D, Helm D, Labischinski H. Microbiological characterizations by FT-IR spectroscopy. *Nature*. 1991 351: 81–82.
- [105] Helm D, Labischinski H, Schallehn G, Naumann D. Classification and identification of bacteria by Fourier-transform infrared spectroscopy. *J Gen Microbiol*. 1991 137 69–79.

- [106] Rebuffo CA, Schmitt J, Wenning M, von Stetten F, Scherer S. Reliable and rapid identification of *Listeria monocytogenes* and *Listeria* species by artificial neural network-based Fourier transform infrared spectroscopy. *Appl Environ Microbiol.* 2006 72: 994–1000.
- [107] Bosch A, Miñán A, Vescina C, Degrossi J, Gatti B, Montanaro P, Messina M, Franco M, Vay C, Schmitt J, Naumann D, Yantorno O. Fourier transform infrared spectroscopy for rapid identification of nonfermenting gram-negative bacteria isolated from sputum samples from cystic fibrosis patients. *J Clin Microbiol.* 2008 46: 2535–2546.
- [108] Harvey TJ, Henderson A, Gazi E, Clarke NW, Brown M, Faria EC, Snook RD, Gardner P. Discrimination of prostate cancer cells by reflection mode FTIR photoacoustic spectroscopy. *Analyst* 2007 132: 292-295.
- [109] Holton SE, Walsh MJ, Bhargava R. Subcellular localization of early biochemical transformations in cancer-activated fibroblasts using infrared spectroscopic imaging. *Analyst.* 2011 136: 2953-2958.
- [110] Gaigneaux A, Decaestecker C, Camby I, Mijatovic T, Kiss R, Ruyschaert JM. The infrared spectrum of human glioma cells is related to their in vitro and in vivo behavior. *Exp Cell Res.* 2004 297: 294-301.
- [111] Diem M, Romeo M, Boydston-White S, Miljkovic M, Matthäus C. A decade of vibrational micro-spectroscopy of human cells and tissue (1994–2004). *Analyst.* 2004 129:880–885.
- [112] Krishna CM, Kegelaerl G, Adt I, Rubin S, Kartha VB, Manfait M., Sockalingum GD. Combined Fourier transform infrared and Raman spectroscopic identification approach for identification of multidrug resistance phenotype in cancer cell lines. *Biopolymers .* 2006 82: 462-470.
- [113] Bhargava R. Towards a practical Fourier transform infrared chemical imaging protocol for cancer histopathology. *Anal Bioanal Chem.* 2007 389: 1155–1169.
- [114]. Matthäus C, Bird B, Miljkovic M, Chernenko T, Romeo M, Diem M. Infrared and Raman Microscopy in Cell Biology. *Methods Cell Biol.* 2008 89: 275–308.
- [115] Zwielly A, Gopas J, Brkic G, Mordechai S. Discrimination between drug-resistant and non-resistant human melanoma cell lines by FTIR spectroscopy. *Analyst .* 2009 134 :294–300.

- [116] Gasper R, Dewelle J, Kiss R, Mijatovic T, Goormaghtigh E. IR spectroscopy as a new tool for evidencing antitumor drug signatures. *Biochim Biophys Acta*. 2009 1788: 1263–1270.
- [117] Draux F, Jeannesson P, Gobinet C, Sule-Suso J, Pijanka J, Sandt C, Dumas P, Manfait M, Sockalingum G. IR spectroscopy reveals effect of non-cytotoxic doses of anti-tumour drug on cancer cells. *Anal Bioanal Chem*. 2009 395: 2293–2230.
- [118] Diem M, Papamarkakis K, Schubert J, Bird B, Romeo MJ, Miljković M. The infrared spectral signatures of disease: extracting the distinguishing spectral features between normal and diseased states. *Appl Spectrosc*. 2009 63: 307A-318A.
- [119] Vileno B, Jeney S, Sienkiewicz A, Marcoux P, Miller L, Forro L. Evidence of lipid proxydation and protein phosphorylation in cells upon oxydative stress photo-generated by fullerols. *Biophys Chem*. 2009 152 :164–169.
- [120] Gasper R, Mijatovic T, Bénard A, Derenne A, Kiss R, Goormaghtigh E. FTIR spectral signature of the effect of cardiotoxic steroids with antitumoral properties on a prostate cancer cell line. *Biochim Biophys Acta*. 2009 1802: 1087–1094.
- [121] Flower K, Khalifa I, Bassan P, Démoulin D, Jackson E, Lockyer N, McGown A, Vaccari L, Gardner P (2010) Synchrotron FTIR analysis of drug treated ovarian A2780 cells: an ability to differentiate cell response to different drugs? *Analyst* 136:498–507
- [122] Gasper R, Vandebussche G, Goormaghtigh E. Ouabain induced modifications of prostate cancer cell lipidome investigated with mass spectrometry and FTIR spectroscopy. *Biochim Biophys Acta*. 2010 1808: 597–600.
- [123] Diem M, Boydston-White S, Chiriboga L. Infrared spectroscopy of cells and tissues: shining light onto a novel subject. *Appl Spectrosc*. 1999 53: 148A-161A.
- [124] Ellis DI, Goodacre R. Metabolic fingerprinting in disease diagnosis: biomedical applications of infrared and Raman spectroscopy. *Analyst*. 2006 131: 875-885.
- [125] Ellis DI, Goodacre R. Metabolomics-assisted synthetic biology. *Curr Opin Biotechnol*. 2012 23:22-28.
- [126] Romeo M, Mohlenhoff B, Jennings M, Diem M. Infrared micro-spectroscopic studies of epithelial cells. *Biochim Biophys Acta*. 2006 1758: 915-922.

- [127] Bellilosa G, Della Peruta M, Vezzalini M, Moratti E, Vaccari L, Birarda G, Piccinini M, Cinque G, Sorio C. Tracking Infra-Red signatures of drugs in cancer cells by Fourier Transform microspectroscopy. *Analyst*. 2010 135: 3077–3086
- [128] Mazur AI, Monahan JL, Miljković M, Laver N, Diem M, Bird B. Infrared microspectroscopy of live cells in aqueous media. *Marcisin EJ, Uttero CM, Miljković M, Diem M. Analyst*. 2010 135: 3227-3232.
- [129] Lendl B, Krieg P, Kellner R. Determination of alkaline phosphatase activity in human sera by mid-FTIR spectroscopy. *Fresenius J Anal Chem*. 1998 360: 717-720.
- [130] Thouverey C, Bechkoff G, Pikula S, Buchet R. Inorganic pyrophosphate as a regulator of hydroxyapatite of calcium pyrophosphate dihydrate mineral deposition by matrix vesicles Osteoarthritis and cartilage. 2009 17: 64-72.
- [131] Frizler M, Lohr F, Furtmann N, Kläs J, Gütschow M. Structural optimization of azadipeptide nitriles strongly increases association rates and allows the development of selective cathepsin inhibitors. *J Med Chem*. 2011 54: 396-400.
- [132] Gillette JM, Nielsen-Preiss SM. The role of annexin 2 in osteoblastic mineralization. *J Cell Sci* 2004 117: 441-449.
- [133] Vaingankar SM, Fitzpatrick TA, Johnson K, Goding JW, Maurice M & Terkeltaub R. Subcellular targeting and function of osteoblast nucleotide pyrophosphatase/phosphodiesterase 1. *Am J Physiol Cell Physiol*. 2004 286: C1177-1187.
- [134] Mosmann T. Rapid colorimetric assay for cellular growth and survival: application to proliferation and cytotoxicity assays. *J Immunol Methods*. 1983 65: 55-63.
- [135] Stanford CM, Jacobson PA, Eanes ED, Lembke LA, Midura RJ. Rapidly forming apatitic mineral in an osteoblastic cell line. *J Biol Chem* 1995 16: 9420-9428.
- [136] Cyboron GW, Wuthier RE. Purification and initial characterization of intrinsic membrane-bound alkaline phosphatase from chicken epiphyseal cartilage. *J Biol Chem* 1981 256: 7262-7268.
- [137] Li WA, Barry ZT, Cohen JD, Wilder CL, Deeds RJ, Keegan PM, Platt MO. Detection of femtomole quantities of mature cathepsin K with zymography. *Anal Biochem* 2010 401: 91-98.

- [138] Georgess D, Mazzorana M, Terrado J, Delprat C, Chamot C, Guasch RM, Pérez-Roger I, Jurdic P, Machuca-Gayet I. Comparative transcriptomics reveals RhoE as a novel regulator of actin dynamics in bone-resorbing osteoclasts. *Mol Biol Cell*. 2014 25: 380-396.
- [139] Wu LN, Yoshimori T, Genge BR, Sauer GR, Kirsch T, Ishikawa Y, Wuthier RE. Characterization of the nucleational core complex responsible for mineral induction by growth plate cartilage matrix vesicles. *J Biol Chem*. 1993 268: 25084-25094.
- [140] Bradford MM. A rapid and sensitive method for the quantitation of microgram quantities of protein utilizing the principle of protein-dye binding. *Anal Biochem*. 1976 72: 248-254.
- [141] Laemmli UK. Cleavage of structural proteins during the assembly of the head of bacteriophage T4. *Nature* .1970 227: 680-685.
- [142] Genge BR, Wu LN, Wuthier RE. Kinetic analysis of mineral formation during in vitro modeling of matrix vesicle mineralization: effect of annexin A5, phosphatidylserine, and type II collagen. *Anal Biochem*. 2007 367: 159-166.
- [143] Wu LN, Sauer GR, Genge BR, Valhmu WB, Wuthier RE. Effects of analogues of inorganic phosphate and sodium ion on mineralization of matrix vesicles isolated from growth plate cartilage of normal rapidly growing chickens. *J Inorg Biochem*. 2003 94: 221-235.
- [144] Jackson M, Mantsch HH. The use and misuse of FTIR spectroscopy in the determination of protein structure. *Critical Reviews in Biochemistry and Molecular Biology*. 1995 30: 95-120.
- [145] Pathi SP, Kowalczewski C, Tadipatri R, Fischbach C. A novel 3-D mineralized tumor model to study breast cancer bone metastasis. *PLoS One*. 2010 5: e8849.
- [146] Suda T, Nakamura I, Jimi E, Takahashi N. Regulation of osteoclast function. *J Bone Miner Res*. 1997 12: 869-879.
- [147] Tsuboi M. Vibrational spectra of phosphite and hypophosphite anions and the 24 characteristic frequencies of PO<sub>3</sub><sup>2-</sup> and PO<sub>2</sub><sup>2-</sup>-groups. *J Am Chem Soc*. 1957 79: 1351-54.
- [148] Wang JW, Xiao DG, Deng H, Webb MR, Callender R. Raman difference studies of GDP and GTP binding to c-Harvey ras. *Biochemistry*. 1998 37: 11106-11116.

- [149] Yamamoto I, Konto A, Handa T, Miyajima K. Regulation of phospholipase D activity by neutral lipids in egg-yolk phosphatidylcholine small unilamellar vesicles and by calcium ion in aqueous medium. *Biochim Biophys Acta*. 1995 1233: 21-26.
- [150] Cox RP, Gilbert PJr, Griffin MJ. Alkaline Inorganic Pyrophosphatase Activity of Mammalian-Cell Alkaline Phosphatase. *Biochem J*. 1967 105: 155-161.
- [151] Baran Y, Ceylan C, Camgoz A. The roles of macromolecules in imatinib resistance of chronic myeloid leukemia cells by Fourier transform infrared spectroscopy. *Biomed Pharmacother*. 2013 67: 221-227.
- [152] Travo A, Desplat V, Barron E, Poychicot-Coustau E, Guillon J, Déléris G, Forfar I. Basis of a FTIR spectroscopy methodology for automated evaluation of Akt kinase inhibitor on leukemic cell lines used as model. *Anal Bioanal Chem*. 2012 404: 1733-1743.
- [153] Hausser HJ, Brenner RE. Low doses and high doses of heparin have different effects on osteoblast-like Saos-2 cells in vitro. *J Cell Biochem*. 2004 91:1062-1073.
- [154] McQuillan DJ, Richardson MD, Bateman JF. Matrix deposition by a calcifying human osteogenic sarcoma cell line (Saos-2). *Bone*. 1995 16: 415-426.
- [155] Fedde KN. Human osteosarcoma cells spontaneously release matrix-vesicle-like structures with the capacity to mineralize. *Bone Miner*. 1992 17: 145-151.
- [156] Lomashvili KA, Garg P, Narisawa S, Millan JL, and O'Neill WC. Upregulation of alkaline phosphatase and pyrophosphate hydrolysis: potential mechanism for uremic vascular calcification. *Kidney Int*. 2008 73: 1024-1030.
- [157] Pegan SD, Tian Y, Sershon V, Mesecar AD. A Universal, Fully Automated High Throughput Screening Assay for Pyrophosphate and Phosphate Release from Enzymatic Reactions. *Comb Chem High Throughput Screen*. 2010 13: 27-38.
- [158] Buchet R, Millán JL, and Magne D. Multisystemic functions of alkaline phosphatases. *Methods Mol Biol*. 2013 1053: 27-51.
- [159] Bleicher KH, Böhm HJ, Müller K, Alanine AI. Hit and lead generation: beyond high-throughput screening. *Nat Rev Drug Discov*. 2003 2: 369-378.

## LIST OF PUBLICATIONS

### Experimental papers:

[1] Guan B, Cui Y, **Ren Z**, Qiao Z-a, Wang L, Liu Y, Huo, Q. Highly ordered periodic mesoporous organosilica nanoparticles with controllable pore structures *Nanoscale*. 2012 4 : 6588-6596.

[2] **Ren Z**, Machuca-Gayet I, Chantal Domenget C, Rene Buchet R, Yuqing Wu Y, Pierre Jurdic P, Mebarek S. Azanitrile Cathepsin K Inhibitors: cell viability viabilities, mineralization and bone resorption properties. Submitted.\*

[3] **Ren Z**, Do L.D, Bechkoff G, Mebarek S, Keloglu N, Ahamada S, Meena S, David M, Pikula S, Wu Y, Buchet R. Direct determination of phosphatase activity from physiological substrates in cells. Submitted.\*

\* Publications reported in the PhD thesis.

## LIST OF PRESENTATIONS

### Posters and Oral Presentation

**Journée scientifique d'Institut de Chimie et Biochimie Moléculaires et Supramoléculaires ICBMS, Lyon, France, 28 Feb 2013**

1. **REN Zhongyuan**, MEBAREK Saïda, WU Yuqing , BUCHET René

Cathepsins inhibitor as a molecular tool to probe mineralization mechanisms and a possible drug target to treat osteoporosis

**Journée scientifique d'Institut de Chimie et Biochimie Moléculaires et Supramoléculaires ICBMS, Lyon, France, 06 June 2013**

2. **REN Zhongyuan**, DO Le Duy, BECHKOFF Géraldine, KELOGU Nermin, AHAMADA Saandia, MEBAREK Saïda, MAGNE David, PIKULA Slawomir, WU Yuqing, BUCHET René

Direct determination of pyrophosphate hydrolysis in matrix vesicles and Osteoblast-like Saos-2 Cells by infrared spectroscopy

**15eme Journées Françaises des Tissus Minéralisés, Palais des Congrès du Futuroscope, Poitiers, France 30 May to 1st June 2013**

3. **REN Zhongyuan**, GEORGES Dan, DOMENGET Chantal, JURDIC Pierre, WU Yuqing, BUCHET René, MEBAREK Saida

Effect of Highly selective azadipeptide nitrile cathepsin K inhibitors on bone formation and resorption

**15eme Journées Françaises des Tissus Minéralisés, Palais des Congrès du Futuroscope, Poitiers, France 30 May to 1st June 2013**

4. **REN Zhongyuan**, DO Le Duy, BECHKOFF Géraldine, KELOGU Nermin, AHAMADA Saandia, MEBAREK Saïda, MAGNE David, PIKULA Slawomir, WU Yuqing , BUCHET René

Direct determination of pyrophosphate hydrolysis in matrix vesicles by infrared spectroscopy

## **RESUME SUBSTANTIEL EN FRANCAIS**

### **Petites molécules régulant la résorption osseuse et l'activité enzymatique dans les cellules osseuses**

La thèse comprend trois parties : la première partie est centrée sur les inhibiteurs de cathepsine K (**CKIs**) qui sont des dérivés d'azanitriles. Les effets des **CKIs** sur la formation de l'os induite par les ostéoblastes et sur la résorption de l'os par les ostéoclastes ont été déterminés. La deuxième partie de ma thèse a été centrée sur le développement de mesure de l'activité de la phosphatase alcaline dans les vésicules matricielles au moyen de la spectroscopie IR. Enfin, la troisième partie de ma thèse est une extension de la méthode de mesure d'activité de phosphatase alcaline par IR applicable sur les cellules. Cette méthode pourrait être utilisée pour le criblage des inhibiteurs de phosphatase alcaline selon les conditions physiologiques.

#### **1) Effets des inhibiteurs de cathepsine K sur la minéralisation et sur la résorption osseuse.**

Dans le squelette osseux en bonne santé, l'équilibre entre la formation de la matrice osseuse et la résorption de l'os est atteint grâce à une activité coordonnée des cellules ostéoblastes responsables de la formation de l'os et des ostéoclastes impliquées dans la résorption osseuse [1,2]. Afin de dégrader l'os, les ostéoclastes doivent d'abord créer une cavité de résorption. De larges ensembles d'actine F capables d'adhérer à la matrice cellulaire, appelés podosomes, sont formés par les ostéoclastes qui contribuent à créer une zone basolatérale étanche à la surface de l'os. Cela permet aux ostéoclastes de contrôler la résorption de l'os par un rapide assemblage et démontage des podosomes en réponse de signaux intracellulaires générés par l'intermédiaire des protéines appartenant aux famille des Rho GTPases et des kinases Src [3]. Une fois que la cavité de résorption s'est formée, les enzymes telles que les cystéine protéases et la cathepsine K sont secrétées afin de faciliter la

dégradation de l'os. La cathepsine K est la seule enzyme de mammifère capable de cliver la forme hélicoïdale des fibres de collagène de type 1 dans l'os minéralisé [4]. Le milieu acide produit par les ostéoclastes à l'intérieur des podosomes, servant à dissoudre l'hydroxyapatite (composant minéral majeur de l'os) et l'activité de la cathepsine K dégradant la matrice organique, contribuent tous les deux à la résorption de l'os.

L'ostéoporose est la sixième plus importante maladie et est considérée comme une atteinte socioéconomique majeure [5,6]. L'ostéoporose est caractérisée par une perte osseuse et une détérioration des microstructures osseuses qui résultent d'une fragilité squelettique et un accroissement de risques de fractures d'os. Des connaissances approfondies de la biologie de l'os, plus particulièrement au niveau de la communication entre les ostéoblastes et ostéoclastes, ainsi que les réseaux de signalisation ont conduit à l'identification de plusieurs cibles thérapeutiques potentielles. Actuellement, un large éventail de thérapies est disponible pour traiter la perte osseuse bien qu'aucune d'entre elles ne sont capables de prévenir complètement l'ostéoporose. En plus de la thérapie à base d'hormone, d'autres traitements impliquent la prise de bisphosphonates, calcitonine, calcium, strontium, et vitamine D. Plusieurs de ces traitements ont des inconvénients soit au niveau de leur efficacité générale, de leur mode d'application ou de leurs effets secondaires. C'est pourquoi, il y a un besoin urgent de développer de traitements plus efficaces et la demande en médicaments sûrs pour le traitement de l'ostéoporose demeure élevée [7].

Un des traitements de l'ostéoporose les plus prometteurs est un traitement par voie orale d'inhibiteur de cathepsine K (**CKI**) permettant de ralentir la résorption osseuse [8,9]. Des efforts considérables ont été effectués dans le développement des inhibiteurs hautement sélectifs [10]. Cinq **CKIs**, Balicatib, Relacatib, Odanacatib (ODN) et MIV-711 ont été évalués comme traitements thérapeutiques de l'ostéoporose [11,12]. MIV-711 a déjà passé avec succès la phase I en recherches cliniques pour le traitement de l'arthrose ainsi que pour ceux d'autres maladies osseuses [13]. Seul l'ODN a passé avec succès la phase clinique III [14,15]. Bien que ces molécules sont des agents anti-résorption, certains des composés ont des effets secondaires [16,13]. C'est pourquoi le développement d'autres **CKIs** se poursuit encore, une attention particulière est portée sur les azanitrides [37-40]. Tout récemment, nous avons développé des **CKIs** dont le **CKI-13**,  $IC_{50} = 0.006 \text{ nM}$  (schéma 1) ayant une très bonne sélectivité et un  $K_i$  de l'ordre du pico molaire [17,18].

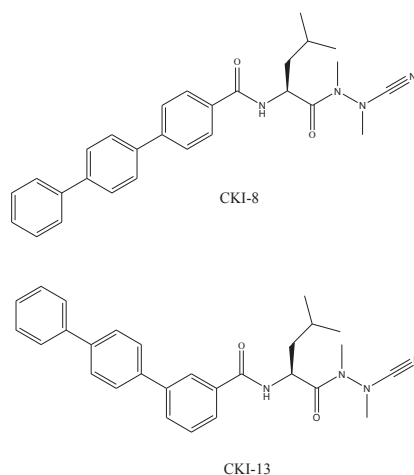


Schéma 1 Structures chimiques des inhibiteurs de cathepsine K : **CKI-8** et **CKI-13**

Afin de consolider la preuve du concept pour l'utilisation de nos inhibiteurs **CKI-8** et **CKI-13** (schéma 1) pour le traitement de l'ostéoporose, nous avons déterminé leurs effets sur la viabilité cellulaire, leur capacité d'induire la minéralisation ainsi que leur propriété de résorption osseuse.

La cytotoxicité de **CKI-8** et de **CKI-13** a été testée sur trois types de cellules : une lignée d'origine humaine Saos-2, une lignée de macrophages de souris RAW 264.7 et les ostéoclastes primaires de souris, en utilisant le test MTT [134]. **CKI-8** (un isomère de **CKI-13**) et **CKI-13** ne sont pas toxiques sur les Saos-2 (Fig. 1a) et les cellules RAW 264.7 (Fig. 1b) jusqu' à une concentration de 1000 nM, tandis qu'ils ne le sont pas jusqu'à une concentration de 100 nM sur les ostéoclastes (Fig. 1c)

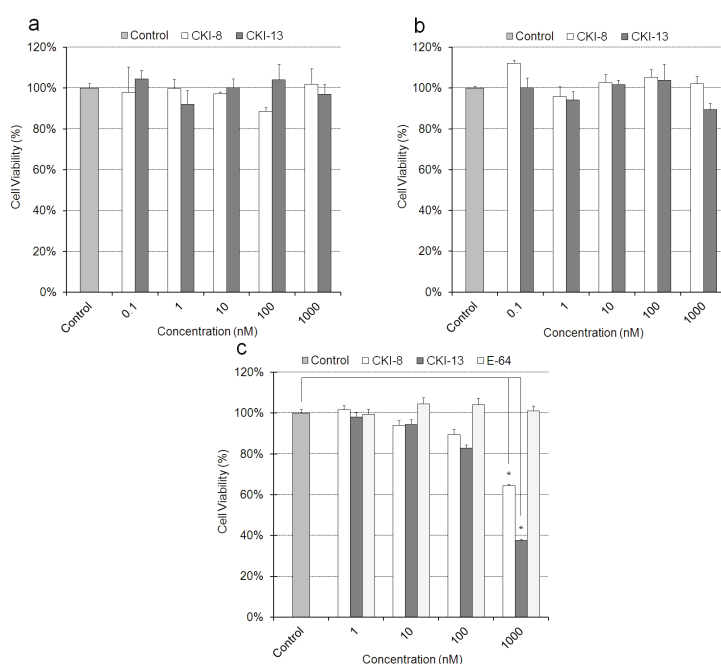


Figure 1. Les inhibiteurs **CKI-8** et **CKI-13** ne sont pas cytotoxiques. A) Tests MTT sur une lignée des cellules d'origine humaine Saos-2. B) Test MTT sur des cellules de souris RAW 264.7. C) Cellules matures d'ostéoclastes primaires de souris. Les résultats ont été effectués trois fois en triplicata (n=9).

La minéralisation est stimulée en ajoutant deux facteurs ostéogéniques, soit l'acide ascorbique (AA) et le béta-glycéro-phosphate ( $\beta$ -GP) [19, 20, 21]. La coloration avec l'AR-S des complexes de calcium a été quantifiée (Fig. 2a et b).

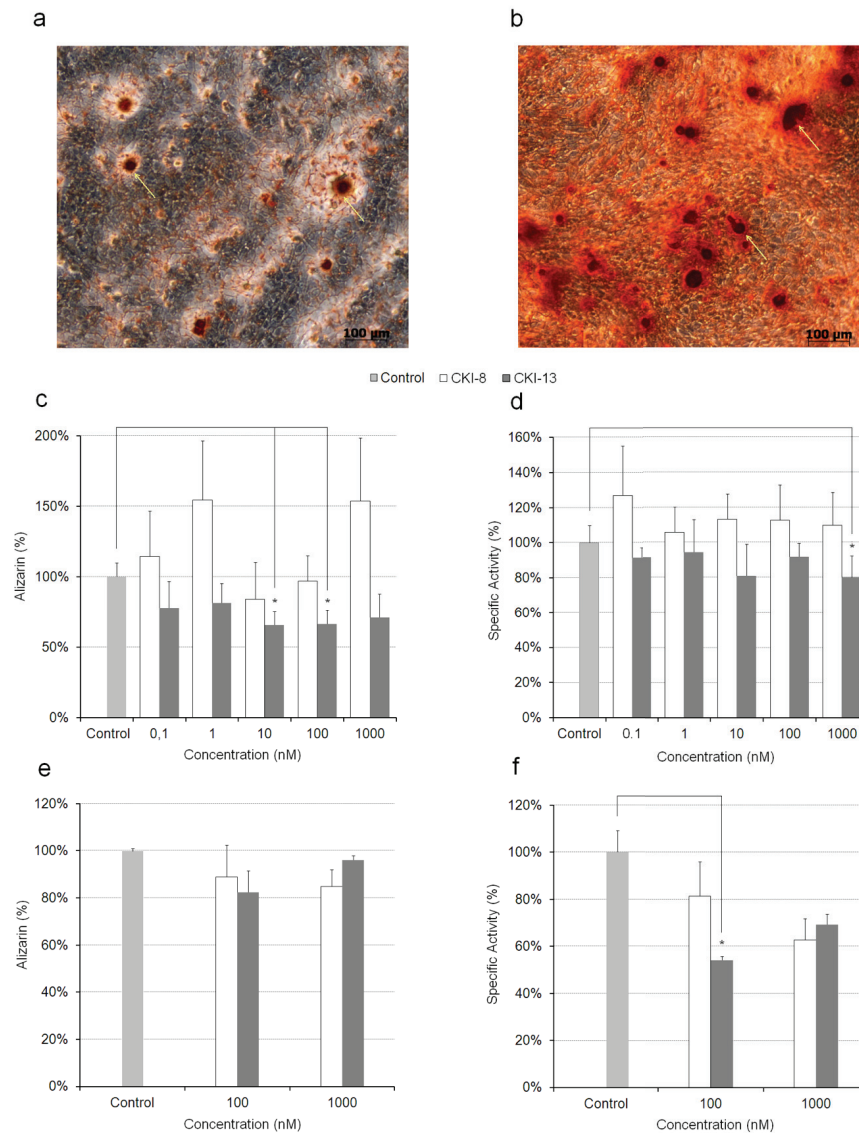


Figure 2. Effets de **CKI-8** et **CKI-13** sur la minéralisation induite par les ostéoblastes. Les Saos-2 ont été incubés pendant six jours sans **(a)** ou avec 50  $\mu$ g ml<sup>-1</sup> AA et 7.5 mM  $\beta$ -GP **(b)** stimulés, puis colorés avec de l'AR-S afin de détecter les complexes de calcium (indiqués par des flèches blanches). Les effets de **CKI-8** et de **CKI-13** sur la minéralisation induite sur les Saos-2 **(c)** et sur les ostéoblastes primaires **(e)** révélés par AR-S ont été quantifiés en fonction de la concentration de **CKI-8** et **CKI-13** en comparaison avec le contrôle (sans inhibiteur). L'activité de phosphatase alcaline durant la minéralisation induite par Saos-2 **(d)** ou par les

ostéoblastes primaires (**f**) a été mesurée en fonction de la concentration de **CKI-8** et **CKI-13** en comparaison avec le contrôle (sans inhibiteur). Les résultats ont été effectués trois fois en triplicata (n=9).

La minéralisation est fortement stimulée en ajoutant les deux facteurs ostéogéniques l'acide ascorbique (AA) et le béta-glycéro-phosphate (Fig. 2b) comme attendu [22]. **CKI-8** n'affecte pas l'activité de phosphatase alcaline (Fig. 2d) ainsi que la minéralisation induite par les Saos-2 (Fig. 2c) et par les ostéoblastes primaires (Fig. 2f). **CKI-13** diminue de 35 % la minéralisation induite par les Saos-2 (Fig. 2c) tandis qu'il n'affecte pas la minéralisation induite par les osteoblastes primaires (Fig. 2f). La résorption osseuse sur des tranches d'os d'origine bovine est diminuée avec 10 nM de **CKI-13**, 100 nM de **CKI-8** et l'inhibiteur commercial **E64** (Fig. 3). **CKI-8** et **CKI-13** diminuent la mobilité des ostéoclastes.

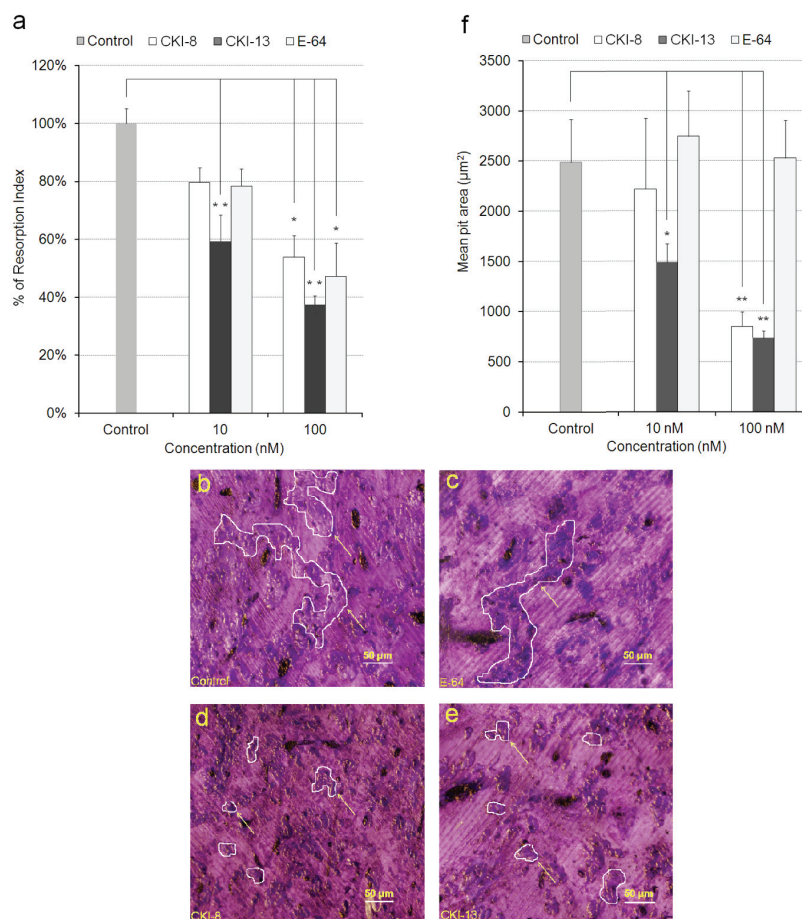


Figure 3. Activité de résorption suivie sur des tranches d'os d'origine bovine. **a**) Index de résorption d'ostéoclastes primaires le contrôle et les inhibiteurs **E-64**, **CKI-8** et **CKI-13**. Surfaces résorbées (indiquées par des contours blancs) sans inhibiteur (**b**), avec **E-64** (**c**), avec **CKI-8** (**d**) et avec **CKI-13** (**e**) à une

concentration de 100nM. Analyse quantitative des surfaces moyennes résorbées en  $\mu\text{m}^2$  sur les tranches d'os avec 100 nM ou sans inhibiteurs (f).

## **1. Développement de mesure de l'activité de la phosphatase alcaline dans les vésicules matricielles et dans les ostéoblastes au moyen de la spectroscopie IR**

La phosphatase alcaline de tissu non-spécifique (TNAP) est exprimée fortement dans l'os, le foie et les reins [23]. Il y a trois enzymes clés dans la régulation du pyrophosphate extracellulaire (ePP<sub>i</sub>), qui est le substrat naturel de la TNAP dans le tissu osseux [24,25]. La première: l'enzyme ankylosante progressive (ANK) est un transporteur de PP<sub>i</sub> et la seconde est l'enzyme nucléotide extracellulaire pyrophosphatase/phosphodiesterase-1 (NPP1) hydrolyse les nucléotides triphosphates en formant du PP<sub>i</sub>. ANK et NPP1 [26,27] contribuent à produire du ePP<sub>i</sub> tandis que la troisième enzyme TNAP hydrolyse l'ePP<sub>i</sub> [28]. L'ePP<sub>i</sub> est un inhibiteur de la formation d'hydroxyapatite (HA). Selon les conditions physiologiques, HA est formé dans l'os. Par contre de l'HA peut être accumulé dans les tissus non squelettiques selon les conditions pathologiques. La TNAP qui hydrolyse ePP<sub>i</sub> est considérée comme une enzyme antagoniste à ANK et NPP1. Le rôle de la phosphatase alcaline a été démontré dans le cas de l'hypophosphatasie chez les patients humains. Cette maladie est causée par une mutation de la TNAP qui conduit à une activité déficiente en TNAP [29,30]. Une forte concentration d'ePP<sub>i</sub>, inhibe la formation d'HA donnant lieu à une ostéomalacie ou à une mauvaise formation de l'os [30,31]. Dans le cas contraire, une forte activité de TNAP peut causer des calcifications pathologiques comme dans le cas des calcifications vasculaires. C'est pourquoi la TNAP, qui est considérée comme un marqueur de la formation osseuse, est une cible thérapeutique attractive pour le traitement des maladies associées aux calcifications vasculaires [32]. Actuellement la sélection des inhibiteurs de la TNAP s'effectue au moyen d'un substrat coloré : le para-nitrophenylphosphate (p-NPP) qui n'est pas un substrat naturel [33]. Les petites molécules sélectionnées de cette façon peuvent agir différemment dans les cellules osseuses. Il y a une forte nécessité de développer des stratégies de criblage des inhibiteurs qui se comportent le plus efficacement possible *in vivo*.

La plupart des mesures de dosage du ePP<sub>i</sub> sont basées sur les essais enzymatiques couplés dosant le NADPH [34], le NADH [35,36] ou par l'intermédiaire de la luciférase [37-43] ou en utilisant le 2-amino-6-mercapto-7-méthylpurine [44,45] ou le luminol [46]. D'autres méthodes colorimétriques ont été développées avec du malachite green [47] des complexes

avec des dérivés de coumarin contenant du Zn (II) et Cd (II) [48]. Aucune de ces méthodes ne permettent de doser simultanément la concentration de protéine, celle du substrat et celle du produit de la réaction, simultanément.

La spectroscopie IR est la seule technique permettant de suivre l'hydrolyse des substrats naturels de la TNAP et de mesurer la concentration de protéine en même temps. Les spectres des substrats AMP, ADP, ATP, UTP,  $\alpha$ -D-glucose-1-phosphate (G-1P)  $\beta$ -glycérophosphate b-GP, para-nitrophenylphosphate (pNPP) sont très différents de celui du produit  $P_i$  (**Fig 4**) rendant possible de déterminer la concentration de substrats et de  $P_i$ .

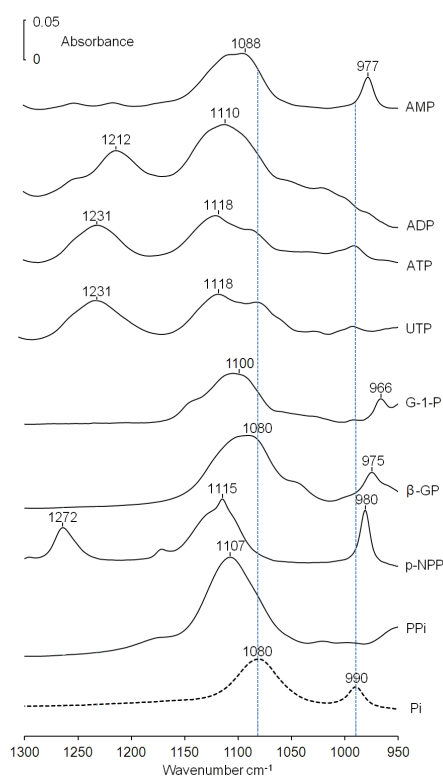


Figure 4. Spectres IR des substrats (50 mM) AMP, ADP, ATP, UTP,  $\alpha$ -D-glucose-1-phosphate (G-1P)  $\beta$ -glycérophosphate b-GP, para-nitrophenylphosphate (*p*NPP),  $PP_i$  et celui du produit  $P_i$ . Deux traits verticaux indiquent la position des bandes de  $P_i$  situées à 1076-1080 et à 990-991  $cm^{-1}$ .

Nous avons développé un dosage d'hydrolyse de  $PP_i$  par la phosphatase alcaline par IR, ayant l'avantage de fonctionner sur des vésicules matricielles et des cellules ostéoblastes avec des substrats naturels à un pH physiologique. Par exemple, la bande de  $PP_i$  localisée à 1107  $cm^{-1}$  ( $\epsilon = 2158 \pm 211 M^{-1}.cm^{-1}$ ) et celles de  $P_i$  localisées à 1076-1080  $cm^{-1}$  ( $\epsilon = 1346 \pm 116 M^{-1}.cm^{-1}$ ) et à 990-991  $cm^{-1}$  ( $\epsilon = 493 \pm 49 M^{-1}.cm^{-1}$ ) ont servis à mesurer les concentrations du substrat et du produit (Fig. 5).

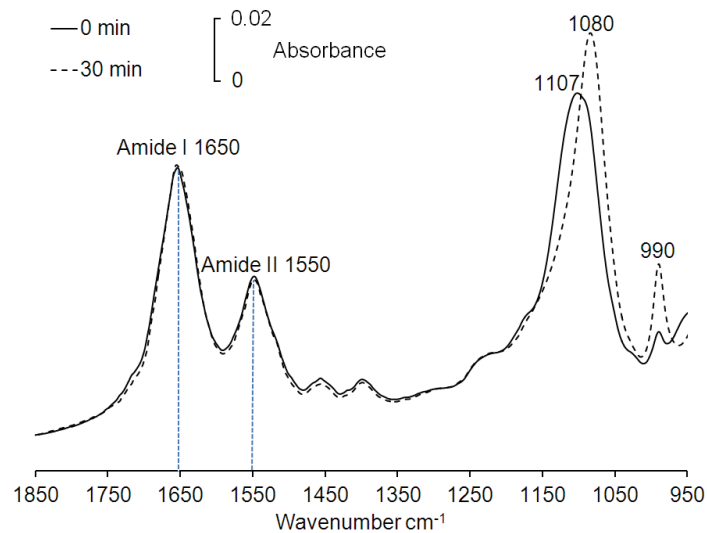


Figure 5. Spectres IR de 50 mM de PPi en présence de cellules Saos-2 mesurés au temps  $t=0$  (trait plein) et après 30 min (tiret).

Le dosage de la concentration de protéines s'est effectué à partir de l'intensité de la bande amide-II car l'intensité de la bande amide-I est plus affectée par la contribution de l'absorption de l'eau. En effectuant des mesures en IR, il est possible de calculer l'activité spécifique de pyrophosphatase.

Nous avons vérifié la faisabilité des mesures enzymatiques sur d'autres substrats tels que AMP, ADP, ATP, UTP, G-1P, b-GP, *p*NPP (Fig. 6).

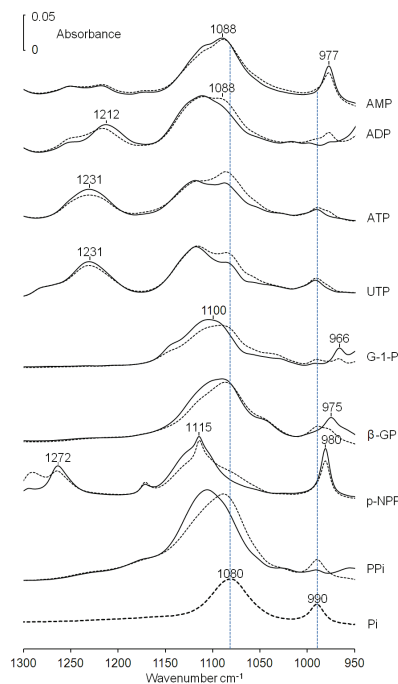


Figure 6. Spectres IR des substrats (50 mM) AMP, ADP, ATP, UTP,  $\alpha$ -D-glucose-1-phosphate (G-1P)  $\beta$ -glycérophosphate, b-GP, para-nitrophenylphosphate (*p*NPP) et celui du produit Pi. Deux traits verticaux indiquent la position des bandes de Pi situés à 1080 et à 990  $\text{cm}^{-1}$ . En présence de cellules Saos-2 (tiret) après 20 min d'incubation et en absence de cellules (trait plein).

Parfois, il est difficile d'observer finement les changements produits au cours de l'hydrolyse des substrats sur les spectres IR. C'est pourquoi nous avons effectué des spectres de différence: soit spectre mesuré après un temps d'incubation moins spectre mesuré à temps =0 (Fig. 6).

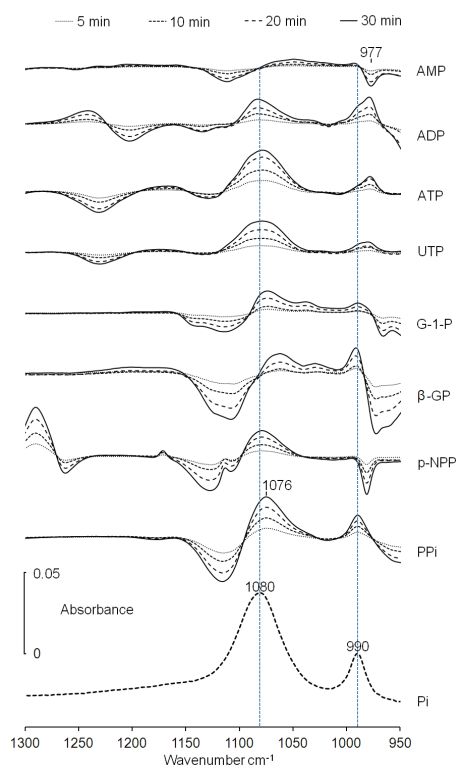


Figure 5. Spectres de différence IR des Cellules Saos-2 en présence de substrats (50 mM) AMP, ADP, ATP, UTP,  $\alpha$ -D-glucose-1-phosphate (G-1P)  $\beta$ -glycérophosphate  $\beta$ -GP, para-nitrophenylphosphate (*p*NPP) et celui du produit Pi. Deux traits verticaux indiquent la position des bandes de Pi situés à 1080 et à 990  $\text{cm}^{-1}$ . Spectres de différence: spectres mesurés selon le temps indiqué moins spectre mesuré en temps =0.

Nous avons démontré que la spectroscopie IR peut déterminer directement une activité de phosphatase dans les ostéoblastes en utilisant des substrats naturels tels que AMP, ADP, ATP, UTP, G-1P,  $\beta$ -GP, *p*NPP. La spectroscopie IR est capable de doser à la fois une concentration de protéines et une activité enzymatique simultanément dans les vésicules matricielles et dans les cellules en milieu aqueux tamponné ou dans un milieu cellulaire. De plus, nous avons pu calculer un  $\text{IC}_{50}$  d'un inhibiteur connu de la TNAP, indiquant que l'activité de phosphatase observée est due pour une grande partie à l'activité de la TNAP. La méthode a été validée pour les Saos-2 et pour les ostéoblastes primaires ainsi que pour des vésicules matricielles

produites par des chondrocytes. Cette approche pourrait servir à doser toute activité de phosphatase dans d'autres types de cellules et pourrait servir d'outil métabolomique.

## Références

- [1] Sturge J, Caley MP, Waxman J. Bone metastasis in prostate cancer: emerging therapeutic strategies. *Nat Rev Clinical Oncology*. 2011 8: 357-369.
- [2] Zaidi M. Skeletal remodeling in health and disease. *Nat Med*. 2007 13: 791–801.
- [3] Heckel T, Czupalla C, Expirto Santo AI, Anitei M, Arantzazu Sanchez-Fernandez M, Mosch K, Krause E, Hoflack B. Src-dependent repression of ARF6 is required to maintain podosome-rich sealing zones in bone-digesting osteoclasts. *Proc Natl Acad Sci*. 2009 106: 1451–1456.
- [4] Garnero P, Borel O, Byrjalsen I, Ferreras M, Drake FH, McQueney MS, Foged NT, Delmas PD, Delaissé JM. The collagenolytic activity of cathepsin K is unique among mammalian proteinases. *J Biol Chem*. 1998 273: 32347–32352.
- [5] Rachner TD, Khosla S, Hofbauer LC. Osteoporosis: now and the future, *Lancet*. 2011 377: 1276-1287.
- [6] Novack DV, Faccio R. Osteoclast motility: putting the brakes on bone resorption, *Ageing Res Rev*. 2011 10: 54-61.
- [7] Yasuda Y, Kaleta J, Brömme D. The role of cathepsins in osteoporosis and arthritis: Rationale for the design of new therapies. *Advanced Drug Delivery Reviews*. 2005 57: 973-993.
- [8] Garnero P, Delmas PD. New developments in biochemical markers for osteoporosis. *Calcif Tissue Int*. 1996 59: 2–9.
- [9] Kim MK, Kim HD, Park JH, Lim JI, Yang JS, Kwak WY, Sung SY, Kim HJ, Kim SH, Lee CH, Shim JY, Bae MH, Shin YA, Huh Y, Han TD, Chong W, Choi H, Ahn BN, Yang SO, Son MH. An orally active cathepsin K inhibitor, furan-2-carboxylic acid, 1-{1-[4-fluoro-2-(2-oxo-pyrrolidin-1-yl)-phenyl]-3-oxo-piperidin-4-ylcarbamoyl}-cyclohexyl)-amide (OST-4077), inhibits osteoclast activity in vitro and bone loss in ovariectomized rats. *J Pharmacol Exp. Ther*. 2006 318: 555-562.

- [10] Boonen S, Rosenberg E, Claessens F, Vanderschueren D, Papapoulos S. Inhibition of cathepsin K for treatment of osteoporosis. *Curr Osteoporos Rep.* 2012 10: 73-79.
- [11] Bone HG, McClung MR, Roux C, Recker RR, Eisman JA, Verbruggen N, Hustad CM, DaSilva C, Santora AC, Ince BA. Odanacatib, a cathepsin-K inhibitor for osteoporosis: a two-year study in postmenopausal women with low bone density. *J Bone Miner Res.* 2010 25: 937-947.
- [12] Stoch SA, Zajic S, Stone JA, Miller DL, van Bortel L, Lassetter KC, Pramanik B, Cilissen C, Liu Q, Liu L, Scott BB, Panebianco D, Ding Y, Gottesdiener K, Wagner JA. Odanacatib, a selective cathepsin K inhibitor to treat osteoporosis: safety, tolerability, pharmacokinetics and pharmacodynamics--results from single oral dose studies in healthy volunteers. *Br J Clin Pharmacol.* 2013 75: 1240-1254.
- [13] Chambers TJ, Tobias JH. Are cathepsin k inhibitors just another class of anti-resorptives?, *J Clin Endocrinol Metab.* 2013 98: 4329-4331.
- [14] Delbeck M, Geerts A, Golz S, Meier H, Mondritzki T, Trubel H, Patent Application. A1 WO. 2012 2012: 156311.
- [15] Nakamura T, Shiraki M, Fukunaga M, Tomomitsu T, Santora AC, Tsai R, Fujimoto G, Nakagomi M, Tsubouchi H, Rosenberg E, Uchida S. Effect of the cathepsin K inhibitor odanacatib administered once weekly on bone mineral density in Japanese patients with osteoporosis--a double-blind, randomized, dose-finding study. *Osteoporos Int.* 2014 25:367-376.
- [16] Fuller K, Lindstrom E, Edlund M, Henderson I, Grabowska U, Szewczyk KA, Moss R, Samuelsson B, Chambers TJ. The resorptive apparatus of osteoclasts supports lysosomotropism and increases potency of basic versus non-basic inhibitors of cathepsin K. *Bone.* 2010 46: 1400-1407.
- [17] Ren XF, Li HW, Fang X, Wu Y, Wang L, Zou S. Highly selective azadipeptide nitrile inhibitors for cathepsin K: design, synthesis and activity assays. *Org Biomol Chem.* 2013 11: 1143-1148.
- [18] Yuan XY, Fu DY, Ren XF, Fang X, Wang L, Zou S, Wu Y. Highly selective aza-nitrile inhibitors for cathepsin K, structural optimization and molecular modeling. *Org Biomol Chem.* 2013 11: 5847-5852.

- [19] Gillette JM, Nielsen-Preiss SM. The role of annexin 2 in osteoblastic mineralization. *J Cell Sci* 2004 117: 441-449.
- [20] Vaingankar SM, Fitzpatrick TA, Johnson K, Goding JW, Maurice M & Terkeltaub R. Subcellular targeting and function of osteoblast nucleotide pyrophosphatase/phosphodiesterase 1. *Am J Physiol Cell Physiol*. 2004 286: C1177-1187.
- [21] Stanford CM, Jacobson PA, Eanes ED, Lembke LA, Midura RJ. Rapidly forming apatitic mineral in an osteoblastic cell line. *J Biol Chem* 1995 16: 9420-9428.
- [22] Mosmann T. Rapid colorimetric assay for cellular growth and survival: application to proliferation and cytotoxicity assays. *J Immunol Methods*. 1983 65: 55-63.
- [23] Millan JL. Mammalian alkaline phosphatases. From Biology to Applications in Medicine and Biotechnology (Wiley-VCH Verlag, Germany). 2012.
- [24] Hessle L, Johnson KA, Anderson HC, Narisawa S, Sali A, Goding JW, Terkeltaub R, Millan JL. Tissue non-specific alkaline phosphatase and plasma cell membrane glycoprotein-1 are central antagonistic regulators of bone mineralization. *Proc Natl Acad Sci*. 2002, 99: 9445-9449.
- [25] Harney D, Hessle L, Narisawa S, Johnson KA, Terkeltaub R, Millán JL. Concerted regulation of inorganic pyrophosphate and osteopontin by *Akp2*, *Enpp1* and *Ank*. *Am J Pathol*. 2004 164: 1199-1209.
- [26] Wang W, Xu J, Du B, Kirsch T. Role of the progressive ankylosis gene (*ank*) in cartilage mineralization. *Mol Cell Biol*. 2005 18: 181-186.
- [27] Zaka R, Williams CJ. Role of the progressive ankylosis gene in cartilage mineralization. *Curr Opin Rheumatol*. 2006 18: 181-186.
- [28] Gollub EE, Boesze-Battaglia K. The role of alkaline phosphatase in mineralization. *Curr Opin Orthopaed*. 2007 18: 444-448.
- [29] Mornet E. Hypophosphatasia. *Best Pract Res Clin Rheumatol*. 2008 22: 113-127.
- [30] Whyte MP. Hypophosphatasia and the role of alkaline phosphatase in skeletal mineralization. *Endocrinol Rev*. 1994 15: 439-461.

- [31] Mebarek S, Hamade E, Thouverey C, Bandorowicz-Pikula J, Pikula S, Magne D, Buchet R. Ankylosing spondylitis, late osteoarthritis, vascular calcification, chondrocalcinosis and pseudo gout: toward a possible drug therapy. *Curr Med Chem*. 2011 18: 2196-203.
- [32] Dahl R, Sergienko EA, Su Y, Mostofi YS, Yang L, Simao AM, Narisawa S, Brown B, Mangravita-Novo A, Vicchiarelli M, Smith LH, O'Neill WC, Millán JL, Cosford ND. Discovery and validation of a series of aryl sulfonamides as selective inhibitors of tissue-nonspecific alkaline phosphatase (TNAP). *J Med Chem*. 2009 52: 6919-6925.
- [33] Sergienko EA, Millán JL. High-throughput screening of tissue-nonspecific alkaline phosphatase for identification of effectors with diverse modes of action. *Nat Protoc*. 2010 8: 1431-1439.
- [34] Lust G, Seegmiller JE. A rapid, enzymatic assay for measurement of inorganic pyrophosphate in biological samples. *Clin Chim Acta*. 1976 66: 241-249.
- [35] Cook GA, O'Brien WE, Wood HG, King MT, Veech RL. A rapid, enzymatic assay for the measurement of inorganic pyrophosphate in animal tissues. *Anal Biochem*. 1978 91: 557-65.
- [36] Sakasegawa S, Hayashi J, Ikura Y, Ueda S, Imamura S, Kumazawa T, Nishimura A, Ohshima T, Sakuraba H. Colorimetric inorganic pyrophosphate assay using a double cycling enzymatic method. *Anal Biochem*. 2011 416:61-66.
- [37] Nyrén P, Lundin A. Enzymatic method for continuous monitoring of inorganic pyrophosphate synthesis. *Anal Biochem*. 1985 151: 504-509.
- [38] Nyrén P. Enzymatic method for continuous monitoring of DNA polymerase activity. *Anal Biochem*. 1987 167: 235-238.
- [39] Nyrén P, Pettersson B, Uhlén M. Solid phase DNA minisequencing by an enzymatic luminometric inorganic pyrophosphate detection assay. *Anal Biochem*. 1993 208: 171-175.
- [40] Nyrén P, Edwin V. Inorganic pyrophosphatase-based detection systems. I. Detection and enumeration of cells. *Anal Biochem*. 1994 220: 39-45.
- [41] Nyrén P, Edwin V. Inorganic pyrophosphatase-based detection systems. II. Detection and quantification of cell lysis and cell-lysing activity. *Anal Biochem*. 1994 220: 46-52.

- [42] Ronaghi M, Karamohamed S, Pettersson B, Uhlén M, Nyrén P. Real-time DNA sequencing using detection of pyrophosphate release. *Anal Biochem.* 1996 242: 84-89.
- [43] Marques SM, Peralta F, Esteves da Silva JC. Optimized chromatographic and bioluminescent methods for inorganic pyrophosphate based on its conversion to ATP by firefly luciferase. *Talanta.* 2009 77: 1497-503.
- [44] Webb MR. A continuous spectrometric assay for inorganic phosphate and for measuring phosphate release kinetics in biological systems. *Proc Natl Acad Sci.* 1992 89: 4884-4887.
- [45] Upson RH, Haugland RP, Malekzadeh MN, Haugland RP. A spectrophotometric method to measure enzymatic activity in reactions that generate inorganic pyrophosphate. *Anal Biochem.* 1996 243: 41-45.
- [46] Jansson, V; Jansson, K. Enzymatic chemiluminescence assay for inorganic pyrophosphate. *Anal Biochem.* 2002 304: 135-137.
- [47] Pegan SD, Tian Y, Sershon V, Mesecar AD. A Universal, Fully Automated High Throughput Screening Assay for Pyrophosphate and Phosphate Release from Enzymatic Reactions. *Comb Chem High Throughput Screen.* 2010 13: 27-38.
- [48] Das P, Bhattacharya S, Mishra S, Das A. Zn(II) and Cd(II)-based complexes for probing the enzymatic hydrolysis of  $\text{Na}_4\text{P}_2\text{O}_7$  by alkaline phosphatase in physiological conditions. *Chem Commun (Camb).* 2011 47: 8118-8120.

## Petites molécules régulant la résorption osseuse et l'activité enzymatique dans les cellules osseuses

### RESUME

La Cathepsine K est parmi la plus efficace des collagénases de mammifère pour cliver la triple hélice de collagène de type-1. Nous avons développé une série d'azanitriles, (**CKI-8** and **CKI-13**) inhibiteurs de cathepsine K. **CKI-8** (un isomère de **CKI-13**) et **CKI-13** ne sont pas toxiques sur les osteoblastes Saos-2 et les cellules RAW 264.7 jusqu' à une concentration de 1000 nM, tandis qu'ils ne le sont pas jusqu'à une concentration de 100 nM sur les osteoclastes. **CKI-8** n'affecte pas l'activité de la phosphatase alcaline ainsi que la minéralisation induite par les Saos-2 et par les osteoblastes primaires. **CKI-13** diminue de 35 % la minéralisation induite par les Saos-2 tandis qu'il n'affecte pas la minéralisation induite par les osteoblastes primaires. L'addition de **CKI-13** diminue l'activité de la phosphatase alcaline d'environ 20% (Saos-2) et de 40 % (osteoblastes primaires). La résorption osseuse sur des tranches d'os d'origine bovine est diminuée avec 10 nM de **CKI-13**, 100 nM de **CKI-8** et 100 nM d'inhibiteur commercial **E64**. **CKI-8** et **CKI-13** diminuent la mobilité des osteoclastes. Nous avons développé un dosage d'hydrolyse de  $PP_i$  par la phosphatase alcaline au moyen de l'IR, ayant l'avantage de fonctionner sur des vésicules matricielles et des cellules avec des substrats naturels à un pH physiologique. La bande de  $PP_i$  localisée à  $1107\text{ cm}^{-1}$  ( $\epsilon = 2158 \pm 211\text{ M}^{-1}.\text{cm}^{-1}$ ) et celles de  $P_i$  localisées à  $1076\text{ cm}^{-1}$  ( $\epsilon = 1346 \pm 116\text{ M}^{-1}.\text{cm}^{-1}$ ) et à  $991\text{ cm}^{-1}$  ( $\epsilon = 493 \pm 49\text{ M}^{-1}.\text{cm}^{-1}$ ) ont servis à mesurer les concentrations du substrat et du produit.

## **Small Molecules regulating Bone Resorption and Enzyme Activity in osseous cells**

### **ABSTRACT**

Cathepsin K is among the most potent mammalian collagenase, capable of cleaving the triple helix in type-I collagen. We developed a series of azanitriles (**CKI-8** and **CKI-13**) which are inhibitors of cathepsin K. **CKI-8** (an isomer of **CKI-13**) and **CKI-13** did not induce significant toxicity on osteoblasts Saos-2 and RAW 264.7 cells up to 1000 nM, while they were not toxic on mature osteoclasts up to 100 nM. Commercial **E64** inhibitor was not toxic in primary osteoclast cells up to 1000 nM. **CKI-8** did not affect alkaline phosphatase activity as well the mineralization induced by Saos-2 cells and by primary osteoblasts. **CKI-13** decreased by 35% the mineralization induced by Saos-2 cells while it did not on mineralization induced by primary osteoblasts. Addition of **CKI-13** decreased alkaline phosphatase activity by around 20% (Saos-2 cells) and 45% (primary osteoblasts). Bone resorption on bovine slices decreased significantly with 10 nM of **CKI-13**, with 100 nM of **CKI-8** and commercial inhibitor **E64**. Our findings indicated that **CKI-8** and **CKI-13** inhibited bone resorption and affected the mobility of osteoclast. To monitor directly the  $PP_i$  hydrolytic activity by alkaline phosphatase, we developed an infrared (IR) assay taking the advantage to use natural substrate under physiological pH in matrix vesicles and in living cells.  $PP_i$  band located at  $1107\text{ cm}^{-1}$  ( $\epsilon = 2158 \pm 211\text{ M}^{-1}\cdot\text{cm}^{-1}$ ) and  $P_i$  bands located at  $1076\text{ cm}^{-1}$  ( $\epsilon = 1346 \pm 116\text{ M}^{-1}\cdot\text{cm}^{-1}$ ) and at  $991\text{ cm}^{-1}$  ( $\epsilon = 493 \pm 49\text{ M}^{-1}\cdot\text{cm}^{-1}$ ) served to measure the substrate and the product concentrations.

**Université Claude Bernard Lyon 1**

**UFR Chimie - Biochimie**

**UMR CNRS UCBL 5246 - ICBMS**

**43 Boulevard du 11 Novembre 1918**

**69622 Villeurbanne Cedex, FRANCE**

**Jilin University**

**State key lab for supramolecular  
structure and materials**

**2699 Qianjin Street**

**130012 ChangChun, CHINE**